ABSTRACT

Influence of Climate and the Expansion of C_4 Grasses on Sequence-Scale Cyclicity and Landscape Development during the Late Miocene to Pleistocene of West Texas

Ryan S. Dhillon, M.S.

Committee Chairman: Stacy C. Atchley, Ph.D.

The Neogene records a period of global climate change and terrestrial ecosystem evolution; however, little is known about whether these changes influenced sedimentary and soil forming processes. The late Miocene to Pleistocene Fort Hancock and Camp Rice Formations from two adjacent isolated basins, southeast Hueco Bolson and northwest Eagle Flat Draw, were analyzed to determine whether changing climate and concomitant C_4 grass expansion influenced fluvial depositional style. Alluvial stacking-pattern analysis of two drill cores reveals sequence-scale trends in paleosol maturity, cycle thickness, and facies proportions. Stable isotope geochemistry of bulk paleosol samples and pedogenic carbonate suggest C_4 expansion at 7.25 Ma and provide a pCO_2 reconstruction of the late Miocene to Pleistocene. C_4 onset coincides with a decreasing sedimentation rate, less frequent channel avulsion events, and an increase in paleosol maturity. Stratigraphic stacking-patterns parallel pCO_2 concentration, suggesting that sedimentation and pedogenesis are influenced by third- to fourth-order global climate cycles.

Influence of Climate and the Expansion of C_4 Grasses on Sequence-Scale Cyclicity and Landscape Development during the Late Miocene to Pleistocene of West Texas

by

Ryan S. Dhillon, B.S.

A Thesis

Approved by the Department of Geology

_____
Steven G. Driese, Ph.D., Chairman

Submitted to the Graduate Faculty of
Baylor University in Partial Fulfillment of the
Requirements for the Degree
of
Master of Science

Approved by the Thesis Committee

_____
Stacy C. Atchley, Ph.D., Chairman

_____
Jason S. Mintz, Ph.D.

_____
Steven G. Driese, Ph.D.

_____
Stephen I. Dworkin, Ph.D.

_____
Steven L. Green, Ph.D.

Accepted by the Graduate School
December 2011

_____
J. Larry Lyon, Ph.D., Dean

Page bearing signatures is kept on file in the Graduate School.

TABLE OF CONTENTS

LIST OF FIGURES

LIST OF TABLES

ACKNOWLEDGMENTS

Dr. Lee Nordt originally conceptualized detailed study of paleosols preserved in cores from the Hueco Bolson as potentially important for recording the onset of C_4 ecosystems in west Texas and I wish to acknowledge this contribution. I would like to thank Dr. Jason Mintz for his day-to-day collaboration and guidance - without his expertise this project would not be where it is today. I am indebted to my advisor, Dr. Stacy Atchley, who supervised my research and shared his knowledge and experience with me through coursework and discussion. He challenged my intellect and pushed me to the best of my potential. I thank my thesis committee for their constructive comments and manuscript review. I'm thankful to Dr. Steve Dworkin, who instructed me on stable isotope geochemistry and helped guide me through lab methodology and sample preparation. I thank Kim Kuijper for her time spent preparing samples, as well as, Dr. Ren Zhang and the Baylor Geology Department's mass spectrometry lab for analyzing hundreds of my samples. I'd like to acknowledge the Bureau of Economic Geology library staff in Austin, Texas for providing maps and geologic reports of my study area. I would also like to show my gratitude to Holly Meier for her helpful discussions and assistance in organization and formatting. Finally, thanks to all my friends and family that supported me during my stay at Baylor University. Financial support for this study was provided by the Baylor Department of Geology and the Baylor Graduate School.

To the loving memory of my father, Bhagat Singh Dhillon, who passed well before his time. He was an honest and loving man, a beautiful musician, an ever-curious intellect, and a father of three sons whom he unconditionally loved through the thick and thin. He inspired me to attend college and encouraged me to chase my dreams and live the life I love. His memory will live on with me forever.

CHAPTER ONE

Introduction

During the Neogene, terrestrial environments experienced a significant change related to global climate evolution and the expansion of C_4 grasses. Miocene to Pleistocene paleoclimate, atmospheric pCO_2, and the expansion of C_4 grasses have been extensively studied (MacGinitie 1962; Nambudiri et al. 1978; Cerling et al. 1997; Ehleringer et al. 1997; Cerling and Harris 1999; Zachos et al. 2001; Tipple and Pagani 2007; Ruddiman 2010). However, little is known about the affects of global climate change and grassland evolution on landscape stability, alluvial sedimentary processes, and pedogenesis. This study builds upon our understanding of Neogene paleoclimate and the nature of late Miocene C_4 grass expansion across North America in order to evaluate the associated impact on sedimentation, pedogenesis, and paleoecology of west Texas, U.S.A.

The earliest fossil evidence of C_4 grasses occur at ~12.5 Ma (MacGinitie 1962; Nambudiri et al. 1978), but the majority of isotope records place the global expansion to C_4-dominated ecosystems between 8 and 6 Ma (Ehleringer et al. 1991, 1997; Morgan et al. 1994; Wang et al. 1994; Quade and Cerling 1995; Cerling et al. 1997, 1998; Latorre et al. 1997; Cerling and Harris 1999; Pagani et al. 1999; Freeman and Colarusso 2001; Passay et al. 2002; Tipple and Pagani 2007; Segalen et al. 2007; Zhang et al. 2009; Edwards and Smith 2010). Causal mechanisms and variability in timing of this ecological shift have long been speculated, and in general, the widely accepted driver is a

decreasing atmospheric pCO_2 of the late Miocene and global climate change (Cerling et al. 1997; Ehleringer et al. 1997; Tripati et al. 2011).

This paper ties a cyclic stratal hierarchy of Neogene paleosol-bearing alluvial deposits with a paleosol-derived paleoclimatic/paleoecological reconstruction to evaluate the relationship (if any) with alluvial sedimentation and landscape stability through time. The study area is in southern Hudspeth County, Texas (Fig. 1) where two cores were drilled through the Miocene to Pleistocene Fort Hancock and Camp Rice Formations of the Santa Fe Group (Fig. 2). These sites are located in the Hueco Bolson and Eagle Flat

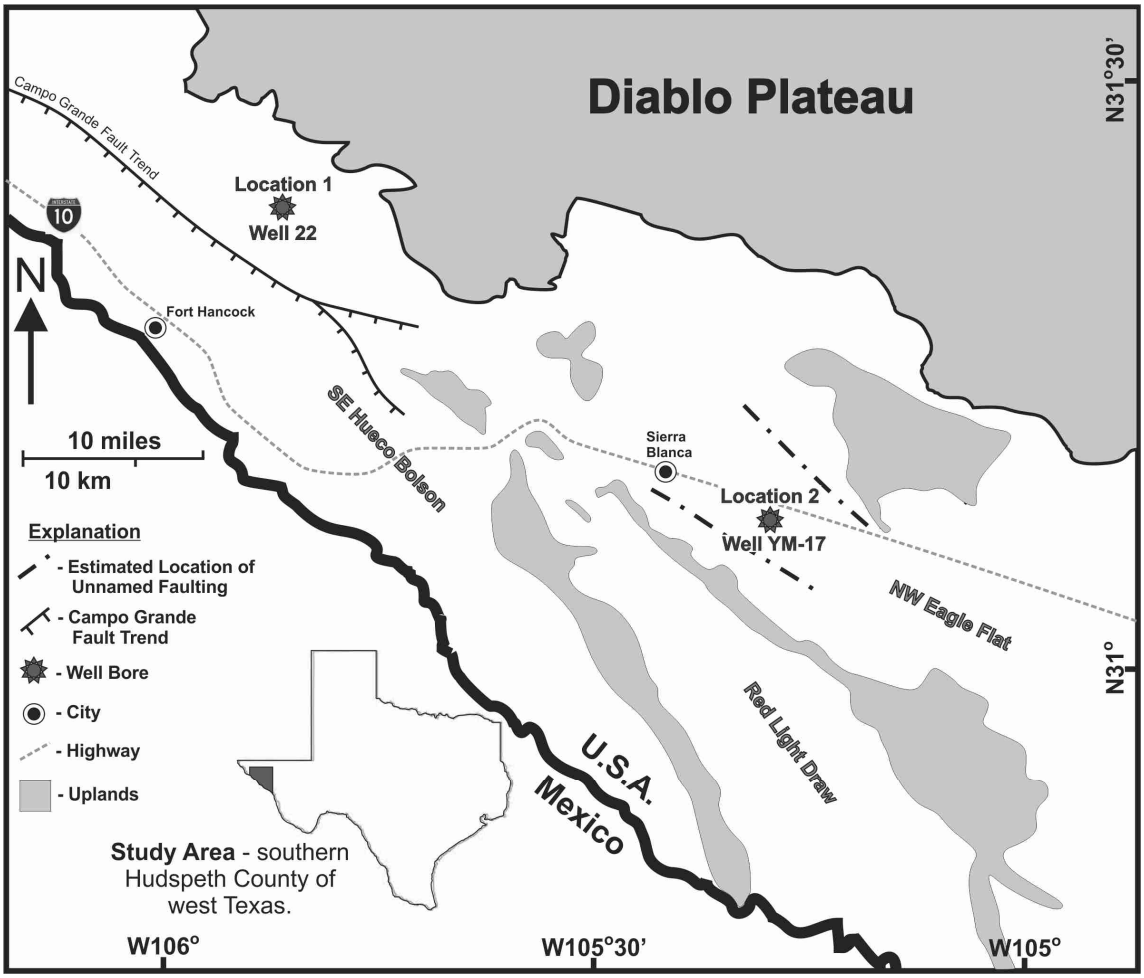

Figure 1. Map illustrating the position of Well 22 (location 1) in the SE Hueco Bolson and YM-17 (location 2) in the NW Eagle Flat basin. The Campo Grande Fault trend location is modified from Collins and Raney (1991).

Basin, which are rift basins that formed within, and associated with, the Rio Grande Rift and Basin and Range province. The goals of this paper are threefold: 1) to evaluate the cyclic alluvial sedimentation within the two isolated basins, in order to understand the local and regional trends of sedimentation and pedogenesis; 2) to reconstruct the paleoecology (C3 vs. C4) from the $\delta^{13}C$ values of soil organic matter (SOM), paleoatmospheric pCO_2 from $\delta^{13}C$ values, and paleotemperatures from $\delta^{18}O$ values of pedogenic carbonate; and 3) to evaluate the effects of climate change and C_4 grass expansion on landscape development during the Neogene in west Texas.

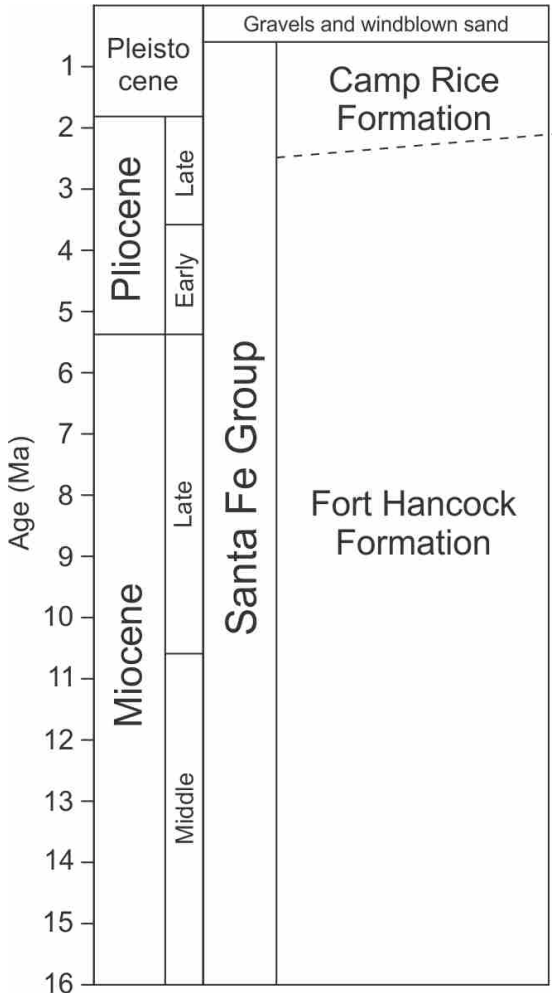

Figure 2. Stratigraphic correlation chart of the study interval within the Hueco Bolson area, Texas (modified from Gustavson 1991).

CHAPTER TWO

Background

Stratigraphy and Depositional Setting

The Fort Hancock Formation and Camp Rice Formation comprise the Santa Fe Group within the study area (Fig. 1 and 2; Albritton and Smith 1965; Strain 1966; Gustavson 1991), which has been previously interpreted as consisting of fluvial, alluvial, and lacustrine sediments of Miocene to Pleistocene age (Gustavson 1991; Langford et al. 1999). Strata time-equivalent to the Fort Hancock and Camp Rice Formations of the Hueco Bolson have been designated the Bramblett and Love Formations, respectively, within the adjacent Red Light Draw (Strain 1966). To avoid confusion, both locations are referred to using the Hueco Bolson terminology in this paper (Fig. 2).

This study examines two cores from southern Hudspeth County, Texas that are part of an 88 core suite that was originally drilled in the late 1980's by the Texas Low Level Radioactive Waste Disposal Authority (TLLRWDA) in a search for a repository site. Well 22 (location 1; 31°23'51"N, 105°43'26"W) is located on the northern edge of the SE Hueco Bolson, about 10 miles (16 km) northeast of Fort Hancock, Texas (Fig. 1). The study interval at location 1 extends from bedrock (depth of 174 meters) to 33 meters below the surface of the basin-fill strata. YM-17 (location 2; 31°8'42"N, 105°15'39"W) is located in the NW Eagle Flat Basin about 7 miles (11 km) east of Sierra Blanca, Texas and about 30 miles (48 km) southeast of location 1 (Fig. 1). The study interval at location 2 extends from bedrock (depth of 207 meters) to 6 meters below the surface.

Absolute age dates of location 2 are constrained by a magnetostratigraphic analysis conducted by Langford and others in 1999.

Located in the south-central North American craton, greater than 650 km from the paleoshoreline, the Eagle Flat Basin and Hueco Bolson are entirely continental basins. Basin-fill sediments are primarily derived from the Diablo Plateau to the north and adjacent northwest-trending fault-block mountain ranges. Basin-fill gravels are composed of limestone and sandstone clasts derived from Cretaceous bedrock (Gustavson 1991; Langford et al. 1999). The SE Hueco Bolson is interpreted as the drainage terminus of the northern ancestral Rio Grande River, from the late Miocene until entrenchment to its modern position, about 0.7 Ma (Kottlowski, 1953; Seager et al. 1984; Gustavson 1991). Stuart and Willingham (1984) described the SE Hueco Bolson as a fluvial-lacustrine basin, in which clays and evaporites were deposited within playa lakes, sandstones and mudstones within low-sinuosity braided channels, and conglomerates within channel lags or alluvial fans along the margin of the bolson. Langford and others (1999) suggested that sedimentation in the NW Eagle Flat Basin was driven by basin morphology, whereby initial basin-fill conglomerates were deposited by extensive alluvial fan systems. As the basin floor aggraded, a low-relief slope formed and deposition evolved into lower competence fluvial systems about 10 Ma.

Significant differences in sedimentation are apparent when comparing basins, the most obvious being the great abundance of mud deposited in the Hueco Bolson, whereas the Eagle Flat Basin is dominantly sand with very little mud. Controls on sedimentation vary between locations because the SE Hueco Bolson and NW Eagle Flat Basin are isolated from each other (Langford et al. 1999). The paleo-Rio Grande River did not

flow through the NW Eagle Flat as it did through the Hueco Bolson, where associated flooding events may account for the high proportion of suspended-load deposits.

Tectonism and Basin Morphology

Late Cenozoic tectonism of the Trans-Pecos Texas southern Rio Grande Rift is part of the western North American Basin-and-Range extension (Seager et al. 1984; Price and Henry 1984, 1985; Henry and Price 1985; Stevens and Stevens 1985; Morgan et al. 1986; Mack and Seager 1990; Collins and Raney 1994). Basin-and-Range extension is inferred to have initiated shortly after Laramide compression ceased, about 29 to 24 Myr before present (Seager et al. 1984; Price and Henry 1984, 1985; Stevens and Stevens 1985). Regional normal faulting across the study area follows the structural trend of the Texas Lineament (a broad subcontinental structural zone, trending NW-SE within the study area; Muehlbereger 1980). Basin-and-Range extension formed a series of north- to northwest-trending fault-bounded basins and adjacent ranges. This study is concerned with two of these normal fault-bounded basins, the southeast Hueco Bolson and northwest Eagle Flat Basin of west Texas.

The Hueco Bolson is a north- to northwest-trending extensional basin approximately 160 km in length and up to 48 km in width from west Texas to southeastern New Mexico. Core from location 1 was obtained from the southeast Hueco Bolson along the southwestern margin of the Diablo Plateau (Fig. 1). Collins and Raney (1991) reported as much as 1850 m of Cenozoic basin-fill sediments within the deepest portion of the southeast Hueco Bolson graben. The Campo Grande Fault trend is a series of normal faults that bound the SE Hueco Bolson on the northeastern edge (Fig. 1), and the fault section adjacent to location 1 is interpreted to have as much as 460 m of offset

(Collins and Raney 1991, 1994). However, location 1 is located northeast of the fault zone on the stable footwall block where Cenozoic basin fill is a maximum of 300 m thick (Collins and Raney 1991, 1994). No evidence for Neogene tectonic activity has been reported northeast of the Campo Grande fault within the study area, and therefore, tectonism at location 1 is assumed to have been relatively stable throughout the late Cenozoic.

The Eagle Flat Basin is a series of three north- to northwest-trending basins, including the Green River Basin, NW Eagle Flat Basin, and SE Eagle Flat Basin (Collins and Raney 1994). Location 2 lies within the NW Eagle Flat Basin which is located east of the Hueco Bolson and south of the Diablo Plateau, and extends 15 miles (24 km) in length and up to 7 miles (11 km) in width (Fig. 1). The basin is relatively shallow, topographically high, and internally drained with a maximum of 219 meters of sediment fill (Collins and Raney 1994; Langford et al. 1999). The tectonic history of the northwest Eagle Flat Basin was studied extensively using seismic and core data by the TLLRWDA, and no evidence of faulting was found within basin-fill strata (Collins and Raney 1994; Langford et al. 1999). Eight-eight wells were drilled throughout the basin and based on the gradually decreasing piedmont slope up-section, Langford and others (1999) interpreted the NW Eagle Flat as a mature basin with tectonism that waned or ceased sometime in the Miocene.

Climate: Miocene to Pleistocene

From assessments of the stratigraphy and paleosols of the SE Hueco Bolson area, Gustavson (1991) suggested that the climate during the Plio-Pleistocene was arid to semi-arid, with cycles of sedimentation and pedogenesis driven by episodic precipitation or

flooding events followed by desiccation. Evidence for an arid to semi-arid climate includes alluvial fan sediments, ephemeral lake deposits, and gypsum evaporite pans in combination with commonly occurring calcic Vertisols indicative of repeated shrink-swell cycles during soil formation (Gustavson 1991).

Following Oligocene glaciation, a warming trend that reduced the global ice volume began at 26 to 27 Ma and persisted through the early and middle Miocene (Miller et. al 1991; Wright et al. 1992; Zachos et al. 2001). This warm trend peaked during the middle Miocene climatic optimum (14-16 Ma) and was succeeded by a gradual global cooling trend that persisted through the late Cenozoic (Zachos et al. 2001). Evidence for global cooling is shown by increasing Antarctic glaciation and increasing $\delta^{18}O$ values of benthic marine organisms (i.e. increasing global ice volume and decreasing deep-ocean temperatures; Miller and Fairbanks 1987; Flower and Kennett 1995; Zachos et al. 2001). Recent work by Pagani and others (2010), Hönisch and others (2009), and Tripati and others (2009; 2011) have provided high resolution atmospheric pCO_2 estimations for the late Cenozoic that correlate closely with trends in glaciation, arctic vegetation, and $\delta^{18}O$ of benthic marine organisms (Ruddiman 2010). An overall decreasing atmospheric pCO_2 is estimated from the middle Miocene to Pleistocene, and this gradually decreasing pCO_2 is believed to be the driver of global cooling and associated increasing aridity (Pagani et al. 2009; Hönisch et al. 2009; Tripati et al. 2009, 2011; Ruddiman 2010).

C_3 and C_4 Plants

Extensive work on the $\delta^{13}C$ values of paleosol organic carbon (SOM), pedogenic carbonate, and fossil tooth enamel commonly show evidence for globally expanding C_4 ecosystems from about 8 to 6 Ma, which has been attributed to decreasing CO_2 and

increasing aridity during the late Cenozoic (Ehleringer et al. 1991, 1997; Cerling et al. 1997, 1998; Cerling and Harris 1999; Pagani et al. 1999; Fox and Koch 2003; Tipple and Pagani 2007; Edwards and Smith 2010). C_4 plants use the Hatch-Slack photosynthetic pathway, a modified Calvin-Benson cycle (C_3 photosynthetic process) in which CO_2 is concentrated at the site of carbon fixation (Hatch 1987). The C_4 photosynthetic pathway is believed to help avoid photorespiration, increased efficiency of photosynthesis under low CO_2 conditions, and increased water-use efficiency (Hatch 1987, Tipple and Pagani 2007). Furthermore, C_4 plants fractionate with a higher preference to the ^{13}C isotope than C_3 plants, which results in the distinctly different isotopic compositions of C_3 and C_4 plants (Cerling and Harris 1999; Tipple and Pagani 2007). The typical $\delta^{13}C$ values of C_3 plants range from about -20 to -35‰ VPDB, whereas the typical $\delta^{13}C$ values of C_4 plants range from about -15 to -10‰ VPDB.

CHAPTER THREE

Methods

Core Description

A total of 342 meters of core from two boreholes (Well 22 and YM-17) were described in detail (Figs. A.1, A.2, and Appendix B). Data collected from the cores include lithotype, grain size, grain sorting, degree of grain rounding, orientation of grains, sedimentary structures (mechanical and biological), stratal thickness, relationships at stratal boundaries, and occurrence of paleosols. These rock attributes were used to assign seven facies designations (Table 1 and Fig. 3) and their distributions were documented within the cores (Figs. A.1 and A.2). Strata are flat-lying at both locations and the maximum burial depth is less than 300 meters (Collins and Raney 1991, 1994); therefore, decompacted thickness estimates were not calculated.

A total of 93 paleosols were classified using USDA Soil Taxonomy (Soil Survey Staff 2010) based on horizonation, ped morphology, carbonate occurrence and depth, color, maturity, density of rooting and burrowing, occurrence of secondary minerals, clay illuviation and eluviation, presence of slickensides, redox features, and relationship with underlying C horizon. Paleosols are categorized into pedotypes, a system of description that focuses on describing a representative profile for a collection of similar paleosols (Table 2 and Fig. 4, Retallack, 2001). Paleosols are assigned a maturity value (1-4) using the paleosol maturity index based on soil thickness, degree of horizonation and percent concentrations of pedogenic minerals (Retallack 1988; 2001). Bulk soil samples and

pedogenic carbonate samples, when present, were collected from each identified paleosol for geochemical analysis.

Table 1. Overview of facies designations, attributes for identification, facies equivalent, architectural element interpretation, and associated depositional setting for each facies (after Miall 1978).

Facies Name	Attributes	Miall Equivalent	Architectural Element Interpretation	Depositional System
Subrounded Pebble Conglomerate - Clast Supported (SPCc)	oligomict to polymict; subrounded to subangular clasts; medium- to fine-grained, calcareous quartz sand matrix; massive to weak horizontal orientation of clasts	Gm	channel bar form, sieve deposit	Alluvial Fan
Subrounded Pebble Conglomerate - Matrix Supported (SPCm)	oligomict to polymict; subrounded to subangular clasts; medium- to fine-grained, calcareous quartz sand matrix; massive to weak horizontal orientation of clasts	Gm, Gms	channel bar form, sieve deposit, debris flow deposit, lag deposit	Alluvial Fan, Eolian
Massive Sandstone (MS)	medium to very fine calcareous quartz sand; < 10% lithoclasts; massive with occasional remnant bedding; burrows and root traces	Sm	scour fill, crevasse splay, upper to lower flow regime, dunes, bed homogenization by biologic activity	Fluvial, Alluvial, Eolian
Cross-Laminated Sandstone (XBS)	fine to very fine, calcareous quartz sand; planar to trough cross-laminations; occasional mud-drapes with flame structures; burrows and root traces	Sr, Sh, Sl	scour fill, crevasse splay, upper to lower flow regime	Fluvial
Red Laminated Mudrock (RLM)	calcareous silt and clay; occasionally interbedded with fine to very fine sand laminations; horizontal laminations to massive; soft-sediment deformation; mud cracks; burrows and root traces	Fl, Fsc, Fm, Fr	overbank or waning flood deposits, drape deposit, seat earth, backswamp deposit	Fluvial, Lacustrine
Intraclastic Conglomerate (IC)	subrounded to angular, elongate mudrock intraclasts (1-35mm); occasional limestone lithoclasts; fine to very fine calcareous quartz sand matrix; massive; burrows and root traces	Se	scour fill, crevasse splay, reworking lacustrine/overbank muds	Lacustrine, Fluvial

Table 1. Overview of facies designations, attributes for identification, facies equivalent, architectural element interpretation, and associated depositional setting for each facies (after Miall 1978).—Continued

Facies Name	Attributes	Miall Equivalent	Architectural Element Interpretation	Depositional System
Intraclastic Sandstone (IS)	fine to very fine, calcareous quartz sand; < 10% subrounded to angular, elongate mudrock intraclasts (1-25mm); occasional limestone lithoclasts; massive; burrows and root traces	Se, Ss, Sm	scour fill, crevasse splay, reworking lacustrine/overbank muds	Lacustrine, Fluvial

Depositional System

Alluvial Fan	SPCc and SPCm facies are massive to poorly stratified sandy gravels, which are commonly deposited as alluvially dominated FACs and typically consist of basal clast-supported conglomerate (SPCc) fining-upward into matrix-supported conglomerate (SPCm) and occasionally massive sandstone (MS).
Fluvial	MS, XBS, and RLM are commonly deposited as channel, crevasse splay, or overbank deposits. Fluvially dominated FACs typically consist of medium to very fine sands (MS, XBS) fining-upward into overbank muds (RLM) and/or a paleosol. Burrowing and rooting is common. IS and IC are fluvial sands to conglomerates with a variable proportion of mudrock intraclasts derived from overbank or lacustrine muds and occasionally occur at the base of a FAC, instead of, or in addition to, MS and XBS.
Lacustrine	RLM is generally deposited in a lacusrine setting and commonly overlain by IC and IS. A lacustrine-dominated FAC typically consists of basal mudrock (RLM) shallowing-upward (gradational transition) into an intraclast conclomerate (IC) and/or intraclast-rich sandstone (IS) and commonly capped by a paleosol. Burrowing and rooting are common.
Eolian	MS and SPCm are occasionally identified as an eolian-dominated FAC in instances in which a thin basal conglomerate (SPCm; lag deposit) is overlain by a thick deposit of very fine to fine sandstone (MS), occasionally capped by a paleosol. Minor rooting and burrowing are present, but deposits are dominantly structureless.

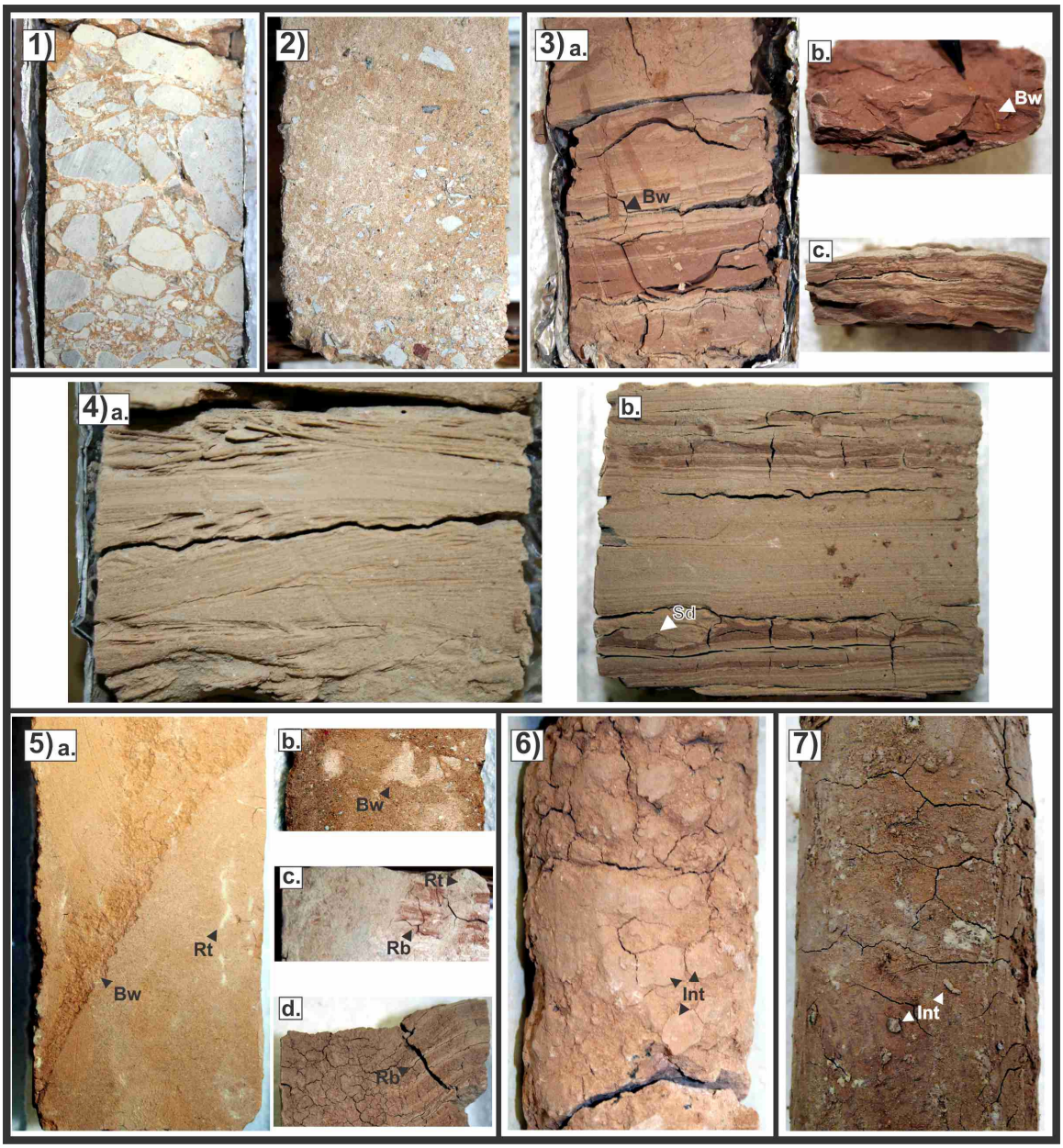

Figure 3. Representative photographs of each facies. Core diameter is 64 mm in all photographs. 1) Subrounded Pebble Conglomerate- Clast Supported (SPCc); 2) Subrounded Pebble Conglomerate- Matrix Supported (SPCm); 3) Red Laminated Mudstone (RLM); 4) Cross-Laminated Sandstone (XBS); 5) Massive Sandstone (MS); 6) Intraclastic Conglomerate (IC); 7) Intraclastic Sandstone (IS). Symbols: Bw = burrow; Rt = root trace; Sd = soft sediment deformation; Rb = remnant bedding; Int = intraclast.

Table 2. Overview of pedotypes, horizonation, paleosol maturity, and attributes for paleosol identification for each pedotype.

Pedotype	Horizon	Structure	Pedogenic features	Precipitates	Rooting	Comments
Paleo-Psamment (Ps) Maturity: 1	A	massive to coarse subangular blocky		sparry calcite around carbonized roots in some paleosols; MnO halos around roots traces or infilling root voids	very fine, common to many carbonized roots or Mn-oxide filled root traces	some A horizons over-thickened cumulative profiles
Color: 7.5YR 6/4 light brown	C	massive silt- or sandstone		none	very fine, none to few carbonized roots	
Paleo-Aquept (Aq)	Bw	medium angular blocky		none	few 1 mm drab haloed root traces	
	Bg1	fine to medium angular blocky	common 3 to 10 mm or 3 to 5 cm diameter mottles (5GY 6/1)	none	Some mottles have linear appearance likely following roots	
	Bg2	medium to coarse angular blocky		none	2-10 cm clay filled root traces	
Maturity: 2	B/C	2nd- very coarse prismatic; 1st-coarse angular blocky		none	none	
Color: 10R 4/3; 10Y 7/1	C	massive sandstone		none	none	
Paleo-Calcid - Fine (Cf)	Ak	strong fine subangular blocky		strong reaction with HCl; some paleosols have abundant fine to very fine rhizolithic carbonate precipitation	very fine, common Mn-oxide filled bifurcating root traces	
	Bw	moderate medium angular blocky		strong reaction with HCl but no nodule formation	very fine, common Mn-oxide filled bifurcating root traces	
Maturity: 2-4	Bk1	structureless to weak medium angular blocky		medium few hard carbonate nodules to only fine to very fine rhizolithic carbonate precipitation	very fine, few Mn-oxide filled bifurcating root traces	

Table 2. Overview of pedotypes, horizonation, paleosol maturity, and attributes for paleosol identification for each pedotype.—Continued

Pedotype	Horizon	Structure	Pedogenic features	Precipitates	Rooting	Comments
	Bk2	2nd-coarse angular blocky; 1st- fine angular blocky		medium common hard carbonate nodules; 5 mm diameter hard rhizolithic carbonates	0.5 cm hard rhizoliths; very fine, few, Mn-oxide filled root traces	finer-grained and stronger pedality than Bk1, potentially epipedon of a soil that was welded into overlying profile
Color: 5YR 6/4 red brown	Bk3	weak coarse angular blocky		medium common hard carbonate nodules	very fine, few Mn-oxide filled bifurcating root traces	higher concentration of carbonate nodules than superseding Bk horizons
	B/C	weak coarse angular blocky		none	few to no roots	
Paleo-Calcid - Coarse (Cc)	Ak	medium angular blocky		few 0.3-0.5 cm hard carbonate nodules	few very fine Mn-oxide filled root traces	A horizon typically truncated and not preserved
Maturity: 3-4	Bk1	massive pebbly sandstone to weak coarse angular blocky		common 0.3-0.5 cm diameter hard carbonate nodules; occasional soft masses in the matrix	few to common very fine Mn-oxide filled root traces	manganese dendrites along void spaces, making clear identification of rooting difficult
	Bk2	massive pebbly sandstone		common 0.5-1.0 cm hard carbonate nodules	few very fine Mn-oxide filled root traces	
Color: 5YR 6/4 red brown	Bk3	none		soft carbonate masses in soil matrix	little to no evidence of rooting	
	C	none		none	none	
Paleo-Calciustert (Cu)	A	fine to medium subangular blocky		none	few to common very fine Mn-oxide filled root traces with Mn-oxide haloes	not commonly preserved

Table 2. Overview of pedotypes, horizonation, paleosol maturity, and attributes for paleosol identification for each pedotype.—Continued

Pedotype	Horizon	Structure	Pedogenic features	Precipitates	Rooting	Comments
Maturity: 3-4	Bkss1	moderate medium subangular blocky	slickensides on ped surfaces	1 cm diameter hard rhizocretions	few to common very fine Mn-oxide filled root traces	some paleosols have gleyed mottles and drab haloed root traces that give these horizons a Bkssg horizon designation
	Bkss2	strong very coarse wedge	master slickensides, wedge-shaped peds	few to common 0.5 cm diameter hard carbonate nodules and 1 cm diameter rhizocretions	common 2-3 mm Mn-oxide and drab haloed root traces	
	Bkss3	strong very coarse wedge	master slickensided surfaces	rare 2-3 mm hard carbonate nodules		
Color: 10R 4/3; 2.5YR 4/4	B/C	thin medium platy	some small bowl shaped cracks	none	none	
	C	red laminated mudrock	none	none	none	
Paleo-Gypsi-torrert (Gt)	Ay	fine to medium angular blocky	pressure faces common on ped surfaces	very few gypsum coatings on ped surfaces	common 2-3 mm Mn-oxide and drab haloed root traces	
Maturity: 3-4	Bssy1	medium angular blocky; 1st-fine angular blocky	common slickensides on ped surfaces and master surfaces	gypsum coating on all ped surfaces marco voids	common 2-3 mm Mn-oxide and drab haloed root traces	no gypsum precipitation within matrix material of peds, only on ped surfaces
	Bssy2	fine to medium wedge	common well defined slickensides on ped faces	gypsum coating on all ped surfaces marco voids	common 2-3 mm Mn-oxide and drab haloed root traces	
	Bssy3	weak blocky ped structure	pressure faces common on ped surfaces	gypsum coating on all ped surfaces marco voids	few 2-3 mm Mn-oxide and drab haloed root traces	
Color: 2.5YR 8/2 pinkish white	B/C	coarse angular blocky	0.5-1 cm burrows filled with light colored fill	none	none	
	C	massive sandstone	none	none	none	5YR 6/4 red brown

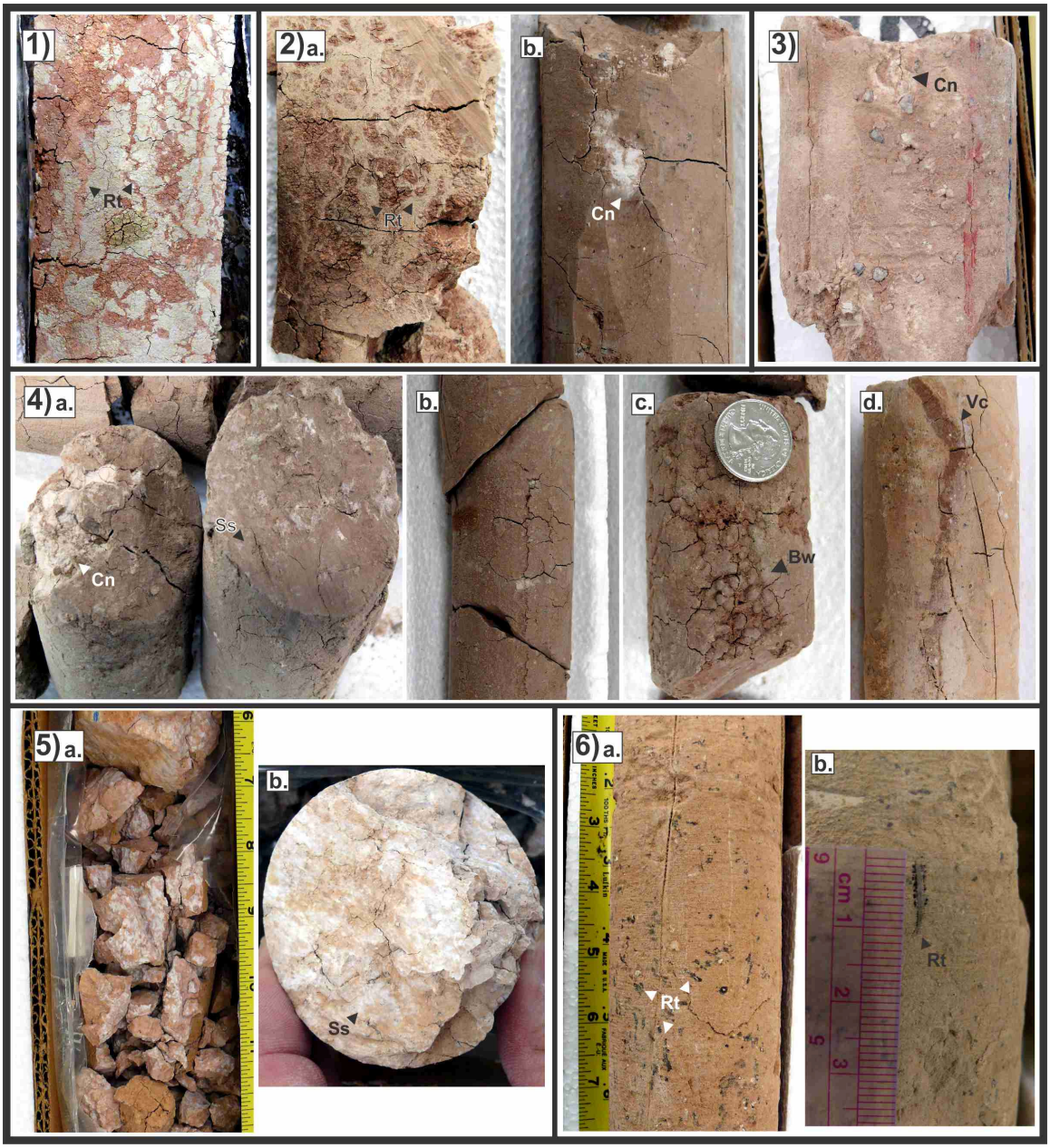

Figure 4. Representative photographs of each pedotype. Core diameter is 64 mm in all photographs. 1) Paleo-Aquept (Aq) – Bg horizon; 2) Paleo-Calcid-Fine (Cf): a. rhizolith-rich Ak to Bk horizon, b. Bk horizon; 3) Paleo-Calcid-Coarse (Cc) – Bk horizon; 4) Paleo-Calciustert (Cu): a. carbonate nodules and slickensides in Bkss horizon, b. wedge-shaped peds in a Bkss horizon, c. fecal pellet lined burrow from Bkss horizon, d. vertical crack into B/C horizon; 5) Paleo-Gypsitorrert (Gt): a. gypsum covered peds within Byss horizon, b. gypsum covered slick-plane from Byss horizon; 6) Paleo-Psamment (Ps): a. A horizon with a high concentration of manganese-filled root traces and a diffuse upper contact with overlying sandstone, b. manganese coated root trace in an A horizon; Symbols: Bw = burrow; Rt = root trace; Cn = carbonate nodule; Ss = slickenside; Vc = vertical crack.

Stacking-Pattern Analysis

Recently, marine stacking-pattern analysis methodology has been adapted for paleosol-bearing alluvial successions (Atchley et al. 2004), in which cycles of fluvial sedimentation occur on a multiple-tier hierarchy and are used in an attempt to decipher autogenic and allogenic controls on terrestrial basin-fill stratigraphy (Kraus 1987, 1999, 2002; Burns et. al. 1997; Retallack 1998; Kraus and Aslan 1999; Atchley et al. 2004; Prochnow et al. 2006; Cleveland et al. 2007; Mintz 2011). This study follows the methodology of Atchley and others (2004) to evaluate potential autogenic and allogenic mechanisms that may account for depositional and pedogenic cyclicity.

Fluvial aggradational cycles (FACs) are the lowest tier of the cyclic stratal hierarchy, and are described as fining-upward, meter-scale successions that are disconformably bound at the base and top (Atchley et al. 2004). An individual FAC is attributed to a single channel avulsion event (Bridge 1984; Kraus 1987; Kraus and Aslan 1999; Atchley et al. 2004; Cleveland et al. 2008; Mintz 2011). FACs stack into decameter-scale FAC-sets, which are disconformably bound at the base and top (Atchley et al. 2004). FAC-sets are interpreted to have been deposited by a series of avulsion episodes as a channel migrated away from, or back toward, a reference point in the alluvial valley (Kraus 1987; Kraus and Aslan 1999; Atchley et al. 2004; Cleveland et al. 2007). Finally, FAC-sets stack into hectometer-scale alluvial sequences that are recognized by a long-period fining-upward trend, thinning-upward of FACs, and the presence of sequence boundaries at the base and top (Atchley et al. 2004). Sequence boundaries are recognized by 1) erosional truncation, 2) long-period inflection from relatively low to high sedimentation rates, 3) the long-period inflection from thinning to thickening of FACs, 4) change in facies proportions from overbank mud dominated

deposits below the boundary to channel sand and gravel dominated deposits above, and 5) the long-period transition from relatively mature and well drained paleosols below the boundary to relatively immature and poorly drained paleosols above (Atchley et al. 2004).

Modified systems tract names are assigned to trends of accommodation change and sedimentation within an alluvial sequence (Atchley et. al. 2004, in review). Trends of increased accommodation gain, high sedimentation, and low paleosol maturity are referred to as transgressive systems tract equivalents (TE), and trends of decreased accommodation gain, decreased sedimentation to erosion, and high paleosol maturity are referred to as highstand- to falling-stage equivalents (HFE; Atchley et. al. 2004). The maximum flooding surface equivalent (MFE) is identified at the inflection of increasing sedimentation/accommodation (TE) and decreasing sedimentation/accommodation (HFE; Atchley et. al. 2004). Alluvial systems tract nomenclature is based solely on stacking-pattern trends and in this study, and have no implications for interpreting eustatic changes.

Previous work using the alluvial stacking pattern analysis methodology has been applied to several types of basins (continental, backarc, passive margin), in which sedimentation and pedogenesis are driven by variations in sea level (Atchley et. al. 2004, in review) or tectonism (Cleveland et. al. 2007, Mintz 2011). In these studies, the greatest and most continuous pedogenic modification occurs during periods of low accommodation. FAC thickness and paleosol maturity have an inverse relationship. Trends of thickening FACs are associated with decreasing paleosol maturity and vice versa.

Paleosol Geochemistry

Pedogenic carbonate samples were collected and analyzed from nodules that were spherical to elliptical in shape, >50 cm from the preserved soil surface, absent of blocky spar, and interpreted to have formed in the vadose zone. Samples were cleaned of siliciclastic material and micritic calcite was collected from each nodule using a small hand drill. Powdered carbonate was analyzed at Baylor University using a Thermo Scientific GasBench II coupled to a Thermo Finnigan Delta V Advantage mass spectrometer, which provided $\delta^{13}C$ and $\delta^{18}O$ values with a precision of $\pm$0.2‰. Approximately 50 mg of powdered bulk paleosol sediment samples were treated to analyze $\delta^{13}C$ values of soil organic matter (SOM). Samples were placed in a small silver cup, treated with a 5% dilute solution of sulfurous acid, dried, and the process was repeated until the reaction digested all the $CaCO_3$. The soil organic matter was analyzed on the Baylor University Costech elemental analyzer coupled to a Thermo Finnigan Delta V Advantage mass spectrometer, which provides $\delta^{13}C$ values with a precision of $\pm$0.1‰.

Soil-derived calcium carbonate (pedogenic carbonate) has been sampled from paleosols throughout the Phanerozoic and is used to estimate the mean annual temperature and paleoatmospheric pCO_2 at the time of carbonate precipitation (Equation 1 and 2; Cerling 1999; Ekardt et al. 1999; Dworkin et al. 2005). Paleotemperature was estimated using the oxygen isotopic composition of pedogenic carbonate ($\delta^{18}O_{cc(SMOW)}$) and the spatial relationship equation (Equation 1) from Dworkin and others (2005) for soil calcite formed in mid-latitude regions:

Equation 1: $$-0.22T^3 + (\delta^{18}O_{cc(SMOW)} + 61.99)T^2 - 2.78 \times 10^6 = 0$$

where T is absolute temperature (^oK).

Atmospheric pCO_2 was estimated using the carbon isotopic composition of pedogenic carbonate and the isotope mass-balance equation (Equation 2; Cerling 1999; Ekardt et al. 1999):

Equation 2: $$[CO_2]_{atm} = Sz([\delta^{13}C_s - 1.0044\delta^{13}C_r - 4.4] / [\delta^{13}C_a - \delta^{13}C_s])$$

where $[CO_2]_{atm}$ is atmospheric pCO_2 (ppmV); Sz is the concentration of soil-respired CO_2 (ppmV); and $\delta^{13}C_s$, $\delta^{13}C_r$, and $\delta^{13}C_a$ are the carbon isotopic compositions of soil pCO_2, soil-respired pCO_2, and atmospheric pCO_2, respectively. Soil pCO_2 concentration (Sz) was estimated to be 1000 ppmV during the formation of the carbonate based on a study of modern soil calcite formation in desert soils and of soil carbonate in Vertisols forming in a humid climate (Breecker et al. 2009, Mintz et al., 2011). The $\delta^{13}C$ values of soil organic matter (SOM) was used to represent $\delta^{13}C_r$ ($\delta^{13}C_r$ = -19 to -25‰). The $\delta^{13}C$ values of pedogenic carbonate and estimated paleotemperature (from Equation 1) were used to calculate the $\delta^{13}C$ values of soil CO_2 from the temperature-dependent carbonate equilibrium fractionation between calcite and CO_2 (Romanek et al. 1992). Finally, $\delta^{13}C_a$ was estimated using $\delta^{13}C_r$ values and the Arens and others (2000) equation ($\delta^{13}C_a = (\delta^{13}C_r + 18.67) / 1.10$).

CHAPTER FOUR

Results

Depositional Facies

A total of seven depositional facies were identified, and then assigned to a Miall (1974) architectural element and depositional system association (Table 1). Facies include subrounded pebble conglomerate, clast-supported (SPCc), subrounded pebble conglomerate, matrix-supported (SPCm), massive sandstone (MS), cross-laminated sandstone (XBS), red laminated mudrock (RLM), intraclast conglomerate (IC), and intraclast sandstone (IS) (Table 1 and Fig. 3). Four depositional systems are interpreted (alluvial, fluvial, lacustrine, and eolian), which are described in Table 1, and are depicted in Figure 5.

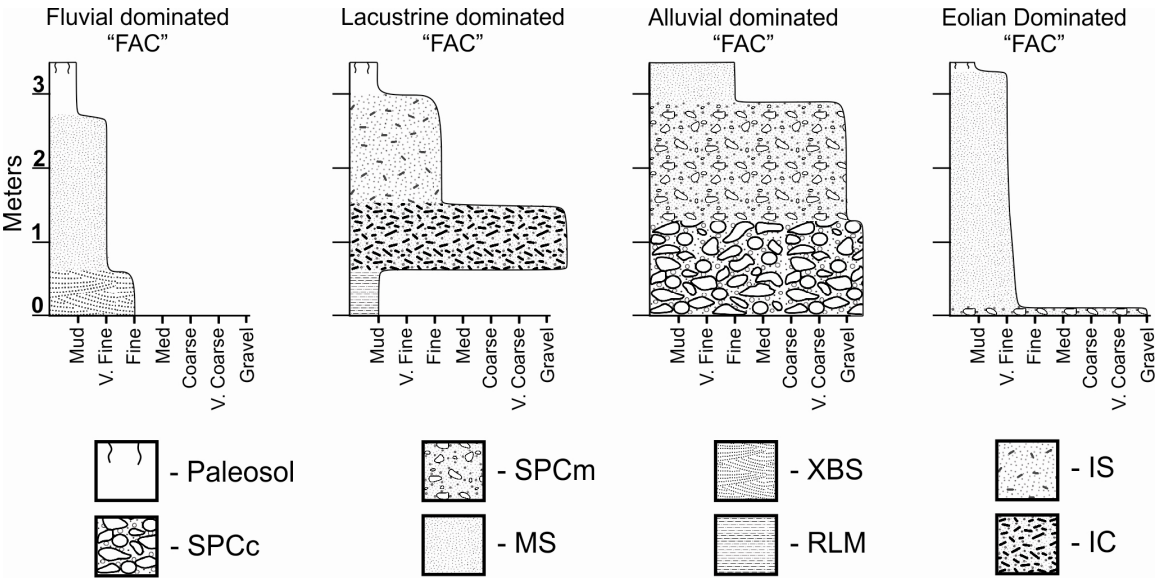

Figure 5. Idealized succession of facies for FACs deposited by fluvial, lacustrine, alluvial, and eolian depositional processes. Compare facies symbols and notation to Table 1.

Pedotypes

A total of six pedotypes are identified that include an Entisol (Paleo-Psamment [Ps]), Inceptisol (Paleo-Aquept [Aq]), two different Aridisols (Paleo-Calcid – fine [Cf] and Paleo-Calcid – coarse [Cc]), and two different Vertisols (Paleo-Calciustert [Cu] and Paleo-Gypsitorrert [Gt]; Table 2 and Fig. 4). Each paleosol was assigned a maturity value and then plotted as cumulative deviation from mean (Fig. 6), and the distribution of pedotypes and paleosol maturity are displayed on the detailed FAC-specific histograms of Figure 7.

Plotting Trends in Sedimentation and Pedogenesis

Cumulative deviation from mean (CDM) FAC thickness, paleosol maturity, and relative abundance of coarse-grained to fine-grained facies (facies proportion) were plotted for each core location to identify long-term stacking patterns (Fig. 6; Sadler et. al. 1993; Drummond and Wilkinson 1993; Lehrmann and Goldhammer 1999; Atchley et. al. 2004). In order to plot CDM facies proportion, site-specific calculations were made to show the relative abundance of fine-grained and coarse-grained facies for each FAC. At location 1, coarse-grained facies include SPCc, SPCm, MS, XBS, IS, and IC, whereas fine-grained facies include RLM and paleosols. At location 2, coarse-grained facies include SPCc and SPCm, whereas fine-grained facies include MS and paleosols. Additionally, distributions of facies and facies thickness, as well as pedotype and paleosol maturity, were plotted for each FAC on histograms for each location to quantitatively assess trends in sedimentation and pedogenesis through time (Fig. 7).

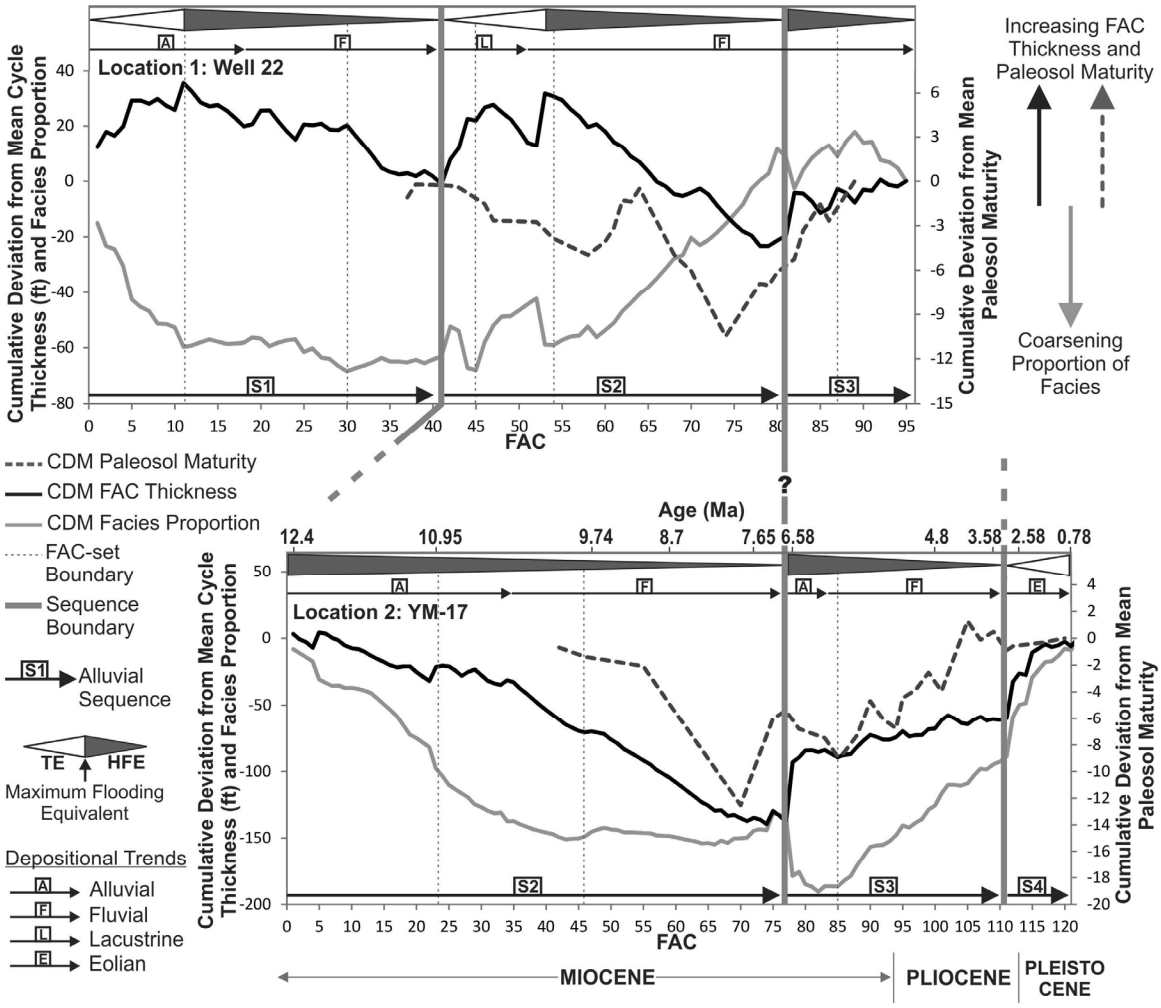

Figure 6. Cumulative deviation from mean (CDM) FAC thickness (bold black line), proportion of facies (bold light gray line), and paleosol maturity (dashed dark gray line) are plotted for both locations. For FAC thickness and paleosol maturity curves, increasing values correspond to increasing thickness/maturity and decreasing trends correspond with decreasing thickness/maturity. For facies proportions, increasing and decreasing trends represent low and high proportions of coarse-grained facies, respectively. Sequences are labeled at the base of each plot with a black arrow and labeled with S1, S2, S3, or S4. TE and HFE are marked with white and dark gray triangles, respectively. Sequence boundaries are designated with thick gray vertical lines and locations are correlated at sequence boundary 2 (SB2). A dashed sequence boundary line means that its position was interpolated. Depositional trends are labeled with arrows just below the systems-tracts (A = alluvial; F = fluvial; L = lacustrine; E = eolian). Sequence boundaries and systems tracts were identified using the methodology from Atchley and others (2004).

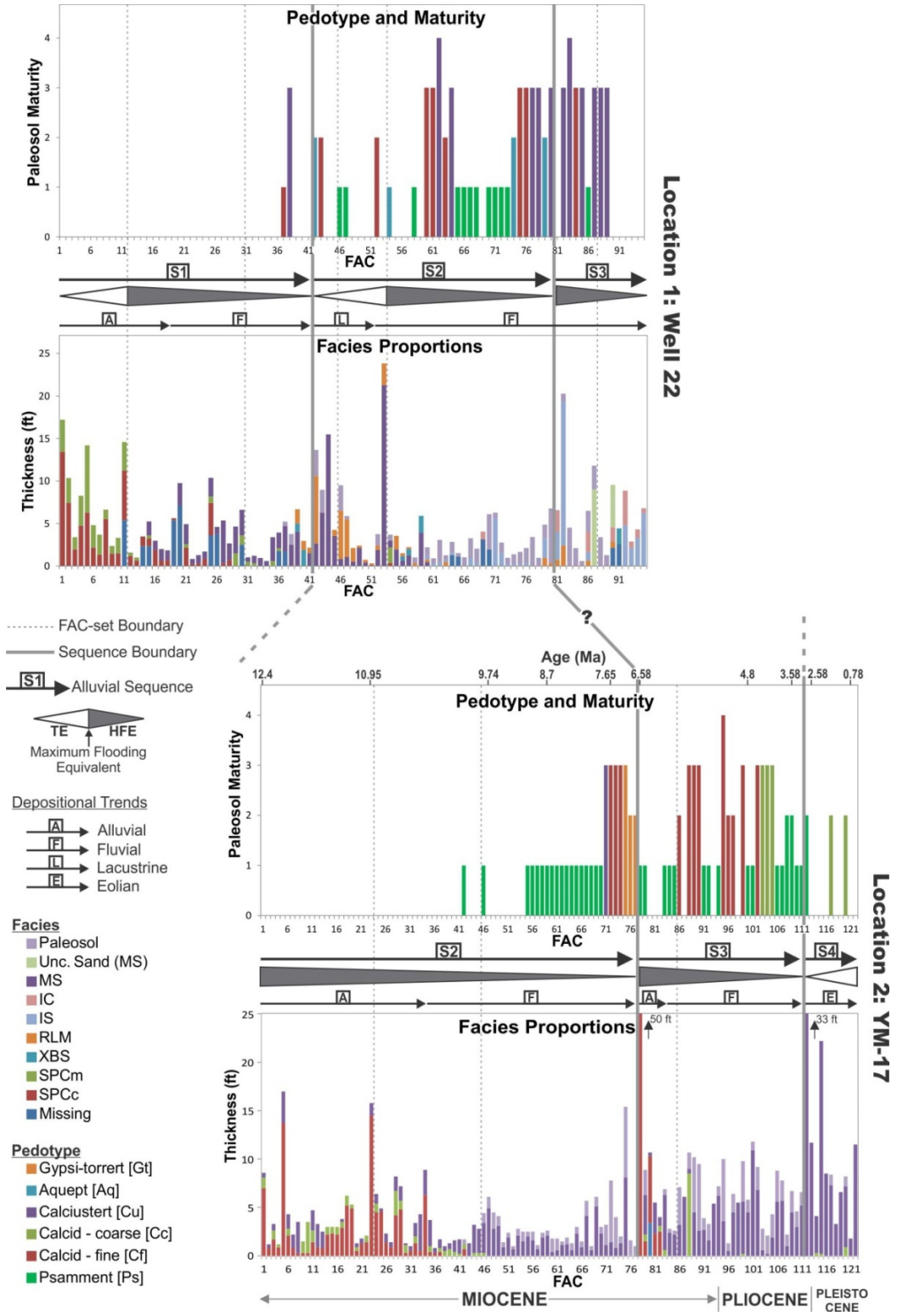

Figure 7. Facies proportions, pedotype, and paleosol maturity histograms for FACs at each location. Depositional trends, sequences, and systems tracts are labeled for each locality. Sequences and systems tracts were identified based on the methodology from Atchley and others (2004).

Potential Sequence-Stratigraphic Correlation

Unlike location 2, location 1 does not have absolute age dates assigned to strata so unequivocal correlation is not possible. However, similarities in long-term trends of FAC thickness, paleosol maturity, and facies proportions are suggestive of equivalence (Figs. 6 and 7). Allogenic processes may produce regionally correlative patterns in sedimentation and pedogenesis (Atchley et al. 2004; Cleveland et al. 2007; Mintz et al. in revision). Thus, the possibility exists that strata at both localities are contemporaneous, at least during the interval of conformable trends.

Sedimentation Rate

The sedimentation rate at location 2 is calculated using the magnetostratigraphic age assignments provided by Langford and others (1999). Sedimentation estimates assume continuous deposition. In reality, the sedimentation rate in a fluvial/alluvial sedimentary system is controlled by rapid deposition during flood events and erosion, non-deposition, or slow deposition during paleosol formation. Initial basin-fill alluvium was deposited at a relatively high rate (2.1 cm/Ky) from about 12 to 10 Ma and then followed by a sudden drop to 0.7 cm/Ky at 9.3 Ma (Figs. 7, 8, and A.2). Paleosol-rich fluvial sandstones deposited from about 10 to 7.5 Ma correspond with low sedimentation rates (~1 cm/Ky; Figs. 7, 8, and A.2). Sedimentation rates gradually increased from 7.5 to 5 Ma and peaked at 2.4 cm/Ky during the deposition of alluvial gravels and subsequent fluvial sands (Fig. 8). At about 5 Ma deposition rates again decreased and remained relatively constant around 1.3 cm/Ky through fluvial and eolian sedimentation of the Plio-Pleistocene (Fig. 8).

No absolute age dates are available for location 1 so detailed sedimentation rates cannot be calculated. However, sequence boundary 2 (SB2) at location 2 is used as a reference point for tentative correlation based on similarities in stacking-pattern trends (Figs. 6 and 7). From this correlation a regional equivalence between the locations is suggested, although not confirmed. "Equivalent" sequences and systems tracts are significantly thinner at location 1, suggesting a lower sedimentation rate (Fig. 6).

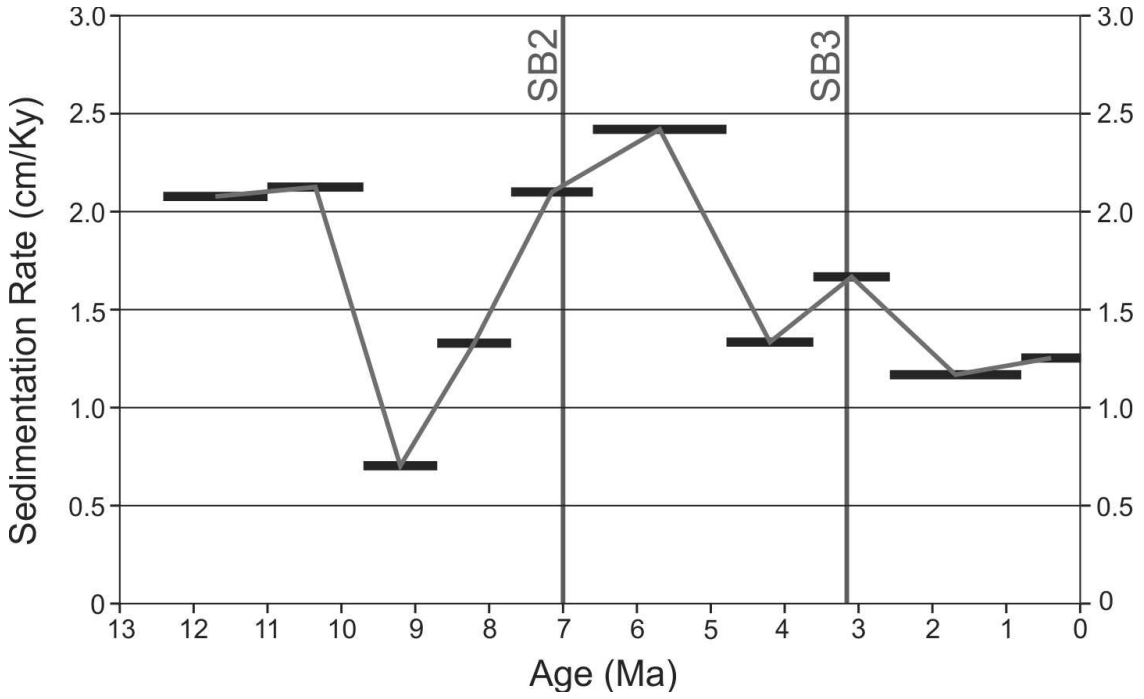

Figure 8. Sedimentation rates from YM-17 (location 2) in cm/Ky were calculated from stratal thicknesses and the absolute age dates of Langford and others (1999).

Alluvial Sequence Stratigraphy

The study interval at location 1 contains 95 FACs that stack into 8 FAC-sets and 3 alluvial sequences through the Fort Hancock Formation (Fig. 6). The facies suggest a variable depositional system through time including alluvial fan, fluvial, and lacustrine processes (Table 1, Figs. 3, 6, and A.1). Thirty-seven paleosols were identified and are

classified as Calciusterts, Aquepts, Calcids (fine), and Psamments with maturity range from 1 to 4 and an average maturity of 2.1 (Table 2, Figs. 4 and 7). Location 2 contains 122 FACs that stack into 6 FAC-sets and 3 alluvial sequences through the Fort Hancock and Camp Rice Formations (Fig. 6). The facies suggest variable trends in depositional style that include alluvial fan, fluvial, and eolian processes (Table 1, Figs. 3, 6, and A.2). Fifty-six paleosols were identified and are classified as Calcids (coarse and fine), Psamments, Gypsitorrerts, and Calciusterts with maturity range from 1 to 4 and an average maturity of 1.7 (Table 2, Figs. 4 and 7).

Sequence 1 (S1) is only present at location 1 where it is bound at the top by sequence boundary 1 (SB1). The underlying sequence boundary is not present. S1 at location 1 has 41 FACs and 3 FAC-sets. The lowest FAC-set has an alluvial fan facies assemblage, thicker than average FACs, coarser than average facies, and is described as occurring within the transgressive equivalent (TE) of S1 (Figs. 6 and A.1). The upper two FAC-sets have a dominantly fluvial facies assemblage, thinner than average FACs, average facies proportion grain-size trend, and are described as occurring within the highstand to falling stage equivalent (HFE) of S1 (Figs. 6 and A.1). Sedimentary structures are rarely preserved due to bioturbation, and pedogenesis is almost completely absent with the exclusion of an Aridisol and a Vertisol (Cf and Cu; average maturity of 2) near the top of S1 (Figs. 7 and A.1).

SB1 is only present at location 1 where it separates the fluvially-dominated HFE of S1 and the lacustrine-dominated TE of sequence 2 (S2). SB1 coincides with the inflection of thinning-upward FACs of S1 and thickening-upward FACs of S2. Paleosol maturity remains relatively uniform below and above SB1, and the grain-size trend of S1 transitions from coarser to finer than average (Figs. 6 and 7).

S2 at location 1 is bound at the base by SB1 and at the top by sequence boundary 2 (SB2) and contains 39 FACs that stack into 3 FAC-sets. The lower two FAC-sets have a lacustrine facies assemblage, thicker than average FACs, finer than average facies proportion trend, lower than average paleosol maturity trend, and are described as the TE of S2 (Figs. 6 and A.1). FACs are lacustrine-dominated, although fluvial sands are also common. Horizontal laminations are observed in lacustrine muds, however, homogenization of the sediment via bioturbation is common. Pedotypes Aq, Cf, and Ps are present and have relatively low maturity values (1 to 2; Fig. 7). The upper FAC-set has a fluvial facies assemblage, thinner than average FACs, finer-grained facies, generally lower than average paleosol maturity, and is the HFE of S2 (Figs. 7 and A.1). FACs are fluvially-dominated, mudrock intraclasts are common within sandstones, and primary sedimentary structures are rarely preserved due to burrowing and rooting. Pedotypes Aq, Cf, Ps, and Cu are present and have highly variable maturities (1-4), although the overall paleosol maturity is lower than average (Figs. 6 and 7).

S2 at location 2 is bound at the top by SB2, but the lower sequence boundary was not penetrated through coring. Seventy-seven FACs stack into 3 FAC-sets with a thinner than average cycle thickness, therefore S2 is described as entirely HFE at location 2 (Fig. 6). The lower two FAC-sets have a dominantly alluvial fan facies assemblage, coarser than average facies, and no sedimentary structures or pedogenic modification is apparent (Figs. 6, 7, and A.2). The upper FAC-set has a fluvial facies assemblage, average to finer than average facies, and a generally lower than average paleosol maturity (Figs. 6 and 7). FACs are fluvially-dominated, with no preserved primary sedimentary structures due to bioturbation. Rooting and pedogenic modification are common, especially near the top of S2, including pedotypes Ps, Cu, Cf, and Gt. Poorly developed Ps (maturity of 1)

paleosols dominate until the upper-most portion of S2, where better developed Cu, Cf, and Gt paleosols (maturity of 2-3) occur (Fig. 7). At both localities, trends in paleosol maturity and FAC thickness reach the lowest recorded value of the entire study interval just prior to SB2 (Fig. 6).

SB2 separates thinning-upward cycles of the S2 HFE and relatively uniform thickness cycles of the sequence 3 (S3) HFE at location 1 and 2. SB2 at location 1 occurs between underlying paleosol-bearing fluvially-dominated FACs of S2 and overlying lacustrine-rich fluvially-dominated FACs of S3 (Figs. 7 and A.1). A higher than average paleosol maturity trend initially decreases across SB2, but overall, maturity increases above SB2 (Figs. 6 and 7). A finer than average facies proportion trend of S2 abruptly changes to a coarser than average trend at SB2 (Fig. 6). SB2 at location 2 separates underlying paleosol-rich fluvially-dominated FACs of S2 and overlying alluvially-dominated FACs of S3 (Figs. 7 and A.2).

S3 at location 1 is bound at the base by SB2 and the upper boundary was not collected during coring. Fifteen FACs stack into 2 FAC-sets, which have a fluvial facies assemblage, average to slightly higher than average FAC thickness, average to coarser than average facies, higher than average paleosol maturity, and are assigned to only HFE (Figs. 6 and 7). Facies are dominated by fluvial sands, although lacustrine mudrocks occur at the base of S3. Sedimentary structures are absent and were likely destroyed by biogenic modification. Paleosols are only present within the lower half of S3. Pedotypes Aq, Cu, and Cf dominate and have moderate to high maturity values (3-4); however, one low maturity (1) Ps is present as well (Figs. 7 and A.1).

S3 at location 2 is bound by SB2 at the base and sequence boundary 3 (SB3) at the top. 34 FACs stack into 2 FAC-sets that have an average to slightly higher than

average FAC thickness trend. S3 is described as HFE (Fig. 7). The lower FAC-set has alluvially-dominated FACs, coarser than average to average facies, and lower than average paleosol maturity (Fig. 6). FACs are initially dominated by poorly-sorted mud-rich gravel (diamict) but fine-upward abruptly into fluvially-dominated FACs (Fig. 7 and A.2). Sedimentary structures are absent and were likely destroyed by bioturbation. Pedotypes Ps and Cf are present, but have very low maturity (1.2 average; Fig. 7). The upper FAC-set has fluvially-dominated FACs, finer than average facies, and sporadic but overall higher than average paleosol maturity. FACs are fluvially-dominated and all sedimentary structures were destroyed by bioturbation. Trends in paleosol development alternate back and forth between low maturity (1-2) Ps and moderate to high maturity (2-4) Cf or Cc (Fig. 7).

SB3 is only present at location 2 where it separates the relatively uniform thickness FACs of the S3 HFE and thickening-upward FACs of sequence 4 (S4). SB3 occurs between paleosol-bearing fluvially-dominated FACs of S3 and eolian-dominated FACs of S4 (Figs. 7 and A.2). Finer than average facies continue across SB3 with no significant change, but paleosol maturity changes from higher than average (S3) to relatively average (S4; Fig. 6).

S4 is only present at location 2 and is bound at the base by SB3. The upper boundary was not sampled during coring. Eleven FACs stack into 1 FAC-set, which has an eolian-dominated thicker than average FACs, finer than average facies, average paleosol maturity, and is described as only TE (Figs. 6 and A.2). Pedogenic modification is low and sedimentary structures were likely destroyed by bioturbation and eolian reworking of sediment. Only 3 weakly developed (maturity of 2) paleosols are present, including pedotypes Ps and Cc (Fig. 7).

Stable Isotopes of Soil Organic Matter and Pedogenic Carbonate

At location 1, 52 samples of bulk soil organic matter (SOM) were analyzed in duplicate for $\delta^{13}C$, and resultant values are relatively consistent through the study interval (average $\delta^{13}C$ of -24.1‰ $\pm$ 0.9‰ relative to VPDB standard) (Fig. 9). Paleotemperature and paleoatmospheric pCO_2 were estimated using the $\delta^{18}O$ and $\delta^{13}C$ values of pedogenic carbonates, respectively (Table 3). Paleotemperature was calculated using equation 1, resulting in an estimated 22.1°C at location 1. Paleoatmospheric pCO_2 was estimated using equation 2 and the resulting concentrations varied from 275 to 1235 ppmV (parts per million by volume). The pCO_2 gradually decreases up-section, with the lowest concentration just below SB2, and rises to the highest concentration just above SB2 (Fig. 9).

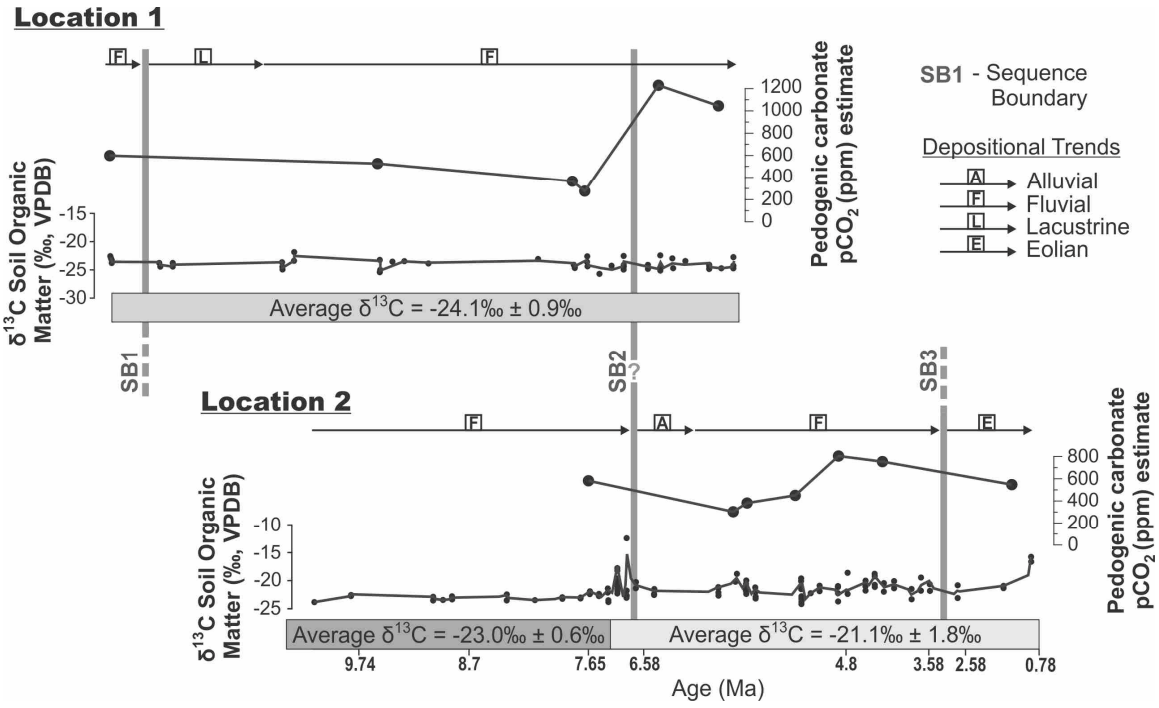

Figure 9. Pedogenic carbonate-derived pCO_2 estimates (from equation 2) and $\delta^{13}C$ values of soil organic matter (SOM) plotted for each location and tentatively correlated at SB2.

Table 3. List of pedogenic carbonate-derived pCO_2 estimates, paleotemperature estimates, and remaining variables used to calculate pCO_2 (equation 2).

Location 1						
Paleosol	**Sz**	**$\delta^{13}C_s$**	**$\delta^{13}C_r$**	**$\delta^{13}C_a$**	**Temp (^{0}C)**	**pCO_2**
W-22-2	1000	-13.1	-22.9	-3.8	22.1	595.4
W-22-8	1000	-13.9	-23.3	-4.2	22.1	526.5
W-22-16	1000	-16.1	-24.4	-5.2	22.1	366.8
W-22-19	1000	-16.3	-23.7	-4.6	22.1	274.5
W-22-22	1000	-12.3	-24.9	-5.6	22.1	1233.0
W-22-24	1000	-12.7	-24.6	-5.4	22.1	1041.4

Location 2						
Paleosol	**Sz**	**$\delta^{13}C_s$**	**$\delta^{13}C_r$**	**$\delta^{13}C_a$**	**Temp (^{0}C)**	**pCO_2**
YM-17-15	1000	-12.8	-22.3	-3.3	24.5	581.6
YM-17-24	1000	-12.4	-19.5	-0.8	24.5	303.1
YM-17-25	1000	-13.1	-21.2	-2.3	24.5	380.5
YM-17-27	1000	-11.7	-19.9	-1.1	24.5	448.3
YM-17-30	1000	-11.4	-22.4	-3.4	24.5	802.4
YM-17-32	1000	-10.5	-20.0	-1.2	24.5	753.5
YM-17-36	1000	-12.0	-21.2	-2.3	24.5	546.3

At location 2, 56 SOM samples were analyzed in duplicate for their $\delta^{13}C$ values, which ranged from about -24 to -12‰ PDB. Depth plots reveal two distinct intervals (Fig. 9). From ~10 Ma to 7.25 Ma the data range from -22.3 to -23.9‰ with an average $\delta^{13}C$ value of -23.0‰ ± 0.61‰, and from ~7.25 to 1 Ma the data range from -12.4 to -24.2‰, with an average $\delta^{13}C$ value of -21.1‰ ± 1.81‰. These two groups of data were analyzed via single-tailed t-test and were determined to be statistically different ($p = 1.7 \times 10^{-12}$).

The $\delta^{13}C$ and $\delta^{18}O$ values of pedogenic carbonates at location 1 provide a paleotemperature estimate of 22.1°C and pCO_2 estimates ranging from 600 to 1230 ppmV (Table 3 and Fig. 9). Paleotemperature at location 2 was estimated at 24.5°C and pCO_2 estimates range from about 300 to 800 ppmV (Table 3 and Fig. 9). An abrupt increase in pCO_2 is apparent adjacent to SB2 at location 1, but is not apparent at location 2, possibly due to the limited availability of pedogenic carbonate samples (Fig. 9). The combined pCO_2 estimates appear to correspond, I a general sense, with trends of global pCO_2; however, the range and amplitudes of the pedogenic carbonate-derived pCO_2 estimates are much higher than the global reconstruction (Fig. 10). This may be due to errors in constraining soil-forming conditions (e.g., soil CO_2 concentration, soil respiration rates, etc.). Recent work on modern soils has greatly improved our understanding of the isotope behavior of carbonates in soil-forming environments (Breecker et al. 2009; Mintz et al. 2011), although more research is needed to constrain these variables.

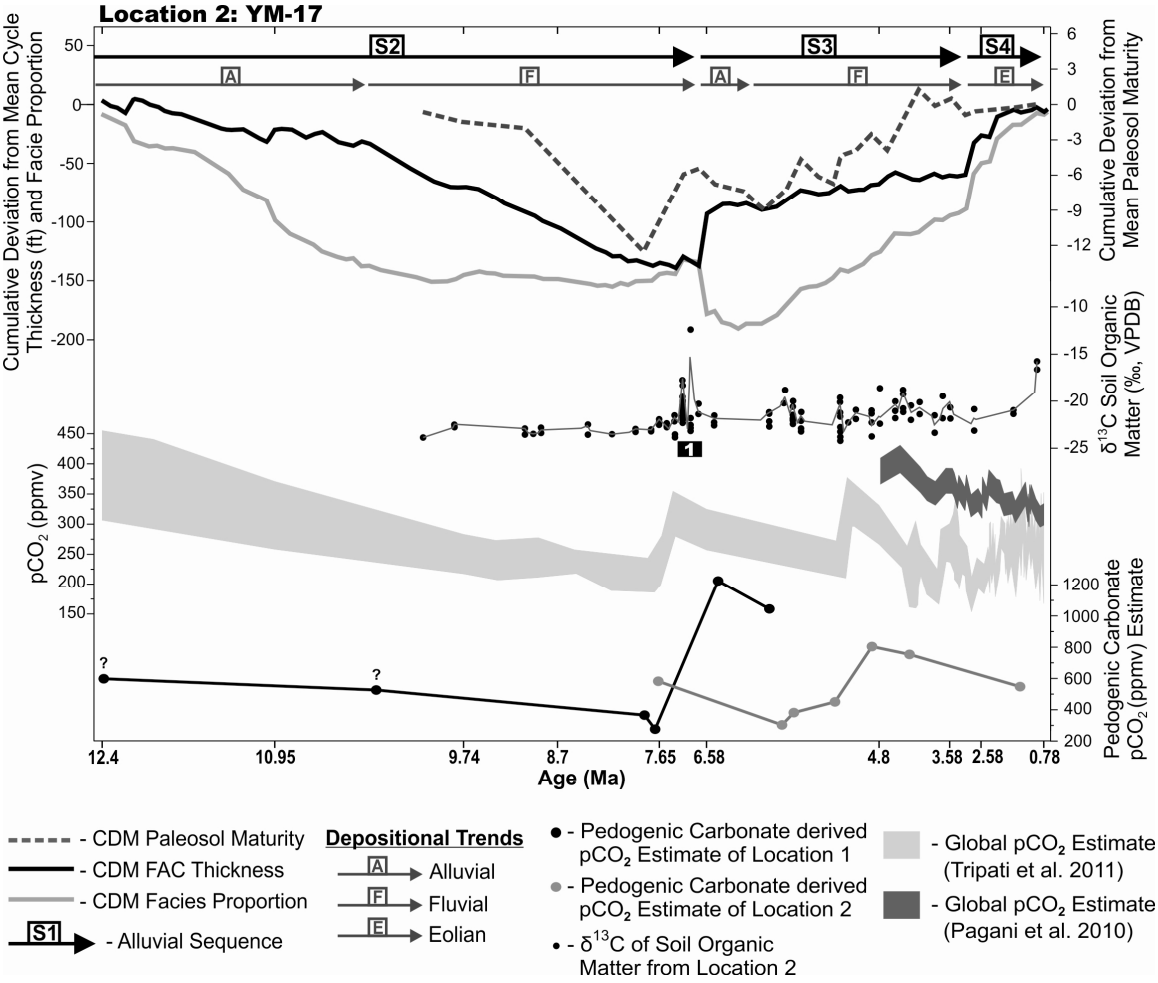

Figure 10. Combined plots of CDM curves from location 2 (see Fig. 6), $\delta^{13}C$ values of soil organic matter from location 2, pedogenic carbonate derived pCO_2 estimates from location 1 (black circles and black line), pedogenic carbonate derived pCO_2 estimates from location 2 (gray circles and gray line), and global pCO_2 reconstructions from alkenone-CO_2 estimates (dark gray; site 925, Pagani et al. 2010) and boron/calcium isotopes of forams (light grey; Tripati et al. 2011). Pedogenic carbonate-derived pCO_2 estimates from location 1 were correlated to the absolute age estimates of location 2 at SB2 (between S2 and S3). Error in correlation increases with distance from the shown correlation point because the sedimentation rate is lower at location 1; thus, the age of the two oldest pCO_2 estimates from location 1 are approximated and marked with "?". Sequences and depositional trends are labeled at the top. The black box labeled "1" marks the onset of C_4 expansion at location 2.

CHAPTER FIVE

Discussion

Discrepancies with Original Alluvial Stacking-Pattern Concepts

Sequence and systems-tract designations are assigned using the original stacking-pattern methodology (see methods section), however, distinct differences are apparent in trends of paleosol maturity. The original model predicts a change from very mature to low-maturity paleosols across sequence boundaries, whereas paleosols in this study appear to increase in maturity or remain relatively stable across sequence boundaries (Fig. 6). Furthermore, paleosol maturity does not decrease with increasing sedimentation/accommodation of the TE, nor increase with decreasing sedimentation/accommodation of the HFE. Contrary to the original alluvial stacking-pattern concepts, increasing paleosol maturity is associated with increasing FAC thickness, and vice versa (Figs. 6 and 7).

Potential Causal Mechanisms

Eustatic Influences

Previous work has identified eustatic fluctuations (Atchley et al. 2004) and regional tectonism (Cleveland et al. 2007; Mintz et al. in revision) as drivers for sequence-scale cyclicity. Atchley and others (2004) conducted their study on a Late Cretaceous-Early Tertiary coastal-plain succession in which sea-level fluctuations were interpreted to have directly affected base level and dynamic equilibrium within the study area. The present study focuses on two rift basins within the craton interior, over 650 km

from the nearest paleocoastline. Therefore, variations in global sea level likely did not have a direct influence on base level, dynamic equilibrium, sedimentation, nor accommodation within the study area.

Tectonic Influences

The southeast Hueco Bolson and northwest Eagle Flat Basin formed from Basin-and-Range extensional tectonism during the Late Cenozoic (Collins and Raney 1994). Langford and others (1999) reported that faulting in the NW Eagle Flat Basin may predate 14 Ma. No evidence was found from seismic or core data to suggest faulting of basin-fill strata (Collins and Raney 1994, Langford et al. 1999). Initial alluvial sedimentation occurred from 12.4 Ma to 10 Ma, possibly during active tectonism (Fig. 6), however, overlying strata show a gradually decreasing piedmont slope up-section (Langford et al. 1999) that suggests tectonic quiescence throughout the remaining history of the basin. Hueco Bolson tectonism began as early as 29 Ma and continues today. Location 1 is positioned on the stable footwall block northeast of the Campo Grande Fault trend and was probably not affected by extensive normal faulting of the Hueco Bolson (Fig. 1). No absolute age dates are available for location 1 so the timing of basin formation within the study area is unknown.

Initial basin-fill stratigraphy at both locations is dominated by thick successions of alluvial conglomerate that fine-upward into fluvial/lacustrine-dominated basins (Figs. 6 and 7). This depositional pattern, in combination with the tectonic history, suggests second- or third-order, tectonically-induced accommodation gain (via rifting). As accommodation was filled, deposition evolved into a relatively lower-gradient depositional system. The occurrence of higher-frequency depositional cycles (e.g.,

sequences) within this longer-period tectonic trend argues for a hierarchy of accommodation periods. Possible higher-frequency mechanisms are evaluated in the following sections.

Climate and Landscape Development

Evidence for climate-driven sequence-scale cyclicity is provided, in part, by discrepancies with prior stacking-pattern analysis records. As discussed above, paleosol maturity does not drastically decrease across sequence boundaries (Fig. 6). Instead, paleosol maturity appears to parallel trends in sedimentation, as shown in Figs. 6 and 8, whereby increasing FAC thickness and sedimentation rate correspond with increasing paleosol maturity, and vice versa. Therefore, sedimentation and paleosol development co-vary, but are inverted from the classic stacking pattern model. This implies that the degree of paleosol development was not influenced by landscape stability and exposure time alone.

The Fort Hancock and Camp Rice Formations were previously interpreted to have been deposited in an arid to semi-arid climate (Gustavson, 1991). Observations from this study support a relatively arid climatic interpretation. Alluvial fan facies may suggest little vegetation covering the landscape (low landscape stability). Evaporite deposits imply occasional flooding events and subsequent evaporation. Thick successions of clay-rich conglomerates (diamicts) are diagnostic of rapid deposition from flooding within an arid climate (flashy flow deposits). Carbonate-rich paleosols, in combination with gypsum-rich Vertisols and calic Aridisols, imply pedogenic modification within a relatively arid climate.

Global pCO_2 reconstructions from the Miocene to Pleistocene were correlated with trends in stacking patterns, $\delta^{13}C$ values of SOM, and pedogenic carbonate-derived pCO_2 estimates (Fig. 10). Figure 10 shows similar patterns between local pCO_2 estimates, global atmospheric CO_2 concentration, and trends in sedimentation and paleosol maturity. Long-term decreasing estimates of pCO_2, from 12.4 to 7.5 Ma, correlate with decreasing FAC thickness and decreasing paleosol maturity (Fig. 10). Abrupt increase in estimated pCO_2 at 7.5 Ma corresponds with the major inflection to increasing FAC thickness, increasing paleosol maturity, SB2 formation, rapid increase in sedimentation rate, deposition of thick successions of diamict (flashy flow deposits), gypsum-bearing paleosols, and the possible onset of C_4 grasses (Figs. 7, 8, 10, and A.2). This pCO_2 "pulse" was followed by multiple episodes of abrupt pCO_2 increases and subsequent more gradual decreases. From 7.5 Ma to 3 Ma, episodic pCO_2 pulses correspond with an interval of sporadic variability in paleosol maturity (Fig. 10). Overall, variability in global pCO_2 concentration appears to have a direct influence on landscape development through time by modifying regional climate and weathering intensity.

Variations in global CO_2 as a driver for sequence-scale trends of sedimentation and paleosol development within an arid environment could be explained by corresponding trends of moisture availability. As atmospheric pCO_2 decreases, global temperatures decrease, global ice volume increases, equatorial evaporation decreases, and moisture is removed from the system. Evidence for this is shown by the eastern Antarctic glacial expansion during the long-term decrease in pCO_2 from about 14 to 10 Ma, following the middle Miocene climatic optimum (Flower and Kennett 1995; Zachos et al. 2001; Tripati et al. 2011). As atmospheric pCO_2 increases, global temperature increases,

glaciers melt, and equatorial evaporation is amplified, increasing atmospheric water vapor on a global-scale. This occurred during the middle Miocene climatic optimum (14-16 Ma) when pCO_2 concentration is estimated to have been at the highest levels in the Neogene and global ice volume was low to absent (Flower and Kennett 1995; Zachos et al. 2001; Tripati et al. 2011). Globally extensive desert formation, eolian deposition, and decreasing vegetation cover during periods of increasing global ice volume suggest that global aridity increases during periods of global cooling (Adams 1997; Zhisheng et al. 1999). In this case, decreasing pCO_2 is associated with increasing global aridity and increasing pCO_2 is associated with increasing global humidity.

This complementary relationship between CO_2 and aridity is archived in trends of paleosol maturity and FAC thickness. During periods of increasing aridity (decreasing pCO_2, 12.4 to 7.5 Ma) the landscape appears to have been relatively static, with low sedimentation rates, sparse vegetation, and weak pedogenesis (Figs. 6 and 10). Increased delivery of moisture (pulses of increased pCO_2, 7.5 to 0.78 Ma) to the area corresponds with flooding and increased sedimentation, as well as increased biological activity, chemical and physical weathering, and high pedogenic modification of the landscape (Figs. 6 and 10). Estimates of pCO_2 show an overall decreasing trend from the middle Miocene to Pleistocene, with pulses of increased CO_2 that occur on a third- to fourth-order scale. These higher-frequency climate pulses are superimposed on longer-period tectonic accommodation gain. Therefore, a composite accommodation history is archived within strata of the southeastern Hueco Bolson and northwestern Eagle Flat Basin.

C_4 Ecosystems and Landscape Development

Although climate may be a driver for depositional cyclicity, the ecology appears to influence deposition as well. The onset of C_4 grasses may have occurred at location 2 at about 7.25 Ma, as suggested by a change in $\delta^{13}C$ values of SOM from relatively constant C_3 values of -23.0‰ ± 0.6‰ PDB, to a more variable range of -21.1‰ ± 1.8‰ PDB (Fig. 9). The timing of potential C_4 expansion at location 2 falls within the same interval as the global record (8-6 Ma; Fig. 11).

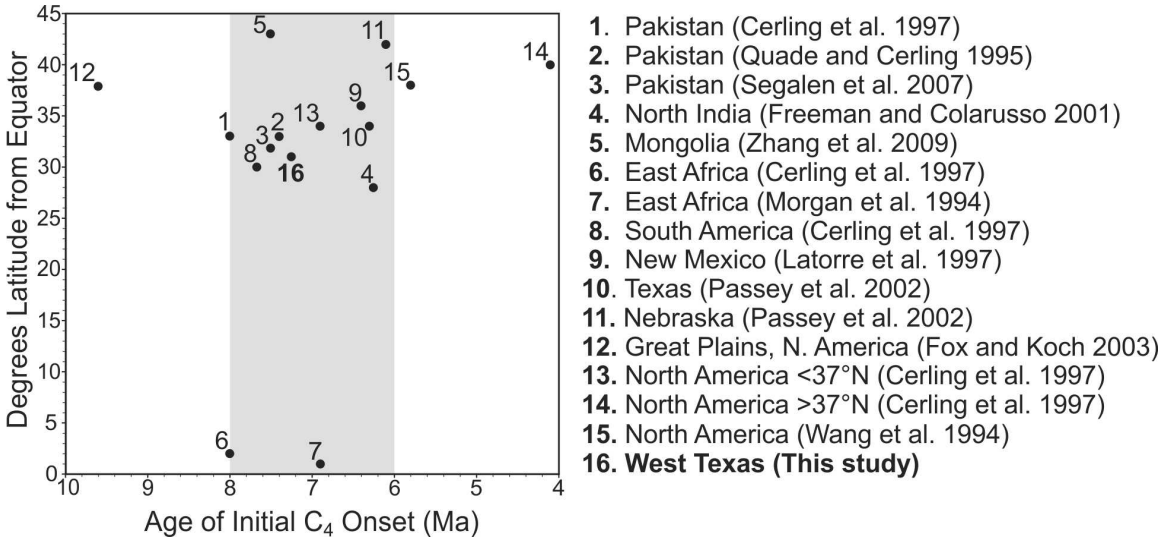

Figure 11. Plot showing the timing of C_4 plant expansion and reconstructed paleolatitude of compiled global data, including this study (**16**). The majority of records report an initial C_4 onset to occur between 8 and 6 Ma (shaded in gray), regardless of latitudinal variability.

Expansion of C_4 grasses may have affected sedimentation and landscape formation at location 2. For example, trends of paleosol maturity and FAC thickness steadily increase and the proportion of facies changes to dominantly fine-grained (MS) following the expansion (Figs. 6 and 7). Sedimentation rate decreases as FAC thickness is increasing, implying that flooding and avulsion events occurred less commonly, but had a higher magnitude when they did occur. C_4 grasses may have filled an ecological

niche within the previously "pure" C_3 environment and promoted increased landscape stability. Increased channel stability, in turn, resulted in reduced avulsion and flooding, and only higher-magnitude flooding events affected the depositional systems.

A shift from weakly developed Entisols (pedotype Ps) to dominantly well-developed Vertisols (pedotype Cu and Gt) and Aridisols (pedotypes Cc and Cf) is contemporaneous with the onset of C_4 grasses at location 2 (Figs. 7 and 10). Whereas the occurrence of well-developed paleosols is attributed to episodic wetting events, the presence of C_4 grasses likely played a role in increased pedogenic modification of the landscape. Grasses have rapid growth rates, deeply penetrating roots, and commonly very high densities, which accelerate chemical and physical weathering and bind the soil. If C_4 grasses did have such an effect on the landscape, modern mixed C_3-C_4 ecosystems should probably not be used as analogs for understanding pre-C_4 sedimentary systems.

C_4 Grasses and Climate

The evolution of C_4 grasses is interpreted to have occurred in the middle Miocene before 12.5 Ma (MacGinitie 1962; Tidwell and Nambudiri 1989), although the majority of records suggest an expansion between 8 and 6 Ma (Fig. 11). Perhaps climate needed to reach a tipping point before C_3 ecosystems were outcompeted by C_4 grasses. Previous research suggested that C_4 plants can outcompete C_3 plants when pCO_2 decreases below a threshold of 400 ± 100 ppmV in low- to mid-latitudes (Cerling et al. 1997; Ehleringer et al. 1997). According to global pCO_2 estimates (Tripati et al. 2011), this threshold was crossed about ~5 Ma before the global expansion of C_4 grasses (Fig. 10). Furthermore, a rapid increase in atmospheric pCO_2 occurred in unison with the putative C_4 expansion at location 2 (~7.5 Ma) and the vast majority of other global records (Figs. 10 and 11).

These records suggest that CO_2 starvation of C_3 plants was not the only driver for C_4 expansion. Decreasing pCO_2 likely influenced C_4 plant evolution (Cerling et al. 1997; Ehleringer et al. 1997), but a global shift to C_4 dominated ecosystems may have also been influenced by abrupt climate change, extensive flooding, and ecosystem disruption associated with rapidly increasing pCO_2.

Some studies report an asynchronous C_4 expansion to the globally established 8 to 6 Ma range (Cerling et al. 1997; Fox and Koch 2003; Sanyal et al., 2010). Cerling and others (1997) suggested an initial onset in equatorial regions, followed by a gradual expansion into higher latitudes; however, a compilation of 16 datasets from varying latitudes show no such trend (Fig. 11; Morgan et al. 1994; Quade and Cerling 1995; Cerling et al. 1997; Latorre et al. 1997; Freeman and Calarusso 2001; Passey et al. 2002; Fox and Koch 2003; Ségalen et al. 2007; Zhang et al. 2009). Sanyal and others (2010) reported a 3 My difference in timing of C_4 expansion between sites less than 200 km apart, in northern India. This asynchronous expansion is attributed to local climate (Indian monsoon) and habitat disturbance overriding global drivers of C_4 onset (Sanyal et al. 2010).

Location 1 does not show evidence for a shift to a C_4 ecosystem (Fig. 9). This may be attributable to either an incorrect time-stratigraphic correlation or to significant differences in environmental conditions between the Eagle Flat Basin and Hueco Bolson. Location 1 shows evidence for common flooding events and consistently moister conditions than location 2, including lacustrine deposits, poorly drained Aquepts and hydromorphic Usterts, more mature paleosols, and an assemblage of pedotypes that typically reflect poor drainage (Figs. 7, A.1, and A.2). Perhaps episodic flooding (via the ancestral Rio Grande) superseded climatic effects and their control on C_4 grass expansion

within the SE Hueco Bolson. If this hypothesis is correct, then the data presented here suggest that asynchronous C_4 expansion is likely related to site-specific environmental conditions, as proposed by Sanyal and others (2010). Absolute age dates for location 1 strata are needed to confirm this.

CHAPTER SIX

Conclusions

1) Patterns in sedimentation and pedogenesis within the SE Hueco Bolson and NW Eagle Flat Basin are found to have a cyclic stratal hierarchy. Alluvial stacking-pattern analysis reveals long-term trends in cycle thickness, paleosol maturity, and facies proportions that allow sequence stratigraphic interpretation.
    a. Location 1 contains 95 FACs that stack into 8 FAC-sets and 3 alluvial sequences and location 2 contains 122 FACs that stack into 6 FAC-sets and 3 alluvial sequences.
    b. Based on significantly similar stacking-pattern trends, absolute ages of strata at location 2 are tentatively correlated to undated strata of location 1 using sequence boundary 2 as a correlation point. This correlation is not absolute but substantial evidence is presented to allow for sequence-stratigraphic correlation.
2) The climate of west Texas during the Neogene is interpreted as arid to semi-arid as suggested by sedimentology, inferred depositional style, pedogenic features, and distribution of pedotypes and paleosol maturity. Additionally, atmospheric pCO_2 gradually decreased through the Neogene and suggests increasing global aridity (Tripati et al. 2011).
3) Tectonism is interpreted to have produced second- and/or third-order accommodation gain that was filled by an overall fining-upward alluvial record within the SE Hueco Bolson and NW Eagle Flat Basin.

4) Higher-frequency cycles of fluvial and lacustrine sedimentation and associated pedogenesis are superimposed onto the overall fining-upward tectonic fill succession. Stacking-pattern trends of FAC thickness, proportion of facies, and paleosol maturity correlate well with global pCO_2 concentrations, suggesting that sequence-scale trends in sedimentation and pedogenesis are controlled by long-term (perhaps third- and/or fourth-order) climate cycles.
5) The expansion of C_4 grasses is interpreted to occur at location 2 at about 7.25 Ma.
    a. Following the onset of C_4 grasses, decreased sedimentation rate corresponded with increased FAC thickness, and suggests that flooding and avulsion events occurred less often and only in conjunction with higher-magnitude floods. Therefore, C_4 grass expansion may have assisted in stabilizing landscapes of west Texas.
    b. Paleosol development increased following the onset of C_4 grasses and may be attributed to the rapid growth rate, deeply penetrating roots, and high density roots of C_4 grasses, as well as decreased sedimentation rate.
6) A rapid increase in pCO_2 occurred in unison with C_4 expansion at location 2 and the majority of other records across the globe (~7.5 Ma). Abrupt climate change and habitat disturbance associated with the rapid increase in pCO_2 may be a driver for the global shift to C_4-dominated ecosystems.
7) The onset of C_4 ecosystems does not occur within the study interval at location 1. This may be due to incorrect correlation, or local conditions that inhibited the expansion of C_4 grasses within the SE Hueco Bolson.

a. Data presented in this study (and an analog study in a monsoonal climate) suggest that asynchronous C_4 expansion is caused by site-specific climatic and landscape conditions.

b. Location 1 shows evidence for common flooding and consistently moister conditions than location 2. Episodic flooding from the ancestral Rio Grande may have superseded climatic effects and their control on C_4 expansion within the SE Hueco Bolson. Absolute ages for location 1 strata are needed to evaluate this possibility.

APPENDICES

APPENDIX A

Stratigraphic Sections

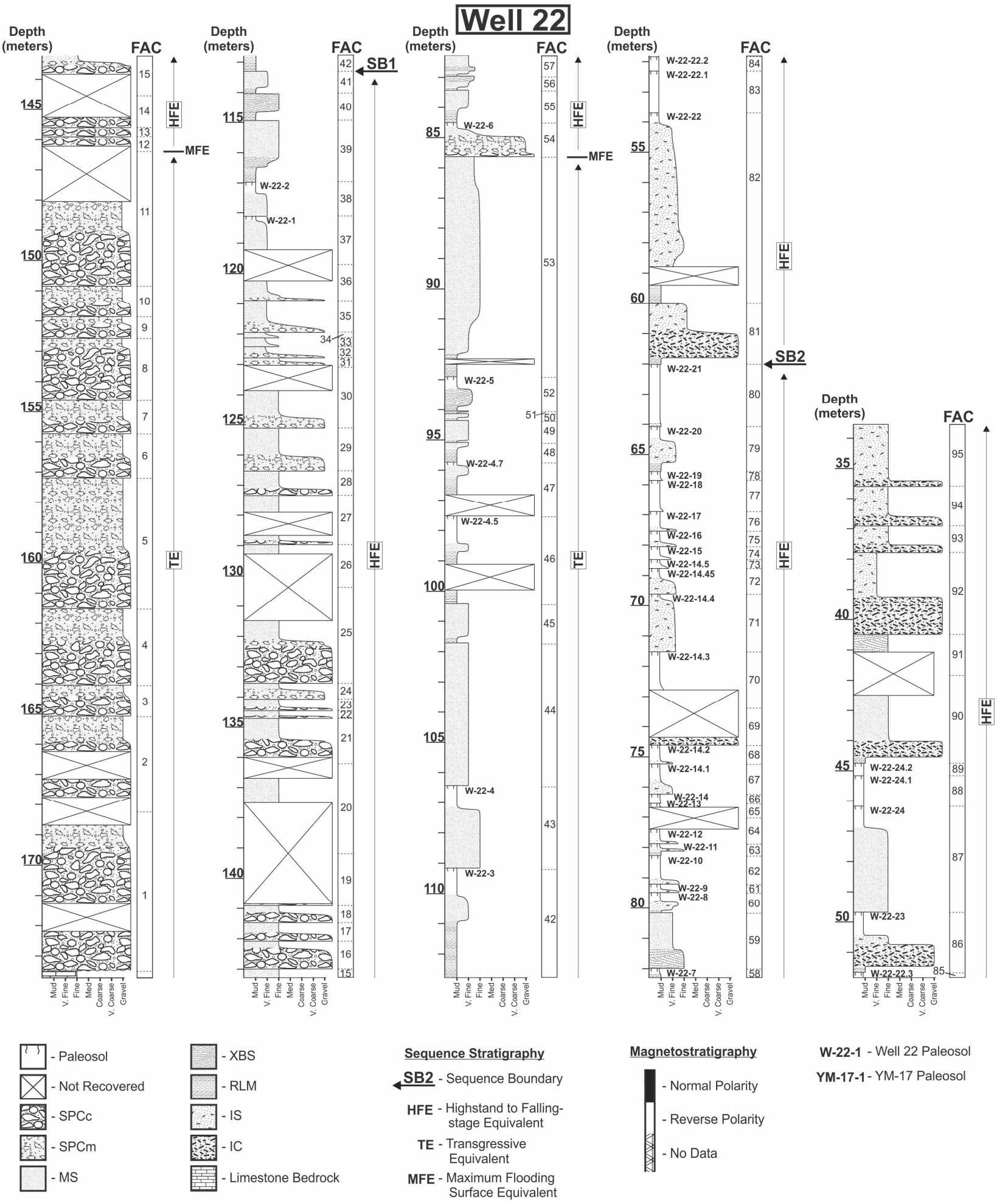

Figure A.1. Stratigraphic section of Well 22 (location 1) from the SE Hueco Bolson. Labeled immediately to the right of the graphical measured section is the fluvial aggradational cycle (FAC) number (from 1 to 95). To the right of the FAC numbers are identified sequence boundaries (sequence 1 is below SB1, sequence 2 is below SB2 and above SB1, etc.) and intra-sequence systems tracts. Small bold labels within the graphical section are paleosols (e.g., W-22-1). Fill patterns within the graphical stratigraphic section represent individual facies and their associated sedimentary structures. For detailed facies distributions and pedotype classification, distribution, and maturity refer to Figure 7. For detailed sequence-stratigraphic interpretations, depositional trends, distribution of FAC-sets, and trends in paleosol maturity, FAC thickness, and grain-size refer to Figure 6.

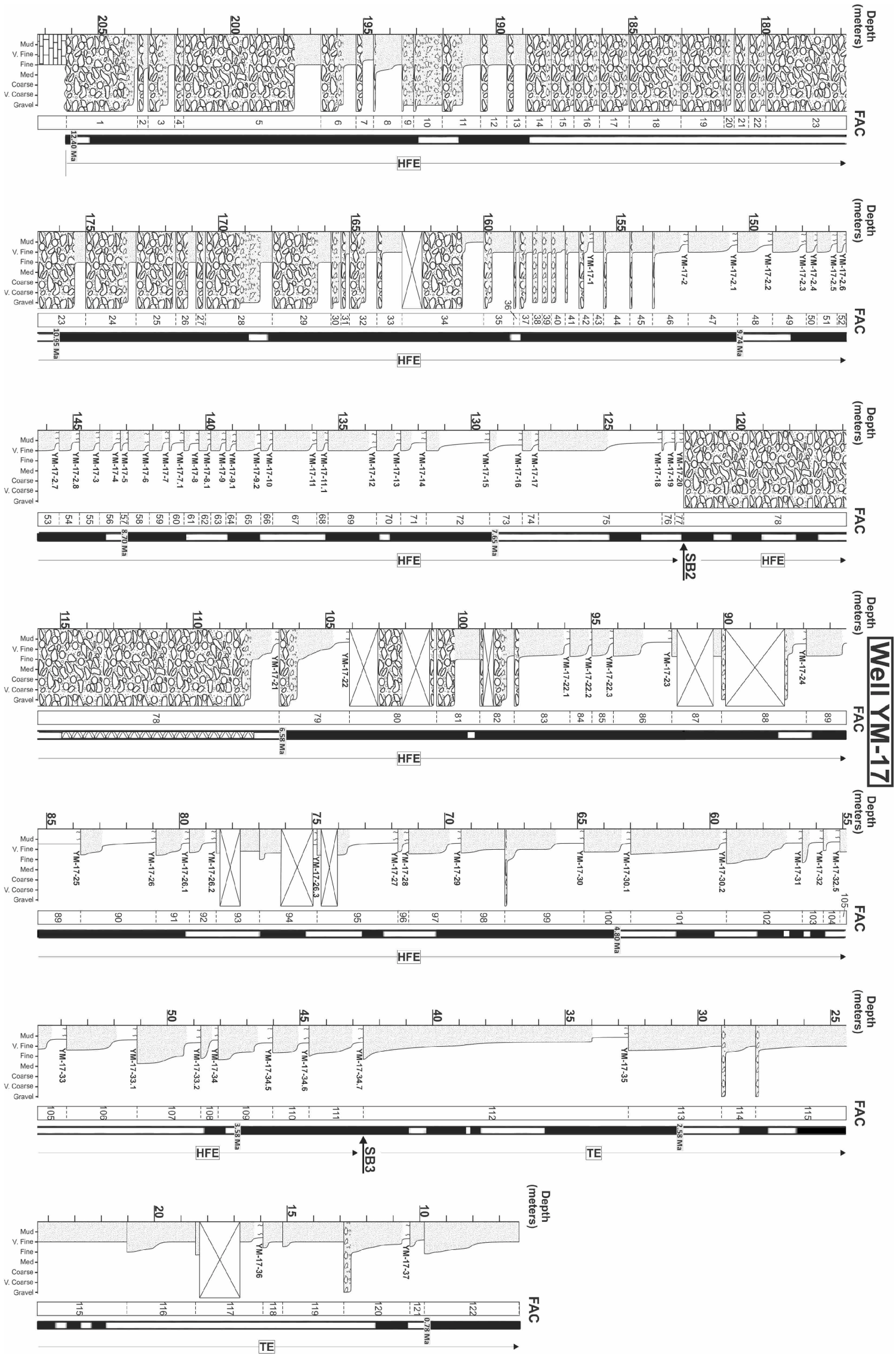

Figure A.2. Stratigraphic section of YM-17 (location 2) from the NW Eagle Flat Basin. The legend is located in Figure A.1. Labeled immediately to the right of the graphical measured section is the fluvial aggradational cycle (FAC) number (from 1 to 122). To the right of the FAC numbers is the magnetostratigraphy and absolute ages from Langford and others (1999). To the right of magnetostratigraphy are identified sequence boundaries (sequence 1 is below SB1, sequence 2 is below SB2 and above SB1, etc.) and intra-sequence systems tracts. Small bold labels within the graphical section are paleosols (e.g. YM-17-1). Fill patterns within the graphical stratigraphic section represent individual facies and their associated sedimentary structures. For detailed facies distributions and pedotype classification, distribution, and maturity refer to Figure 7. For detailed sequence-stratigraphic interpretations, depositional trends, distribution of FAC-sets, and trends in paleosol maturity, FAC thickness, and grain-size refer to Figure 6.

APPENDIX B

Core Description Logs

Symbols

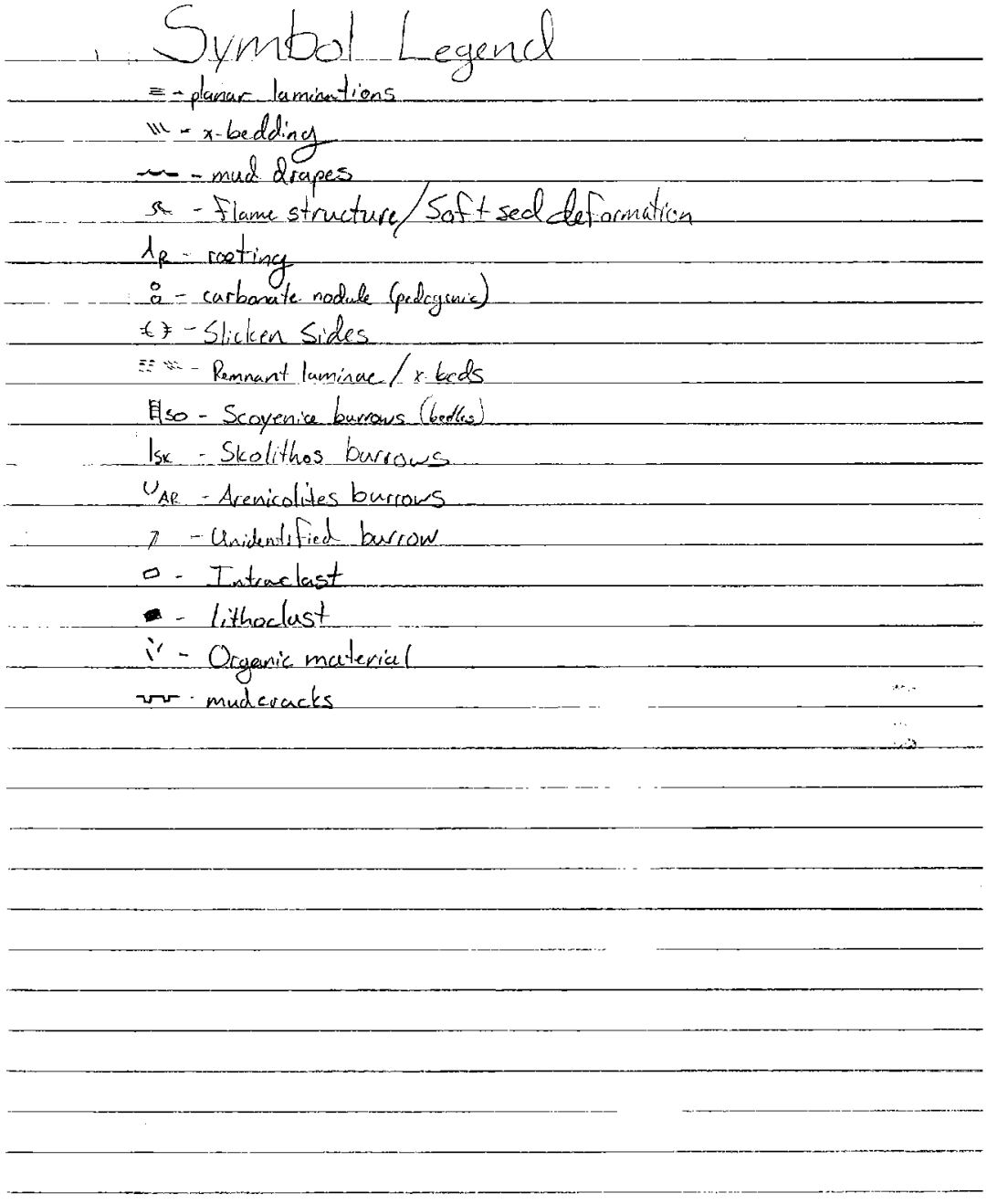

Well YM-17

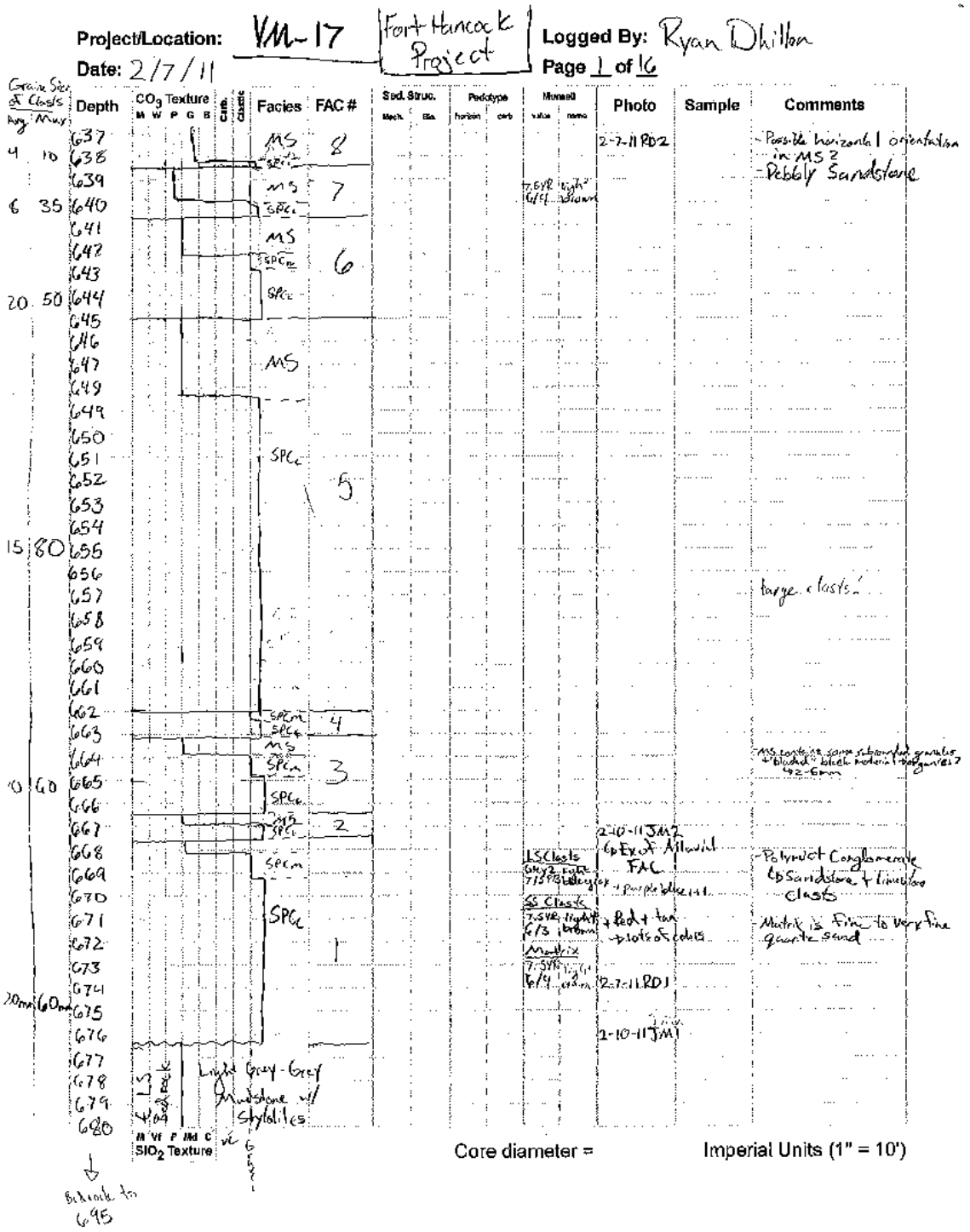
Project/Location: YM-17 Fort Hancock Project
Logged By: Ryan Dhillon
Date: 2/7/11
Page 1 of 16
Depth
Facies
FAC #
Photo
Sample
Comments
Core diameter =
Imperial Units (1" = 10')

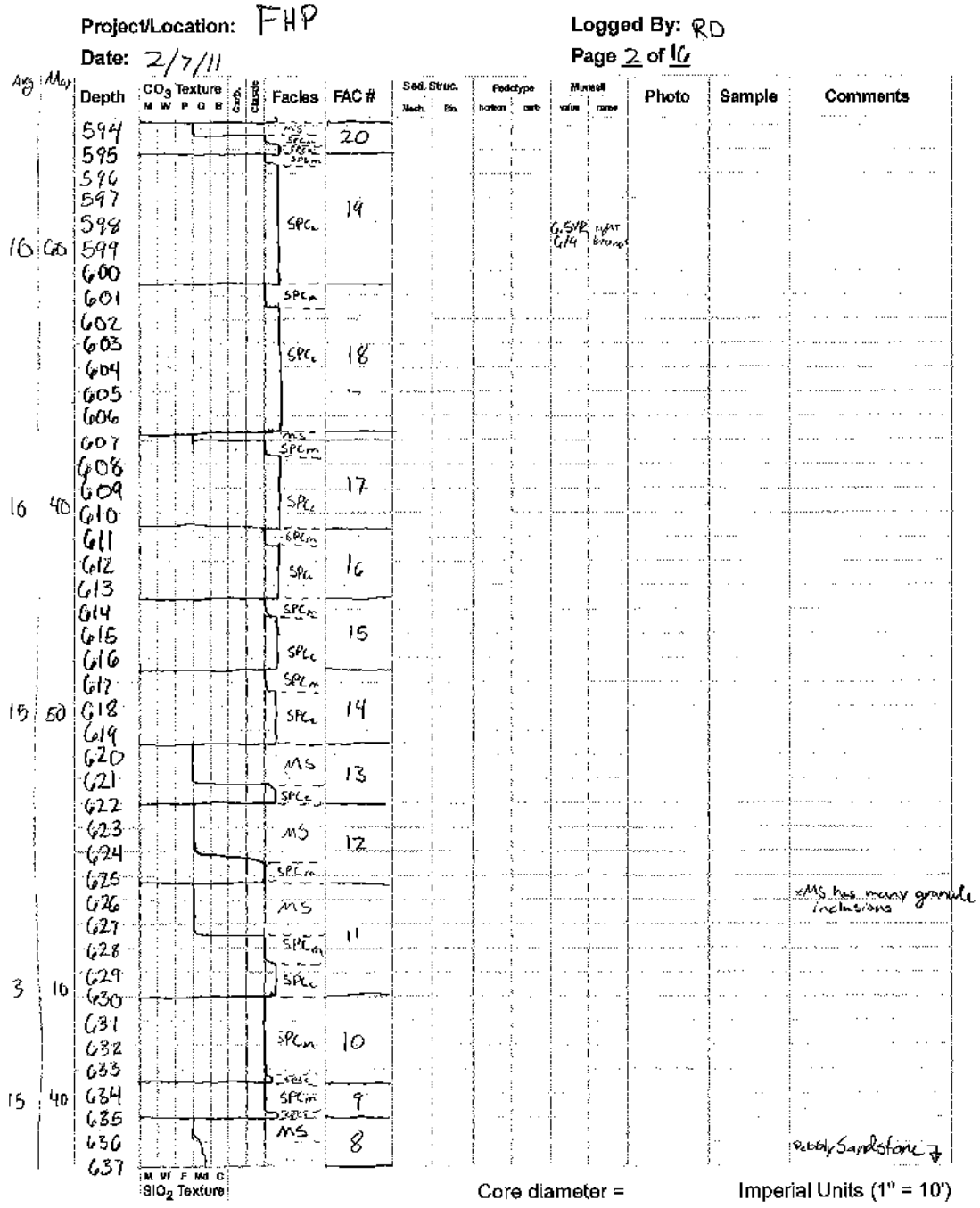
Project/Location: FHP
Logged By: RD
Date: 2/7/11
Page 2 of 16
Depth
CO3 Texture
Facies
FAC #
Sed. Struc.
Pedotype
Munsell
Photo
Sample
Comments
SiO2 Texture
Core diameter =
Imperial Units (1" = 10')
xMS has many granule inclusions
Pebbly Sandstone

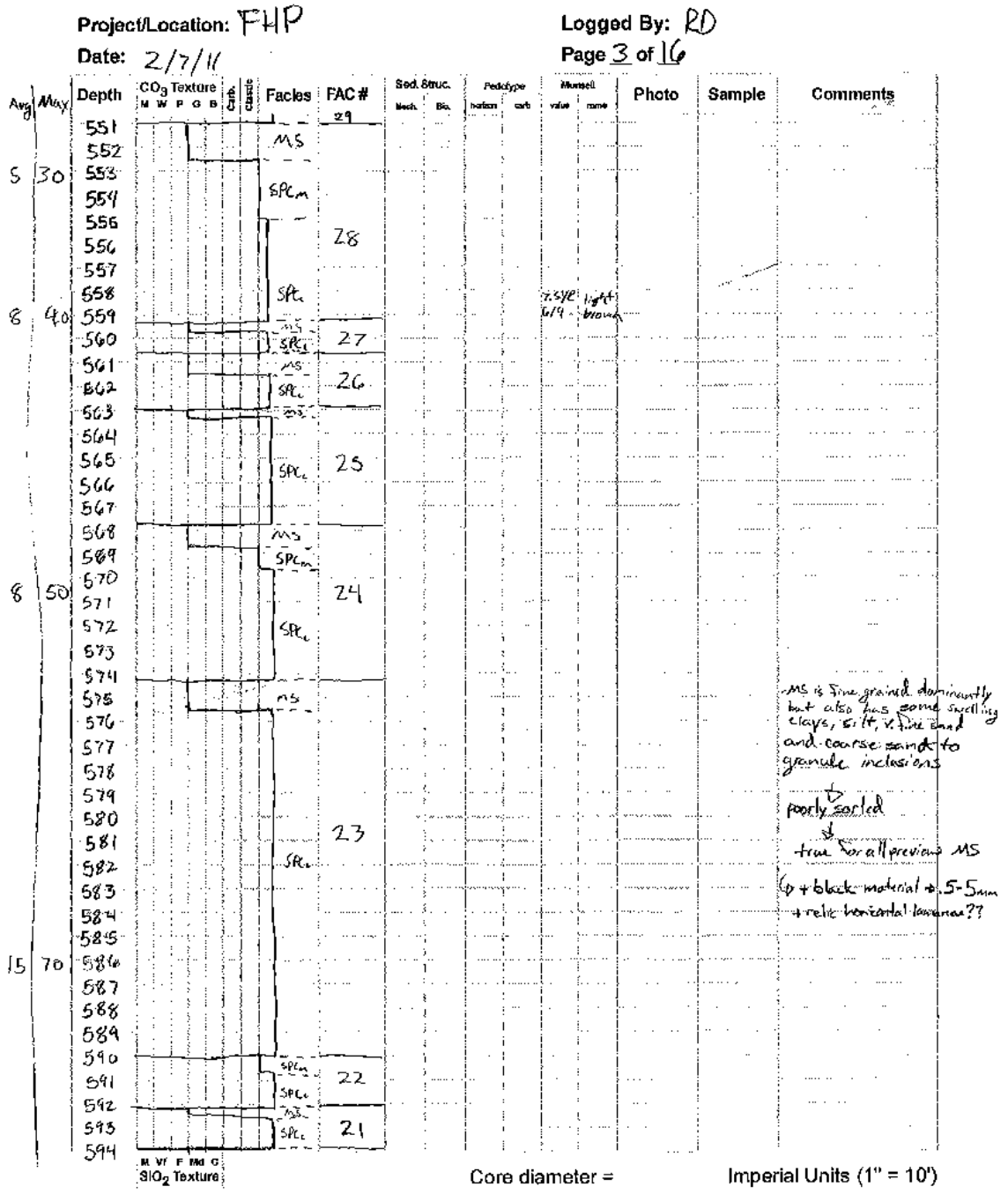
Project/Location: FHP
Logged By: RD
Date: 2/7/11
Page 3 of 16
Depth
Facies
FAC #
Sed. Struc.
Peddype
Munsell
Photo
Sample
Comments
MS
SPCm
SPCc
28
27
26
25
24
23
22
21
MS is fine grained dominantly but also has some swelling clays, silt, v. fine sand and coarse sand to granule inclusions
poorly sorted
true for all previous MS
+ black material ~.5-5mm
+ relic horizontal laminae??
Core diameter =
Imperial Units (1" = 10')

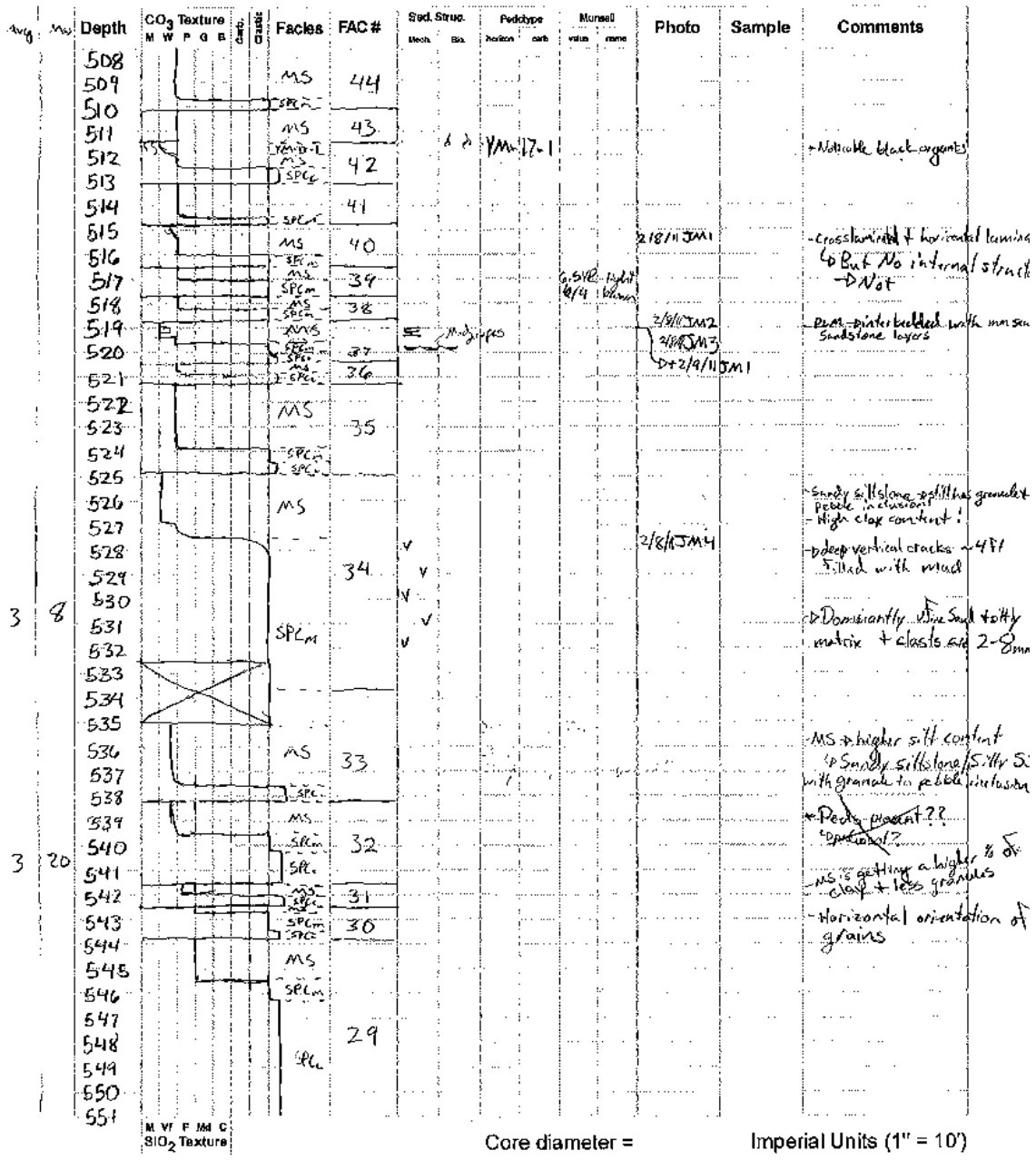
Project/Location: FHP
Logged By: RD
Date: 2/7/11
Page 4 of 16
Depth
Facies
FAC #
Sed. Struc.
Peddype
Munsell
Photo
Sample
Comments
Core diameter =
Imperial Units (1" = 10')

Project/Location: FHP

Logged By: RD

Date: 2/8/11

Page 5 of 16

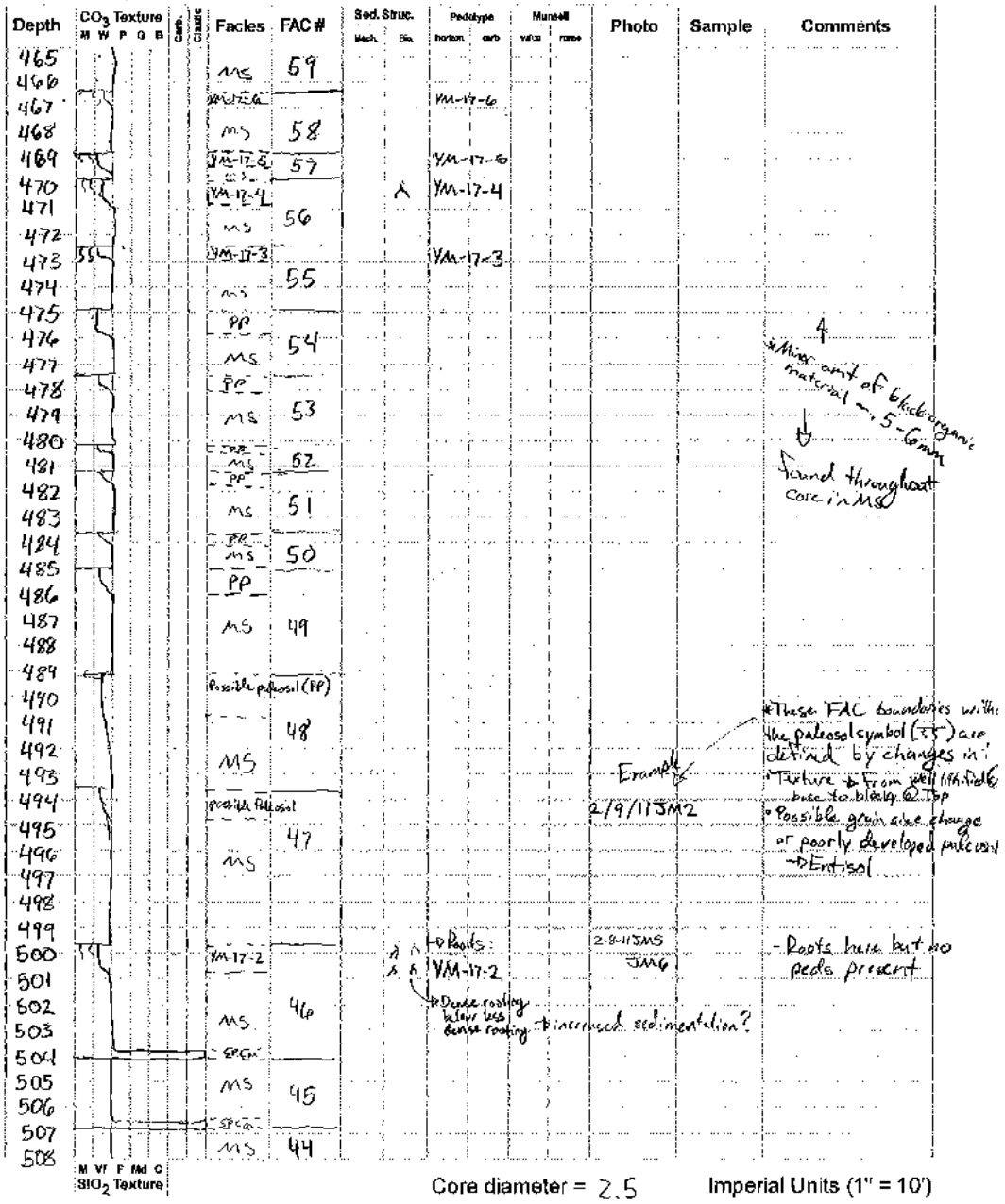

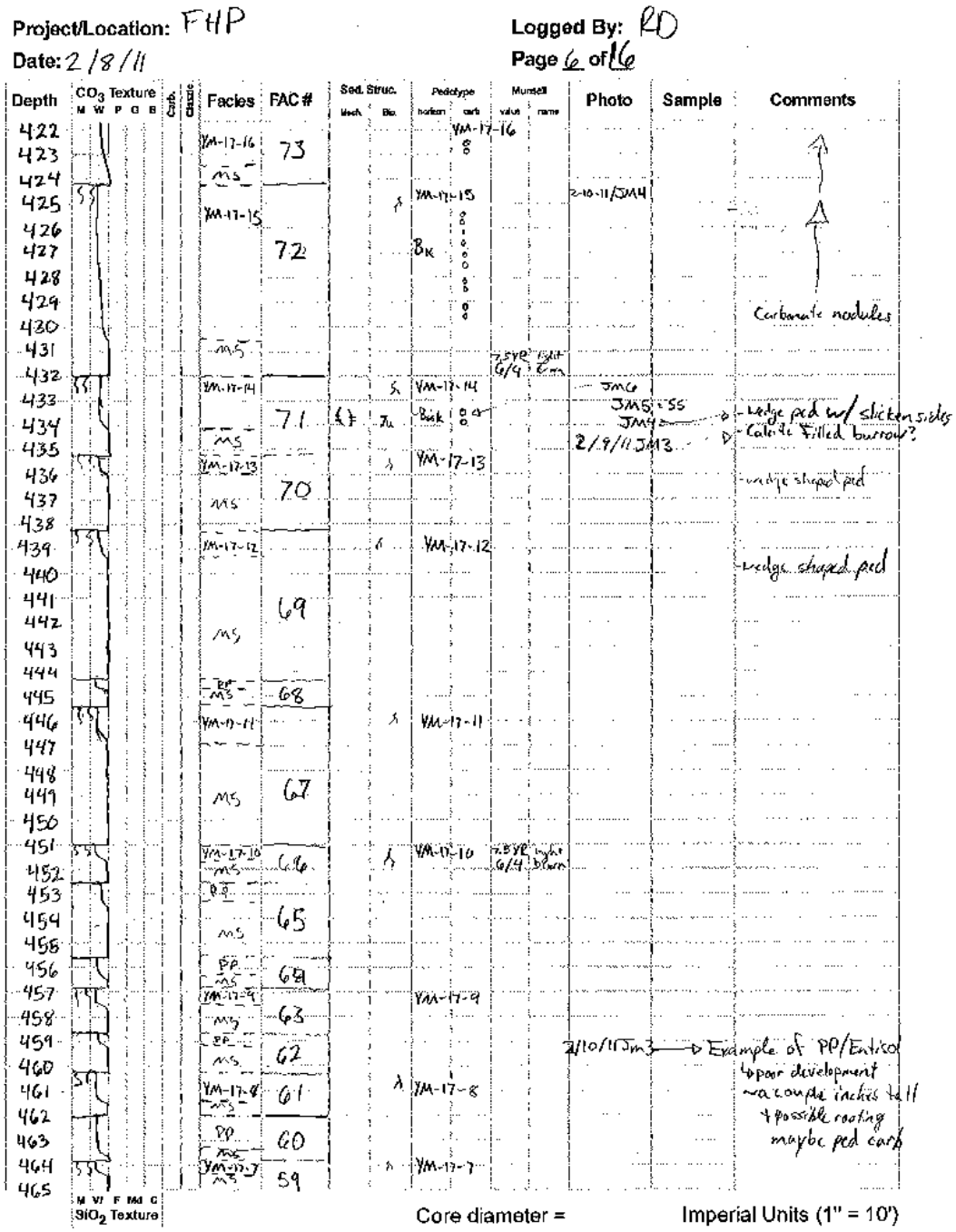
Project/Location: FHP
Logged By: RD
Date: 2/8/11
Page 6 of 16
Depth
CO3 Texture
M W P G B
Carb. Clastic
Facies
FAC #
Sed. Struc.
Mech
Bio
Pedotype
horizon
carb
Munsell
value
name
Photo
Sample
Comments
422
423
424
425
426
427
428
429
430
431
432
433
434
435
436
437
438
439
440
441
442
443
444
445
446
447
448
449
450
451
452
453
454
455
456
457
458
459
460
461
462
463
464
465
YM-17-16
MS
YM-17-15
MS
YM-17-14
MS
YM-17-13
MS
YM-17-12
MS
PP
MS
YM-17-11
MS
YM-17-10
MS
PP
MS
PP
MS
YM-17-9
MS
PP
MS
YM-17-8
MS
PP
MS
YM-17-7
MS
73
72
71
70
69
68
67
66
65
64
63
62
61
60
59
YM-17-16
YM-17-15
Bk
YM-17-14
Bwk
YM-17-13
YM-17-12
YM-17-11
YM-17-10
YM-17-9
YM-17-8
YM-17-7
7.5YR 6/4 light brown
2-10-11/JM4
JM6
JM5
JM4
2/9/11 JM3
Carbonate nodules
- ledge ped w/ slickensides
- Calcite filled burrow?
- wedge shaped ped
- wedge shaped ped
2/10/11 Jm3 → Example of PP/Entisol
- poor development
- ~a couple inches tall
+ possible rooting
maybe ped carb
M VF F Md C
SiO2 Texture
Core diameter =
Imperial Units (1" = 10')

Project/Location: FHP **Logged By:** RD

Date: 2/8/11 **Page** 7 **of** 16

Depth	CO_3 Texture (M W P G B) / Carb. / Clastic	Facies	FAC #	Sed. Struc. (Mech. / Bio.)	Pedotype horizon	Pedotype carb	Munsell value	Munsell name	Photo	Sample	Comments
379	"Washed Out"										
380											
381											
382											
383											
384							5YR 7/6	Reddish Yellow			
385											
386	Gm Se = granules										
387			78								
388	to pebbles										↑
389	up to 150mm										
390											* Muddy matrix supporting gravel
391		SPCc									
392											↳ diamict
393									2-10-11-JM8		
394											↑ Not well lithified
395											
396											↓ Conglomerate is very well lithified.
397											
398											↳ calcified? reacts w/ HCl
399											
400											
401		YM-17-20	77		YM-17-20				2-10-11 JM5 JM6 JM7		
402		YM-17-19	76		YM-17-19						
403							2.5YR 8/2	Pinkish White			
404		YM-17-18			YM-17-18						
405											
406											Heavily slicked, blocky peds
407									2-8-11 JM7		↳ slicked surface is covered in gypsum??
408											
409											↳ very smooth + waxy
410			75				5YR 6/4	light red-brown			
411											
412											
413		MS									
414											slickensides present
415											
416											
417											
418									Rooting		
419		YM-17-17 MS	74		YM-17-17				→ 2/9/11 JM7		heavily rooted ↳ Manganese halos
420											
421		YM-17-16	73		YM-17-16						
422					Bk						

M VF F Md C
SIO_2 Texture

Core diameter =

Imperial Units (1" = 10')

Project/Location: FHP

Logged By: RD

Date: 2/8/11

Page 8 of 16

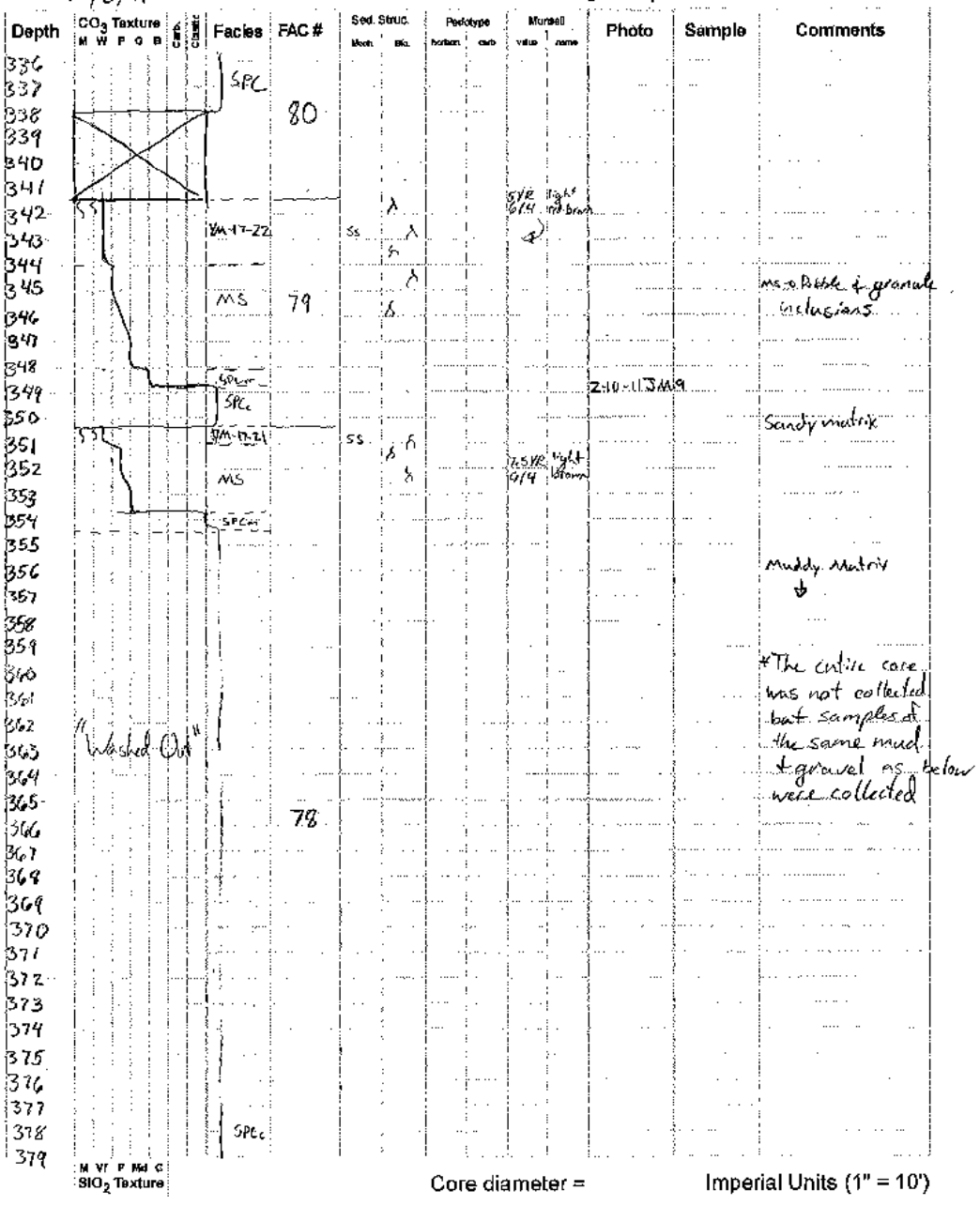

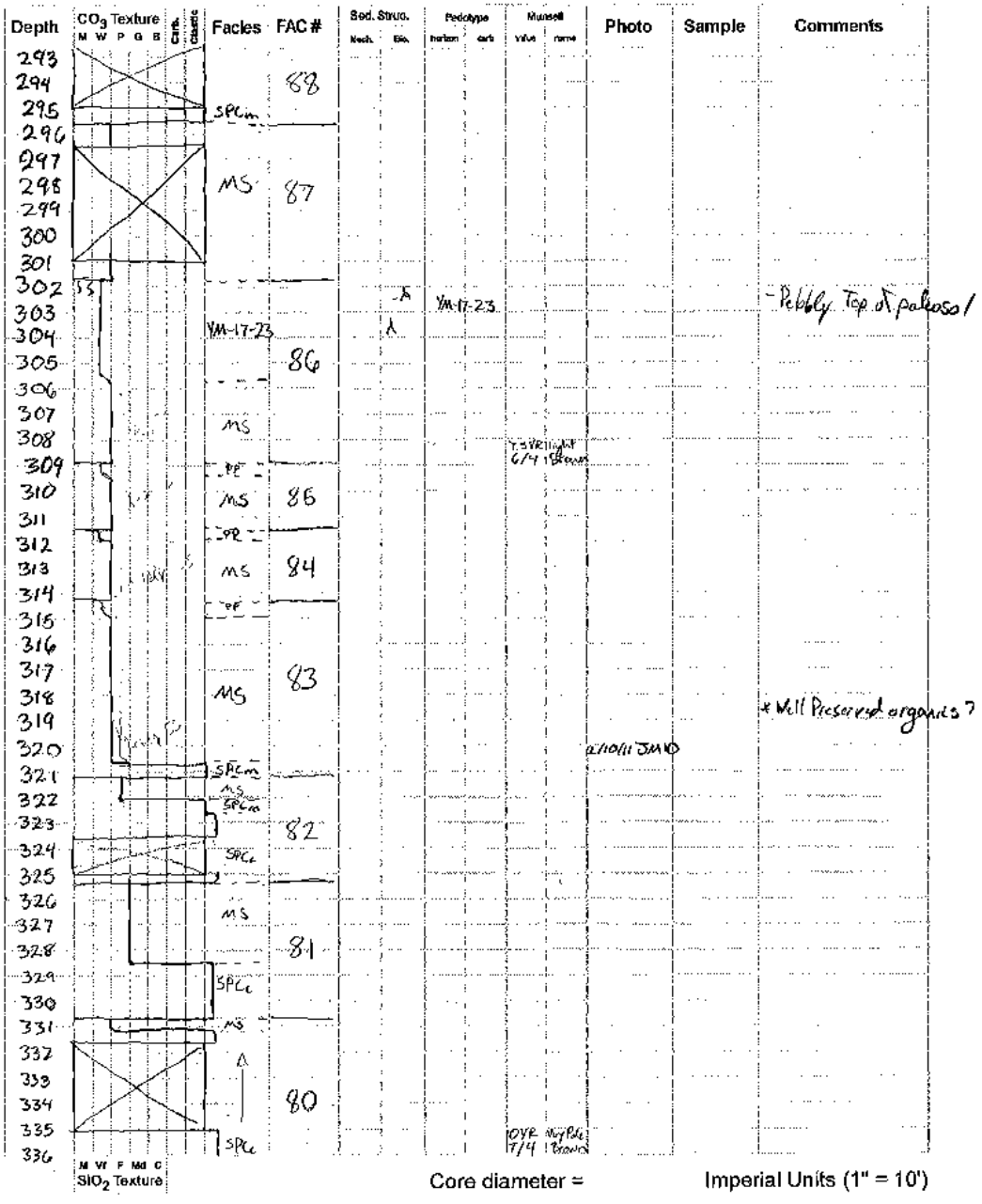
Project/Location: FHP
Logged By: RD
Date: 2/9/11
Page 9 of 16
Depth
CO3 Texture
M W P G B Carb. Clastic
Facies
FAC #
Sed. Struc.
Bioturb.
Pedotype
horizon
carb
Munsell
value
rome
Photo
Sample
Comments
293
294
295
296
297
298
299
300
301
302
303
304
305
306
307
308
309
310
311
312
313
314
315
316
317
318
319
320
321
322
323
324
325
326
327
328
329
330
331
332
333
334
335
336
SPCm
88
MS
87
YM-17-23
86
MS
PF
MS
86
PR
MS
84
PF
MS
83
SPCm
MS
SPCm
82
SPCc
MS
81
SPCc
MS
80
SPCc
- Pebbly Top of paleosol
* Well Preserved organics ?
2/10/11 JM
M Vf F Md C
SiO2 Texture
Core diameter =
Imperial Units (1" = 10')

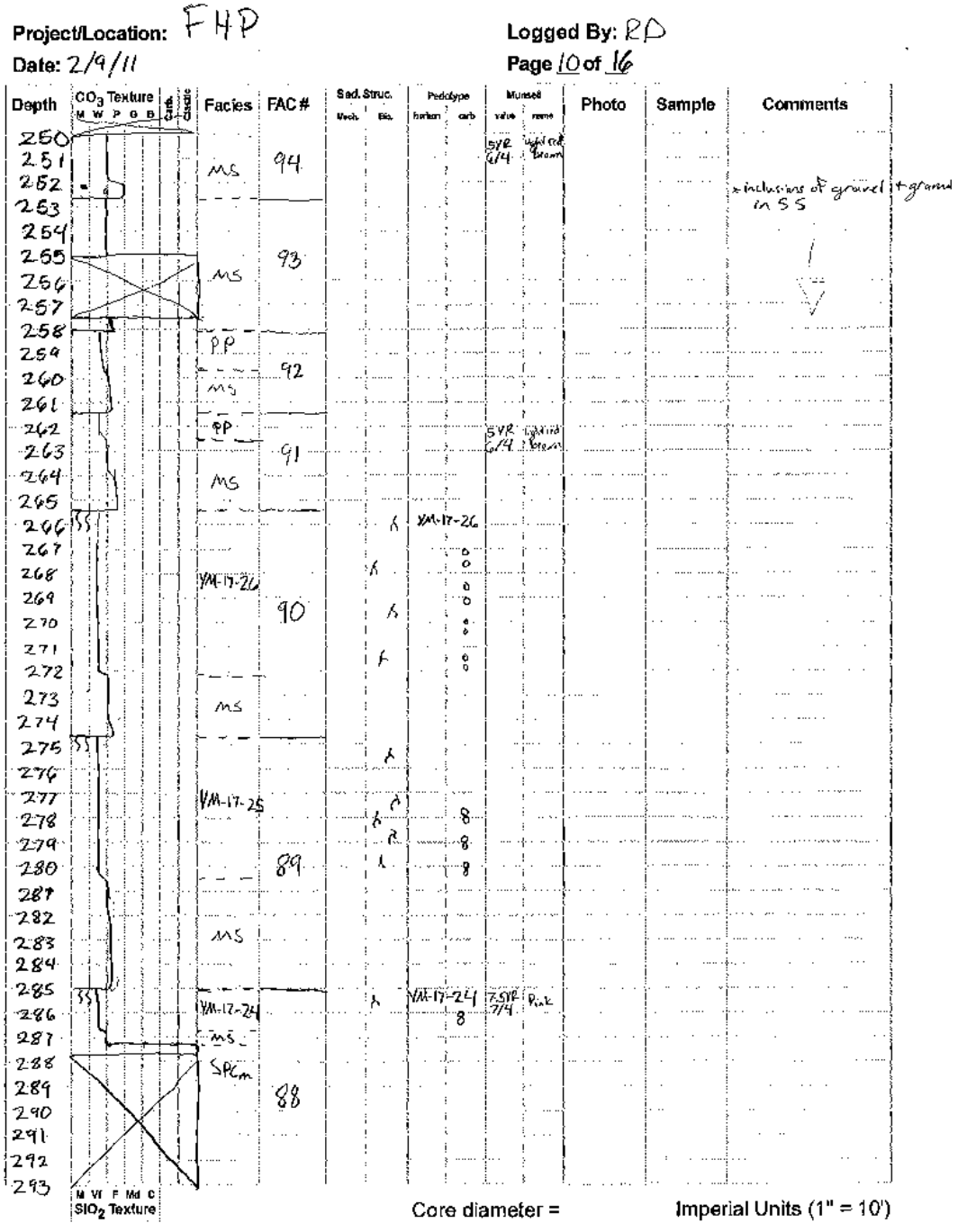
Project/Location: FHP
Logged By: RD
Date: 2/9/11
Page 10 of 16
Depth
CO3 Texture
M W P G B
Facies
FAC #
Sed. Struc.
Mech. Bio.
Pedotype
horizon carb
Munsell
value rxnne
Photo
Sample
Comments
250
251
252
253
254
255
256
257
258
259
260
261
262
263
264
265
266
267
268
269
270
271
272
273
274
275
276
277
278
279
280
281
282
283
284
285
286
287
288
289
290
291
292
293
MS
94
MS
93
PP
92
MS
PP
91
MS
YM-17-26
90
MS
YM-17-25
89
MS
YM-17-24
MS
SPCm
88
5YR 6/4
light red brown
5YR 6/4
light red brown
7.5YR 7/4
Pink
inclusions of gravel + grand in SS
M VF F Md C
SiO2 Texture
Core diameter =
Imperial Units (1" = 10')

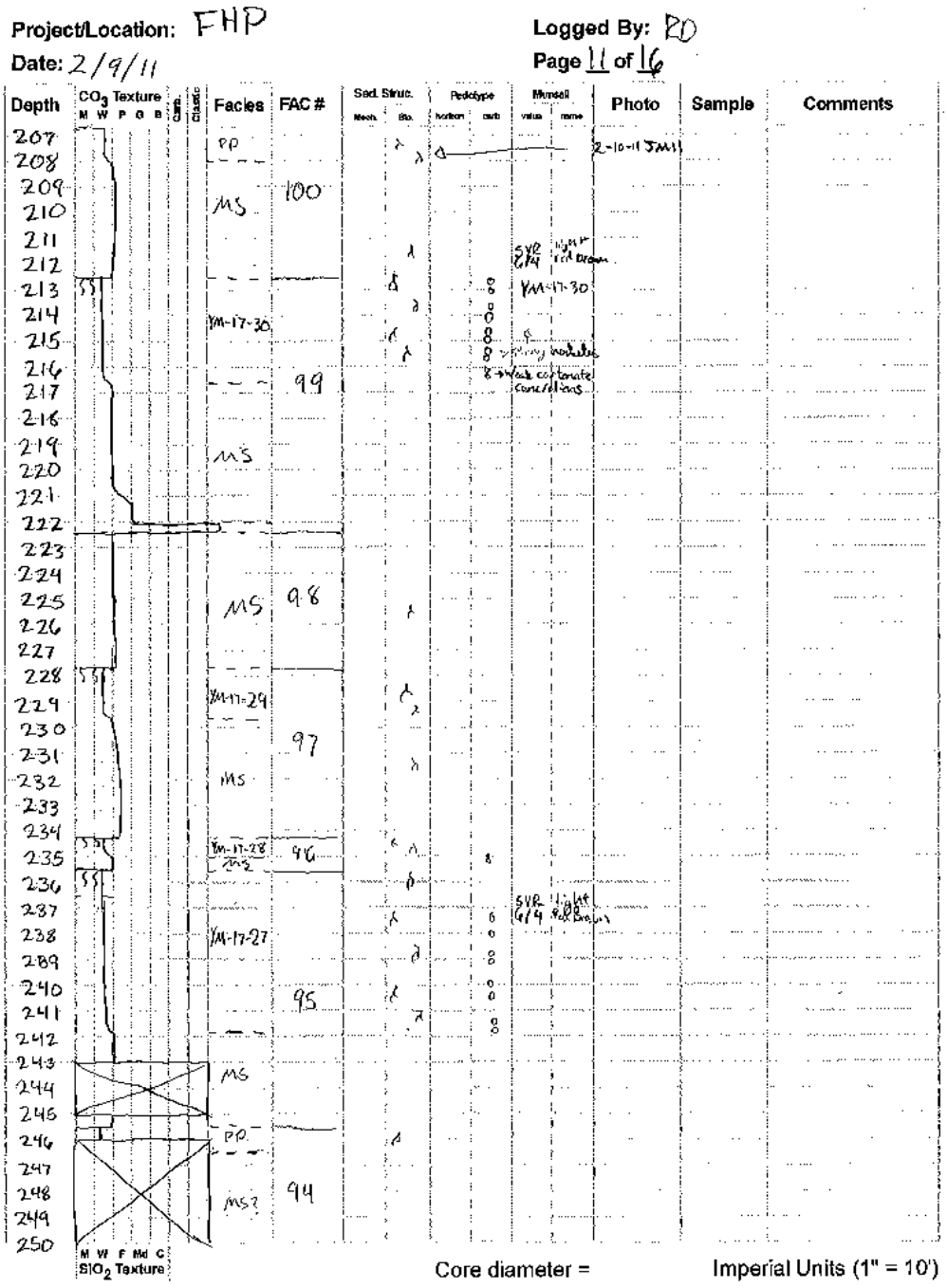
Project/Location: FHP
Logged By: RD
Date: 2/9/11
Page 11 of 16
Depth
CO3 Texture
M W P G B
Facies
FAC #
Sed. Struc.
Pedotype
Munsell
Photo
Sample
Comments
PP
MS
100
YM-17-30
99
MS
MS
98
YM-17-29
97
MS
YM-17-28
96
YM-17-27
95
MS
PP
MS?
94
M W F Md C
SiO2 Texture
Core diameter =
Imperial Units (1" = 10')

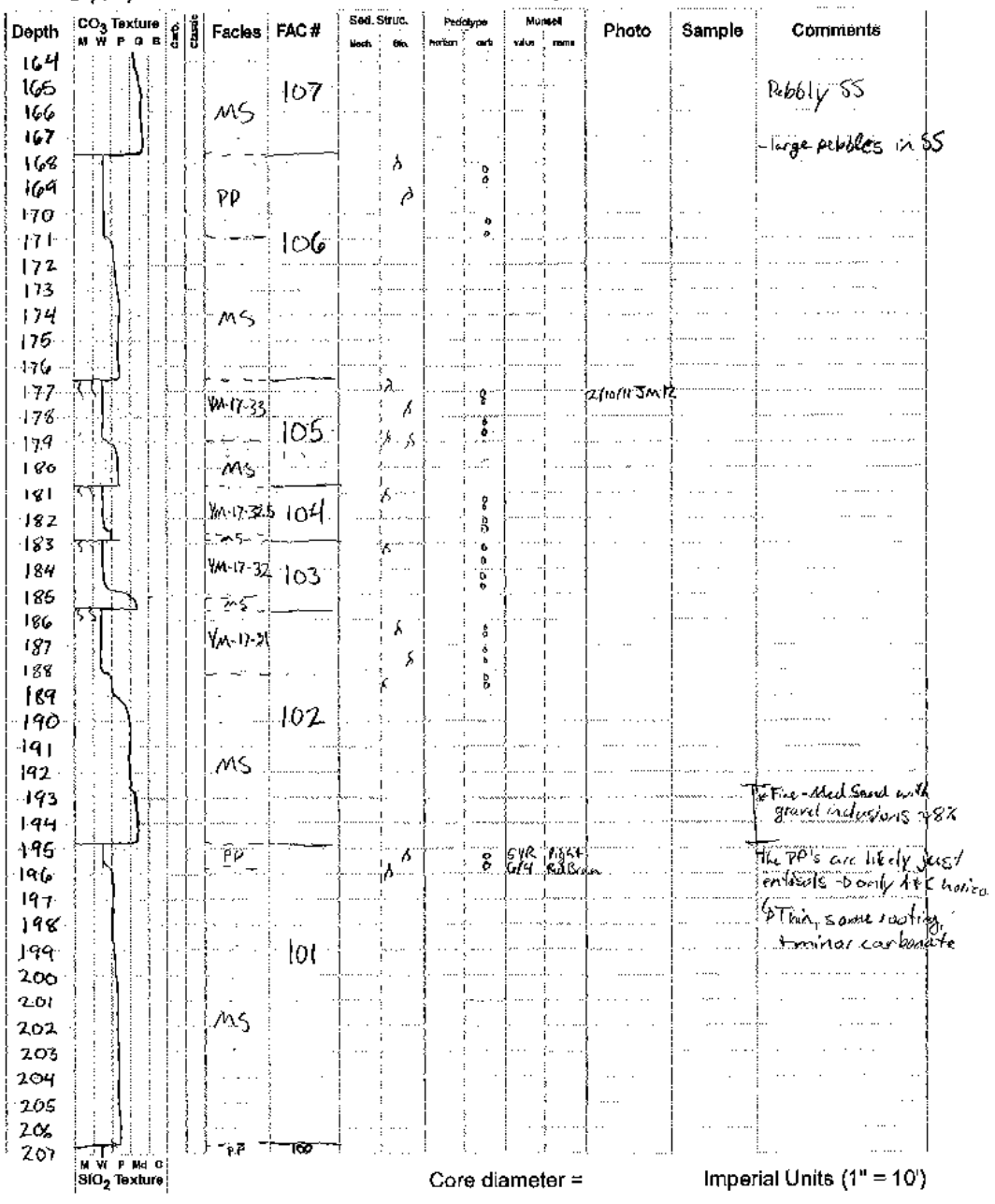
Project/Location: FHP
Logged By: RD
Date: 2/10/11
Page 12 of 16
Depth
CO3 Texture
M W P G B
carb
classic
Facies
FAC #
Sed. Struc.
Pedotype
horizon
carb
Munsell
value
rems
Photo
Sample
Comments
Pebbly SS
-large pebbles in SS
MS
PP
107
106
105
104
103
102
101
160
YM-17-33
YM-17-32.5
YM-17-32
2/10/11 JM12
Fine-Med Sand with gravel inclusions ~8%
The PP's are likely just entisols - barely AC horizon
Thin, some rootlets, laminar carbonate
5YR 6/4 Light Reddish Brown
M VF F Md C
SiO2 Texture
Core diameter =
Imperial Units (1" = 10')

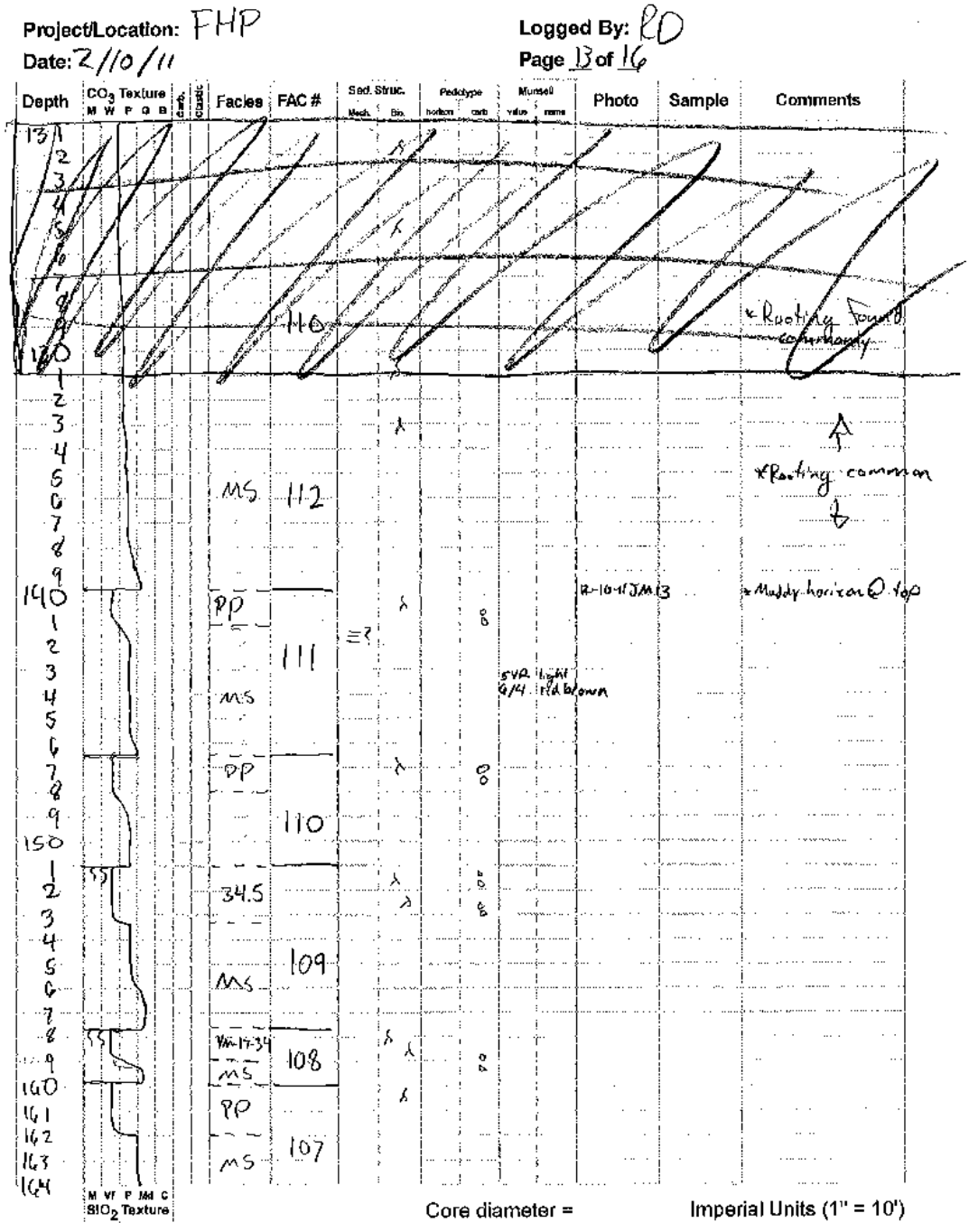
Project/Location: FHP
Logged By: RD
Date: 2/10/11
Page 13 of 16
Depth
CO3 Texture
M W P Q B
Carb. Clastic
Facies
FAC #
Sed. Struc.
Mech. Bio.
Peds/type
horizon carb
Munsell
value chroma
Photo
Sample
Comments
MS
112
PP
111
MS
PP
110
34.5
109
MS
108
MS
PP
107
MS
R-10-1 JM 13
5YR light red/brown
*Rooting found commonly
*Rooting common
*Muddy horizon @ top
M VF P Md C
SiO2 Texture
Core diameter =
Imperial Units (1" = 10')

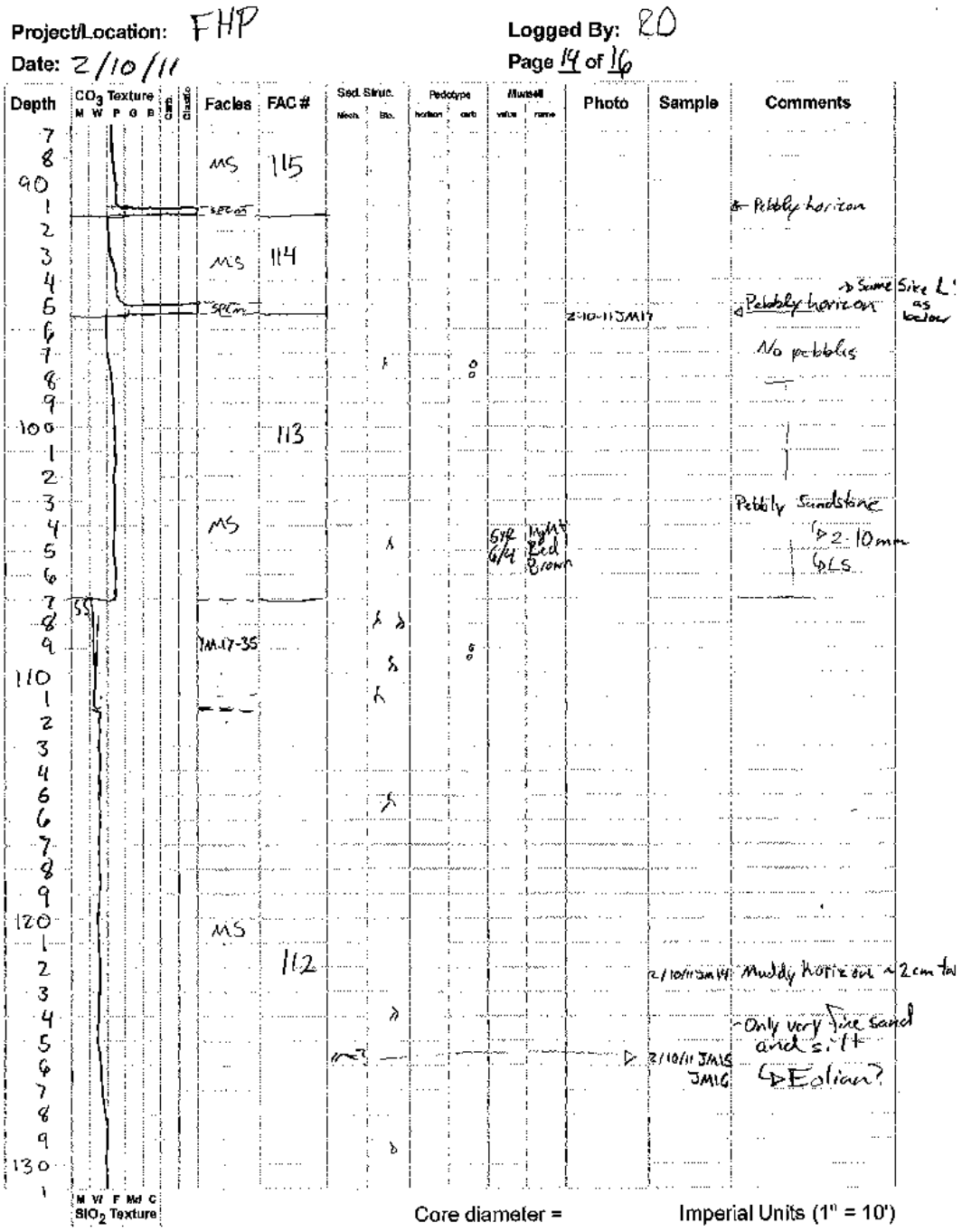
Project/Location: FHP
Logged By: RD
Date: 2/10/11
Page 14 of 16
Depth
CO3 Texture
M W P G B
Facies
FAC #
Sed. Struc.
Mech.
Bio.
Pedotype
horizon
carb
Munsell
value
name
Photo
Sample
Comments
MS
115
114
113
112
JM17-35
2-10-11 JM17
Pebbly horizon
Same Site L as below
No pebbles
Pebbly Sandstone
2-10mm
GLS
5YR 6/4 Light Reddish Brown
2/10/11 JM14 Muddy horizon ~2cm thick
Only very fine sand and silt
2/10/11 JM15
JM16
Eolian?
M Vf F Md C
SiO2 Texture
Core diameter =
Imperial Units (1" = 10')

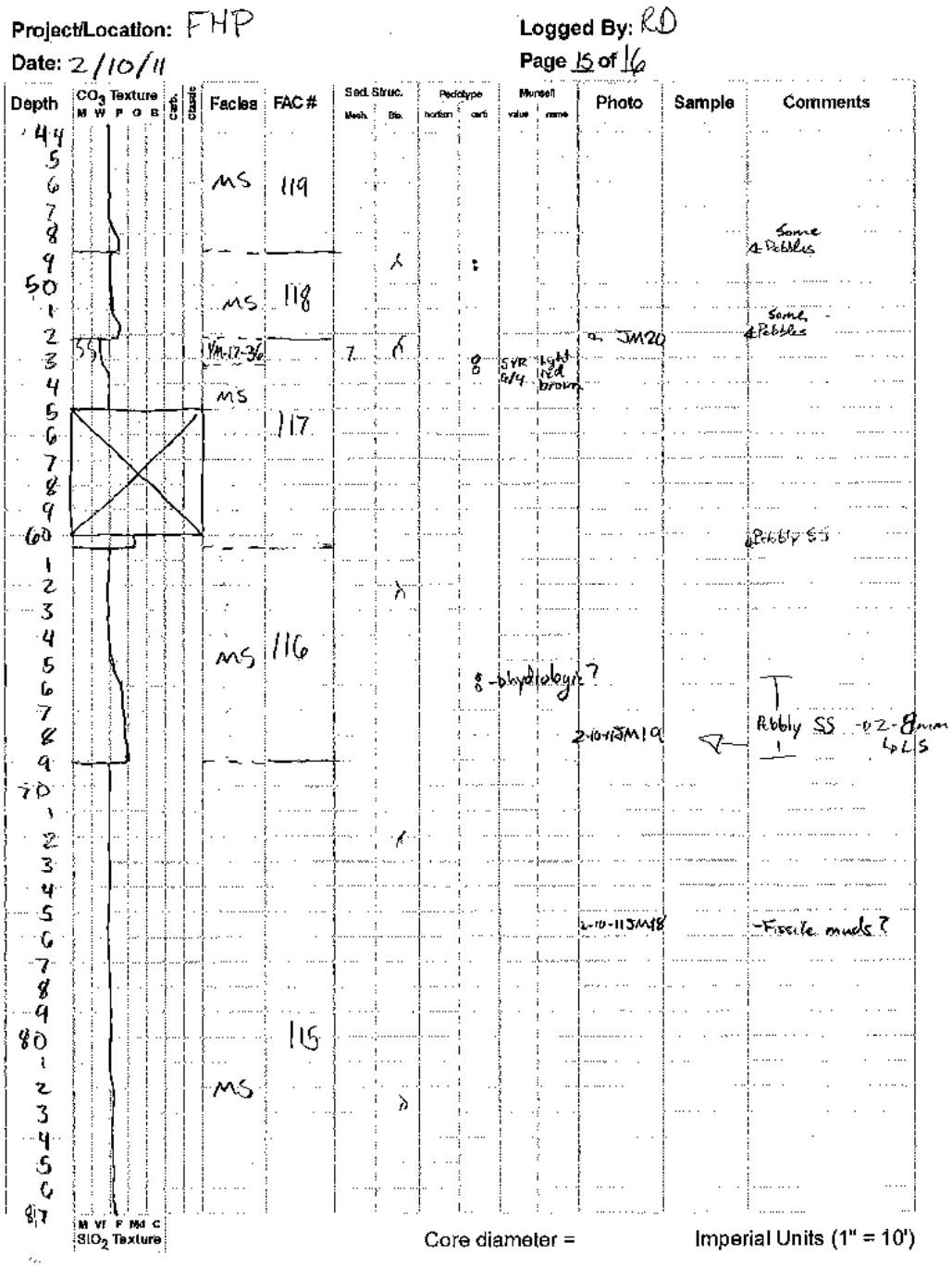
Project/Location: FHP
Logged By: RD
Date: 2/10/11
Page 15 of 16
Depth
CO3 Texture
M W P O B
Facies
FAC #
Sed. Struc.
Bio.
Pedotype
Munsell
value
Photo
Sample
Comments
MS
119
118
117
116
115
Some 4 Pebbles
Some 4 Pebbles
2-10-11JM20
5YR 6/4 light red brown
Pebbly SS
8 - physiologic?
2-10-11JM19
Pebbly SS -0.2-8mm 4 LS
2-10-11JM18
-Fissile muds?
M VF F Md C
SiO2 Texture
Core diameter =
Imperial Units (1" = 10')

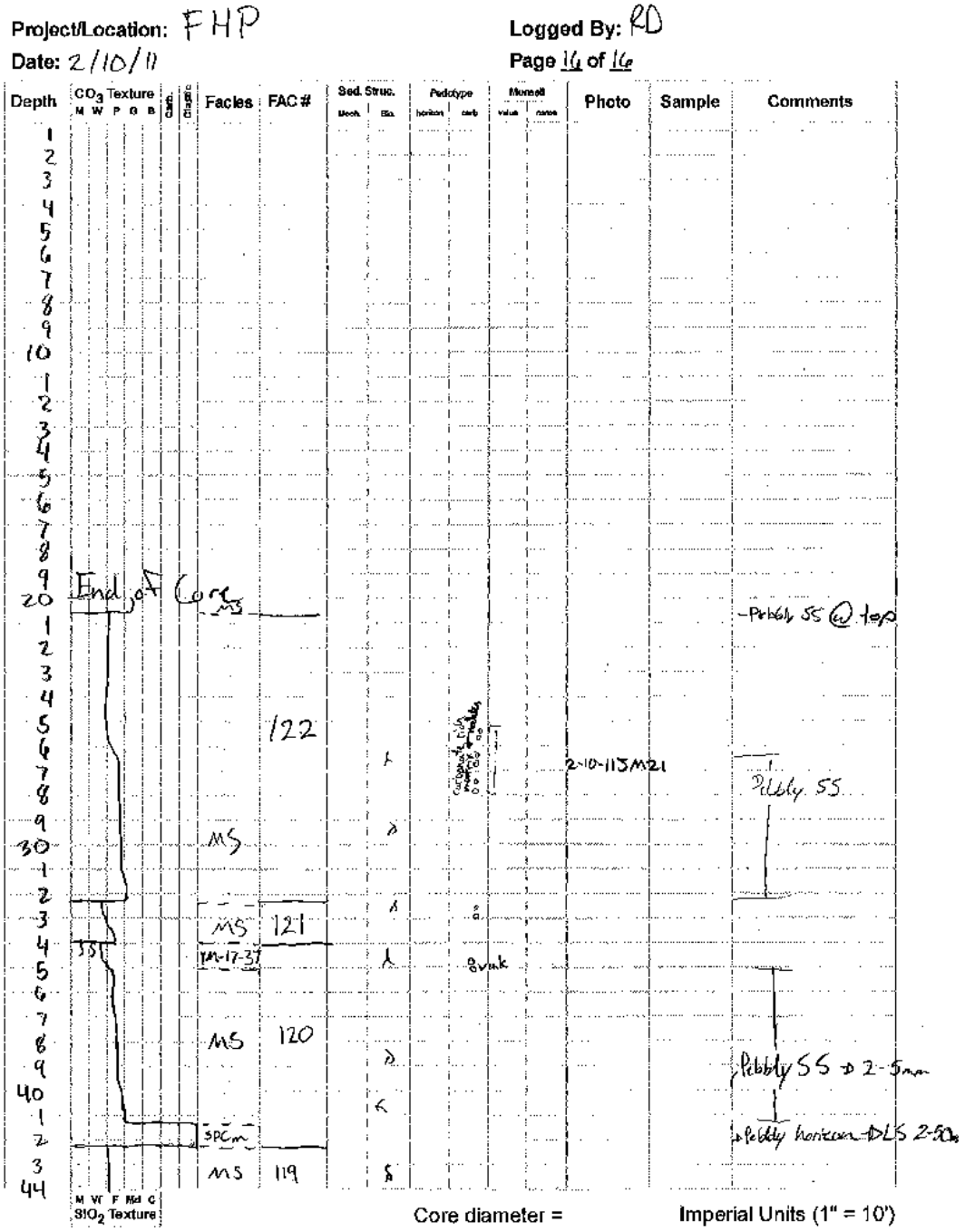
Project/Location: FHP
Logged By: RD
Date: 2/10/11
Page 14 of 16
Depth
CO3 Texture
M W P G B
Facies
FAC#
Sed. Struc.
Pedotype
Munsell
Photo
Sample
Comments
End of Core
MS
122
MS
MS
121
MS
120
SPCm
MS
119
2-10-11 SM21
Pebbly SS
Pebbly SS @ top
Pebbly SS → 2-5mm
Pebbly horizon → LS 2-50mm
M VF F Md C
SiO2 Texture
Core diameter =
Imperial Units (1" = 10')

Well 22

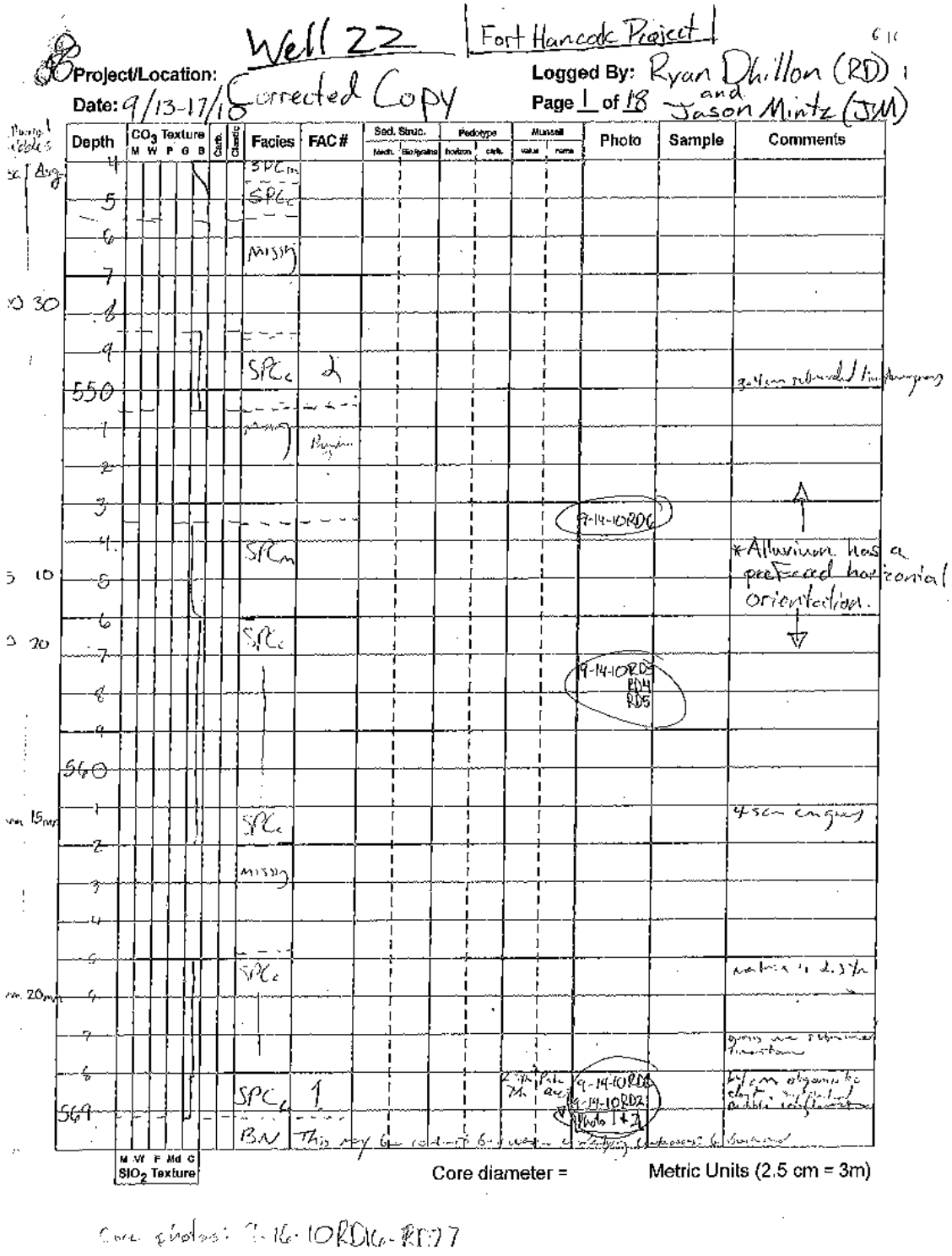

Core photos: 9-16-10RD6-RD7

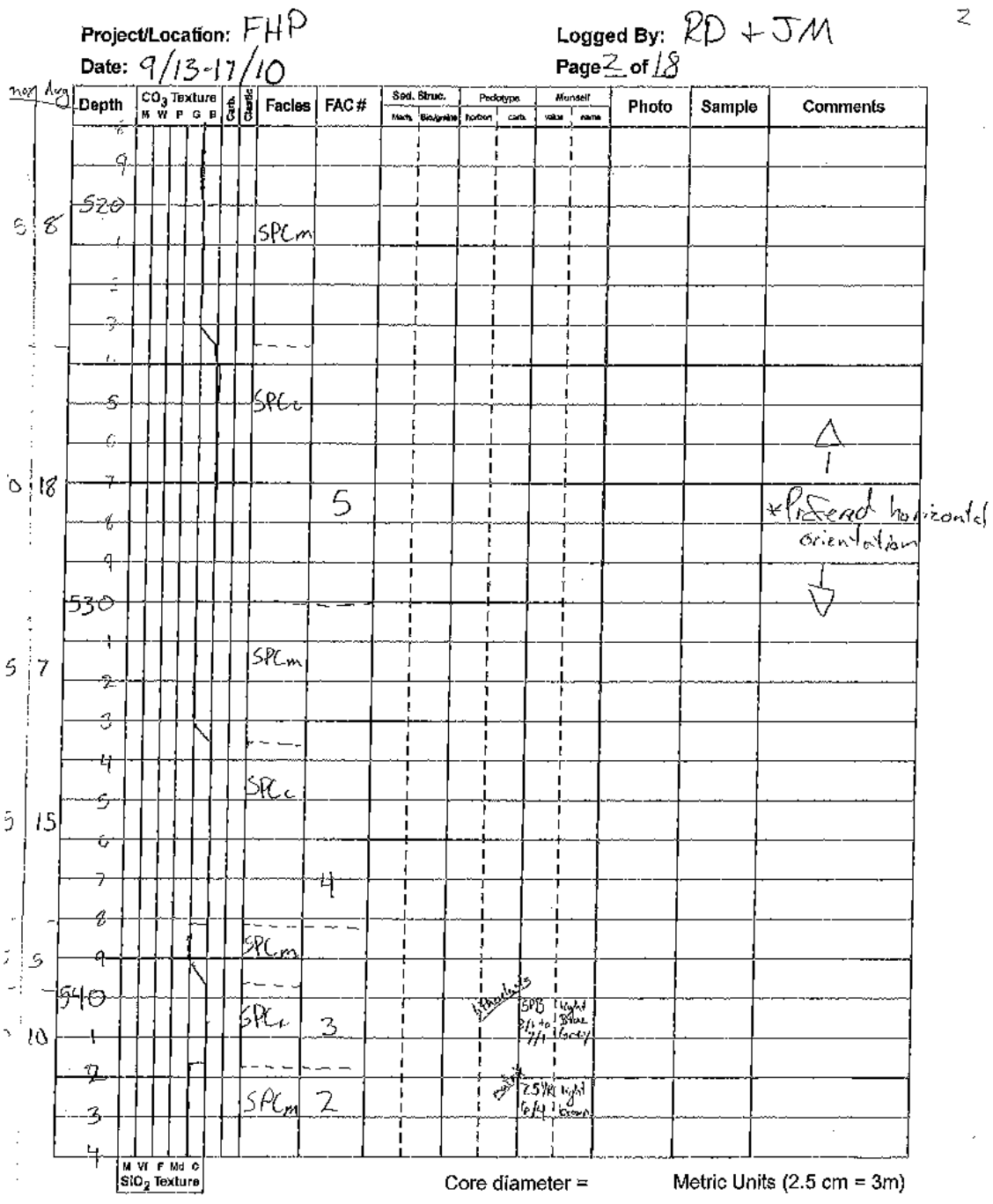
Project/Location: FHP
Logged By: RD + JM
Date: 9/13-17/10
Page 2 of 18
Depth
CO3 Texture
Facies
FAC #
Sed. Struc.
Pedotype
Munsell
Photo
Sample
Comments
SPCm
SPCc
SPCm
SPCc
SPCm
SPCc
SPCm
5
4
3
2
*Record horizontal orientation
M VF F Md C
SiO2 Texture
Core diameter =
Metric Units (2.5 cm = 3m)

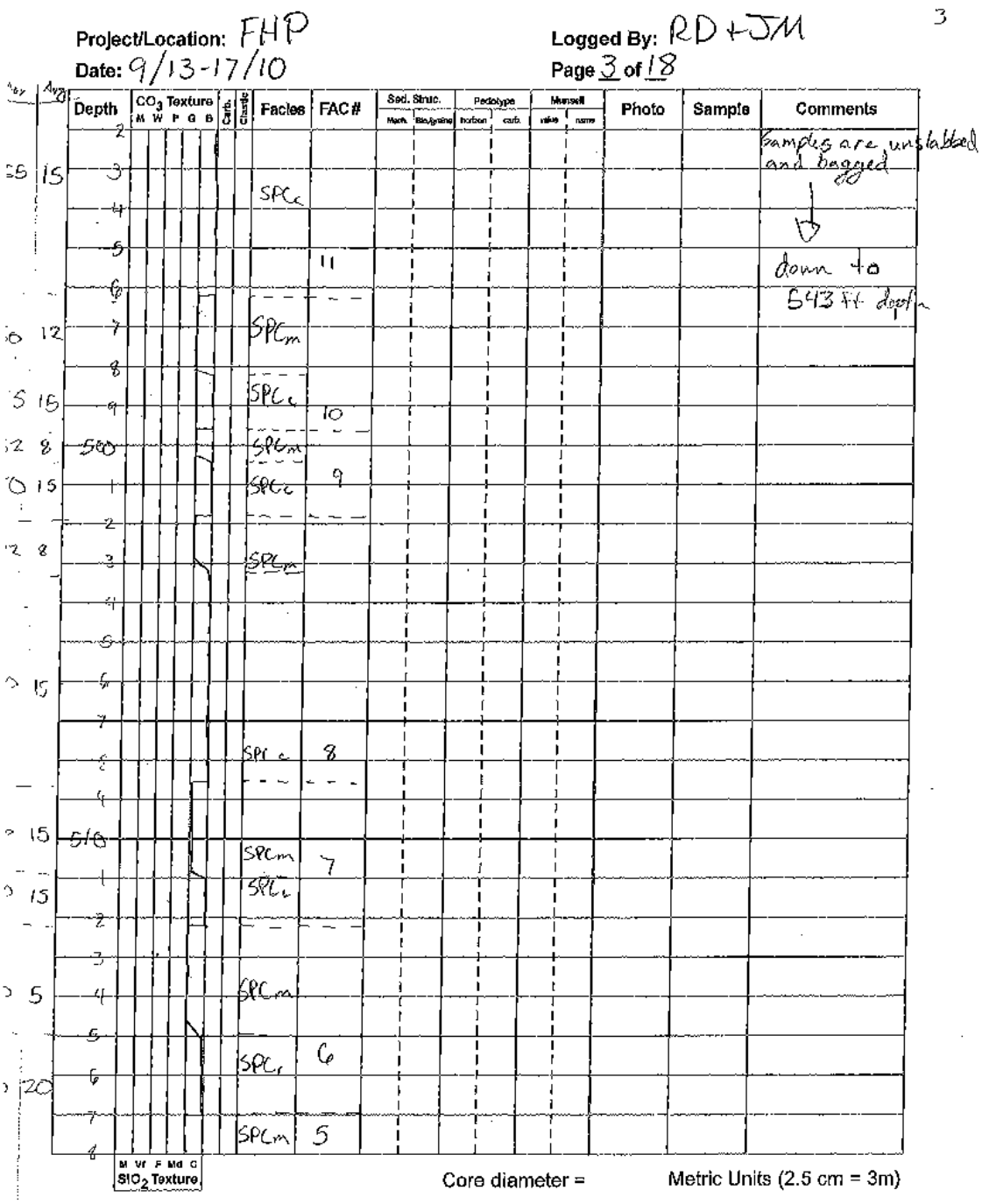
Project/Location: FHP
Logged By: RD + JM
Date: 9/13-17/10
Page 3 of 18
3
Depth
CO3 Texture
M W P G B
Carb. Clastic
Facies
FAC #
Sed. Struc.
Mech. Biog/phys
Pedotype
horizon carb.
Munsell
value name
Photo
Sample
Comments
Samples are unlabled and bagged
down to 543 ft depth
SPCc
SPCm
SPCc
SPCm
SPCc
SPCm
SPCc
SPCm
SPCm
SPCc
SPCm
SPCc
11
10
9
8
7
6
5
M Vf F Md C
SiO2 Texture
Core diameter =
Metric Units (2.5 cm = 3m)

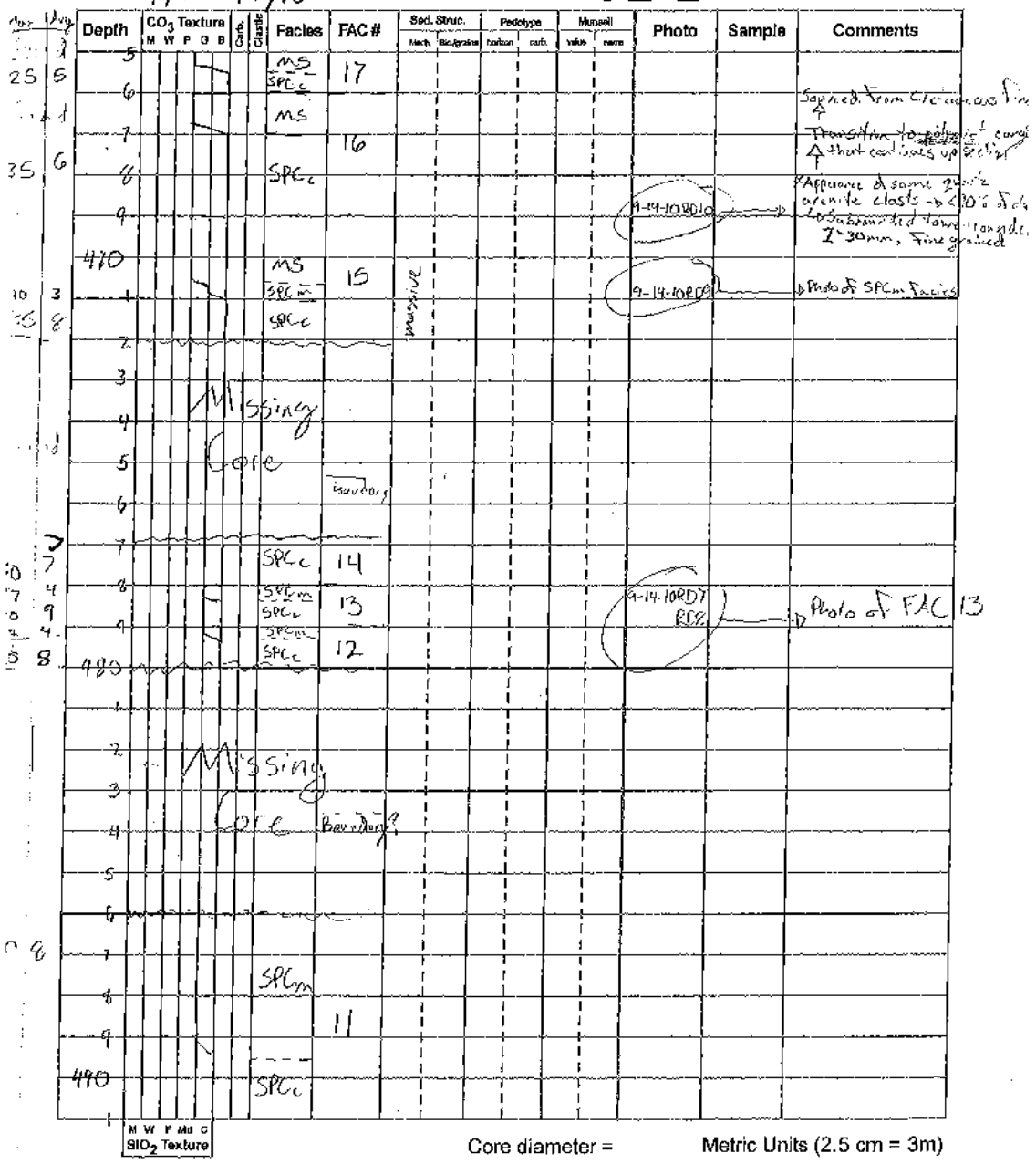
Project/Location: FHP
Date: 9/13-17/10
Logged By: RD + JM
Page 4 of 18
Depth
CO3 Texture
M W P G B
Carb. Clastic
Facies
FAC #
Sed. Struc.
Mech. Biological
Pedotype
horizon carb.
Munsell
value chroma
Photo
Sample
Comments
MS
SPCc
17
MS
16
SPCc
MS
SPCm
15
SPCc
Missing
Core
Boundary
SPCc
14
SPCm
SPCc
13
SPCm
SPCc
12
Missing
Core
Boundary?
SPCm
11
SPCc
massive
9-14-10RD10
9-14-10RD9
9-14-10RD7
RD8
Photo of FAC 13
M VF F Md C
SiO2 Texture
Core diameter =
Metric Units (2.5 cm = 3m)

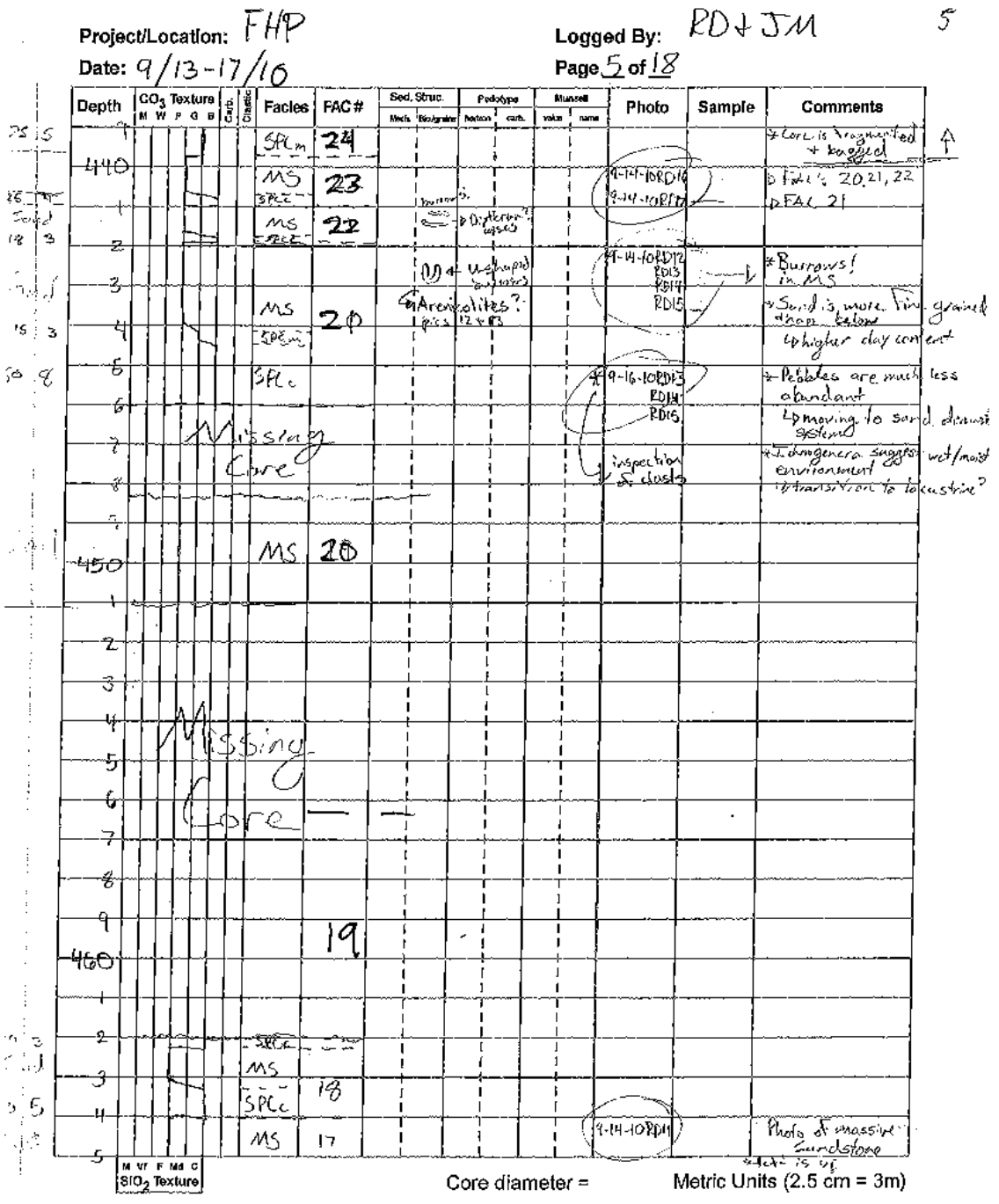
Project/Location: FHP
Logged By: RD & JM
Date: 9/13-17/10
Page 5 of 18
Depth
CO3 Texture M W P G B
Carb. Clastic
Facies
FAC #
Sed. Struc. Mech. Biogenic
Pedotype horizon curb.
Munsell value name
Photo
Sample
Comments
SPLm 24
MS SPLc 23
MS SPLc 22
MS SPLm 20
SPLc
Missing Core
MS 20
Missing Core
19
SPLc
MS
SPLc 18
MS 17
9-14-10RD16
9-14-10RD17
9-14-10RD12 RD13 RD14 RD15
9-16-10RD13 RD14 RD15
inspection & closed
9-14-10RD11
* Core is fragmented + bagged
FACs 20, 21, 22
FAC 21
* Burrows! in MS
* Sand is more fine grained than below
↳ higher clay content
* Pebbles are much less abundant
↳ moving to sand dominated system
* Ichnogenera suggests wet/moist environment to lacustrine?
Photo of massive sandstone
M VF F Md C
SiO2 Texture
Core diameter =
Metric Units (2.5 cm = 3m)

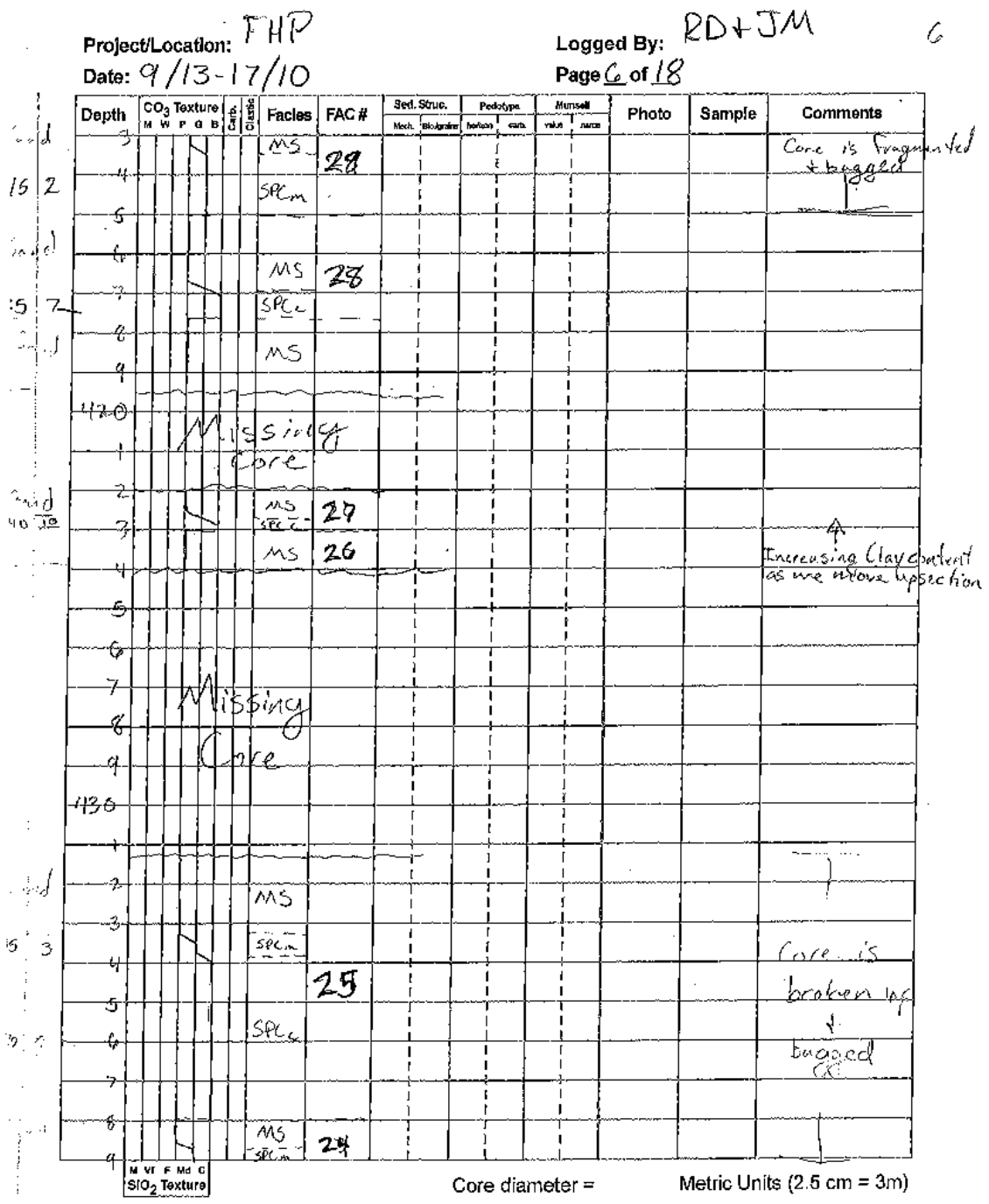
Project/Location: FHP
Logged By: RD+JM
Date: 9/13-17/10
Page 6 of 18
Depth
CO3 Texture
M W P G B
Carb.
Clastic
Facies
FAC #
Sed. Struc.
Mech.
Bio.
Pedotype
horizon
carb.
Munsell
value
chroma
Photo
Sample
Comments
MS
SPCm
28
SPCc
Missing Core
27
26
Increasing Clay content as we move upsection
25
broken up & bagged
24
M VF F Md C
SiO2 Texture
Core diameter =
Metric Units (2.5 cm = 3m)

Project/Location: FHP **Logged By:** RD + JM 7

Date: 9/13-17/10 **Page** 7 **of** 18

Depth	CO3 Texture (M W P G B)	Carb.	Clastic	Facies	FAC #	Sed. Struc. Mech.	Sed. Struc. Bioturb.	Pedotype horizon	Pedotype carb.	Munsell value	Munsell name	Photo	Sample	Comments
7				MS FHP-T	38		AR	Bw	no	5YR 5/2-5/4	Reddish Brown	see FHP-1 photo	X	* First Paleosol – Roots & color changes – No slicks, carb
8						AR								
9				MS	37	AR								
390														
1														
2				Missing										
3				Core										
4														
5														
6				MS	36									
				SPCm										
7														
8				MS	35									
9				SPCm										
400				MS	34									* Very thin FACs – Bands fining up into clay rich very fine sands + losing pebbles
1				MS	33							9-14-10 FOTO <DPAC32>		
2				MS SPCm	32									
3				MS SPCm	31									
4														
5				Missing										
6				Core boundary?										
7														
8				MS										
9				SPCm	30									
410														
1														Core is broken
2					29									+ bagged
3				MS										→ Not stacked

M VF F Md C
SiO2 Texture

Core diameter = Metric Units (2.5 cm = 3m)

Project/Location: FHP

Logged By: RD+JM

Date: 9/13-17/10

Page 8 of 18

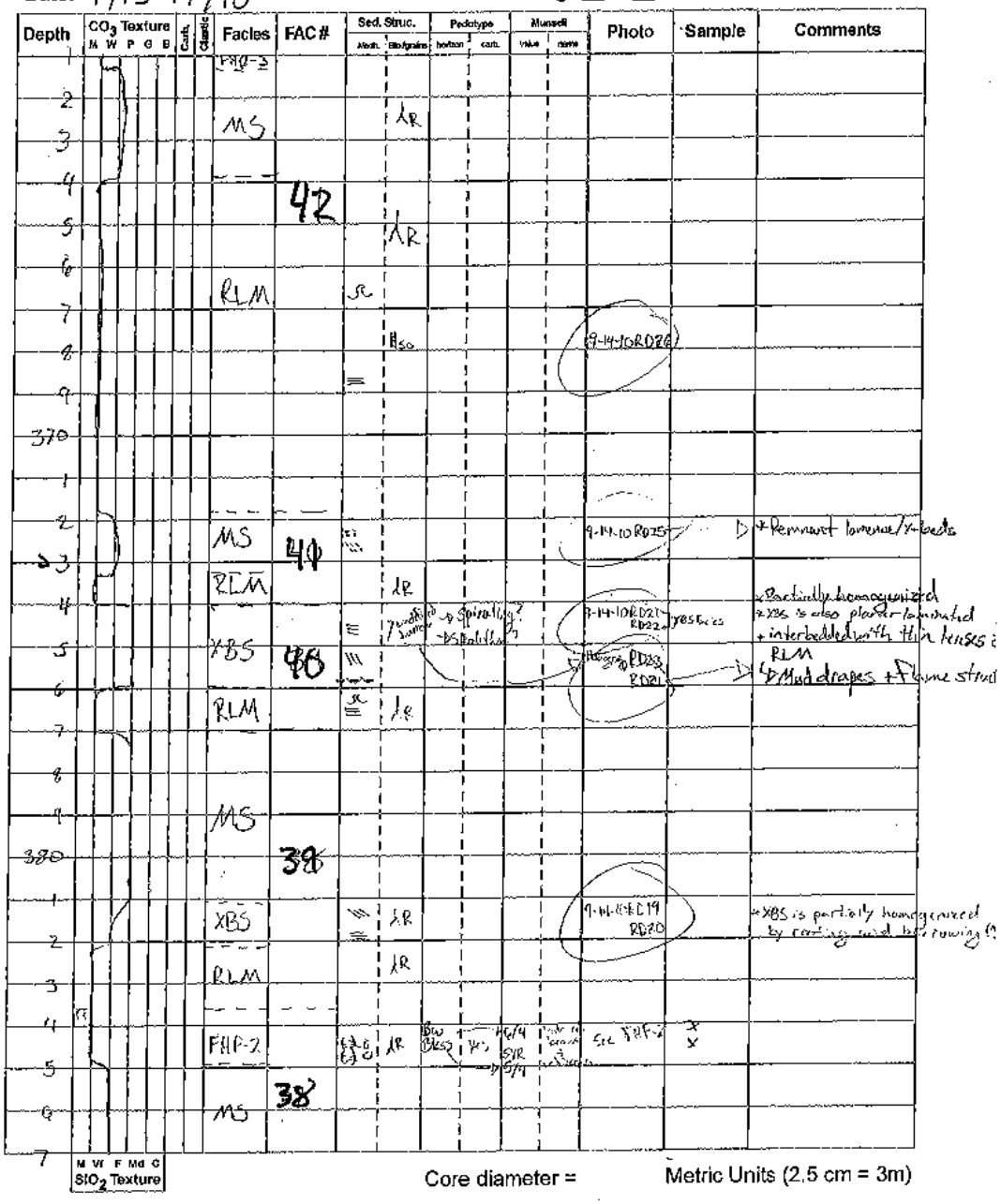

Project/Location: FHP

Logged By: RD + JM

Date: 9/13-17/10

Page 9 of 18

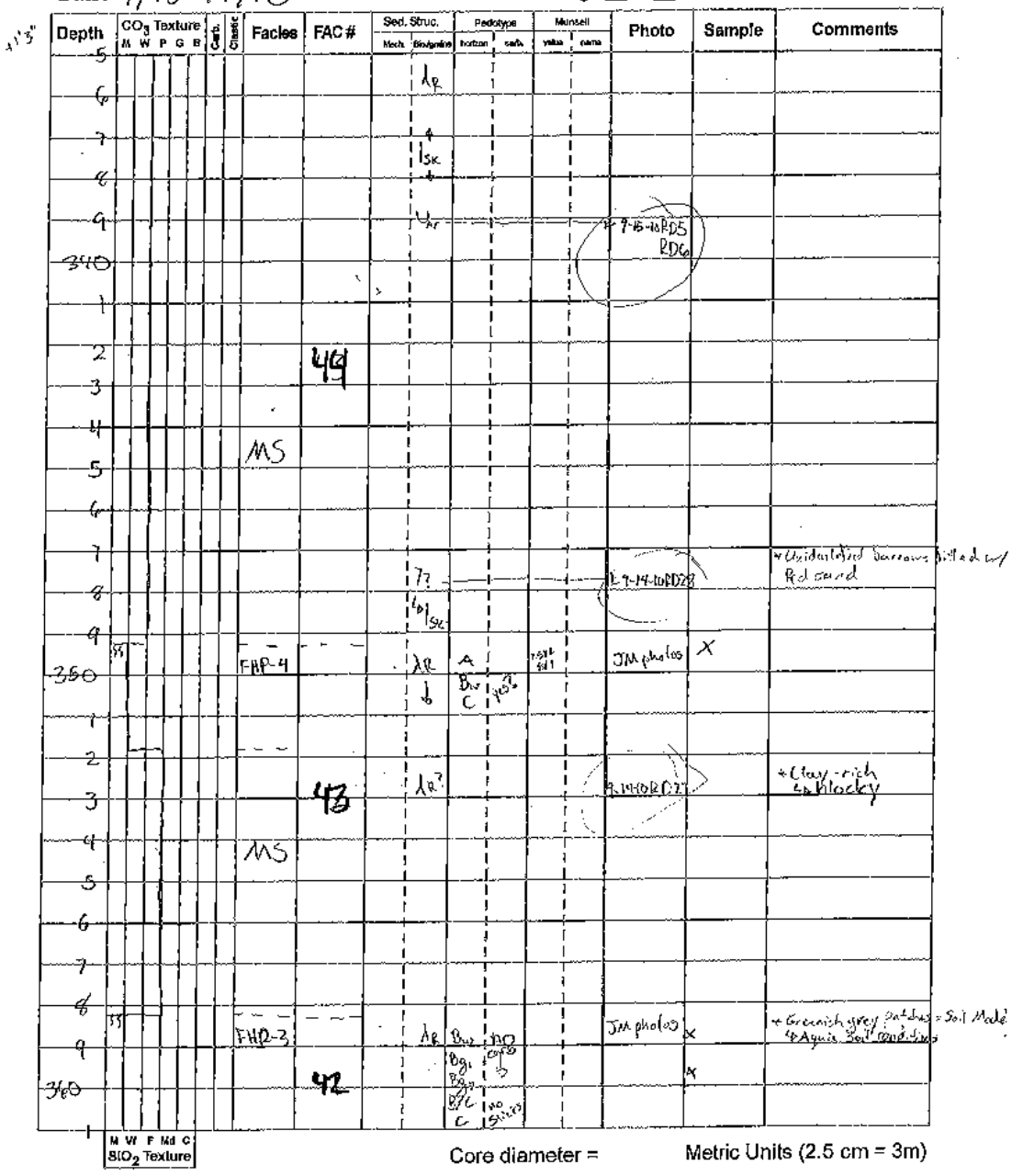

Project/Location: FHP

Logged By: RD + JM

Date: 9/13-17/10

Page 10 of 18

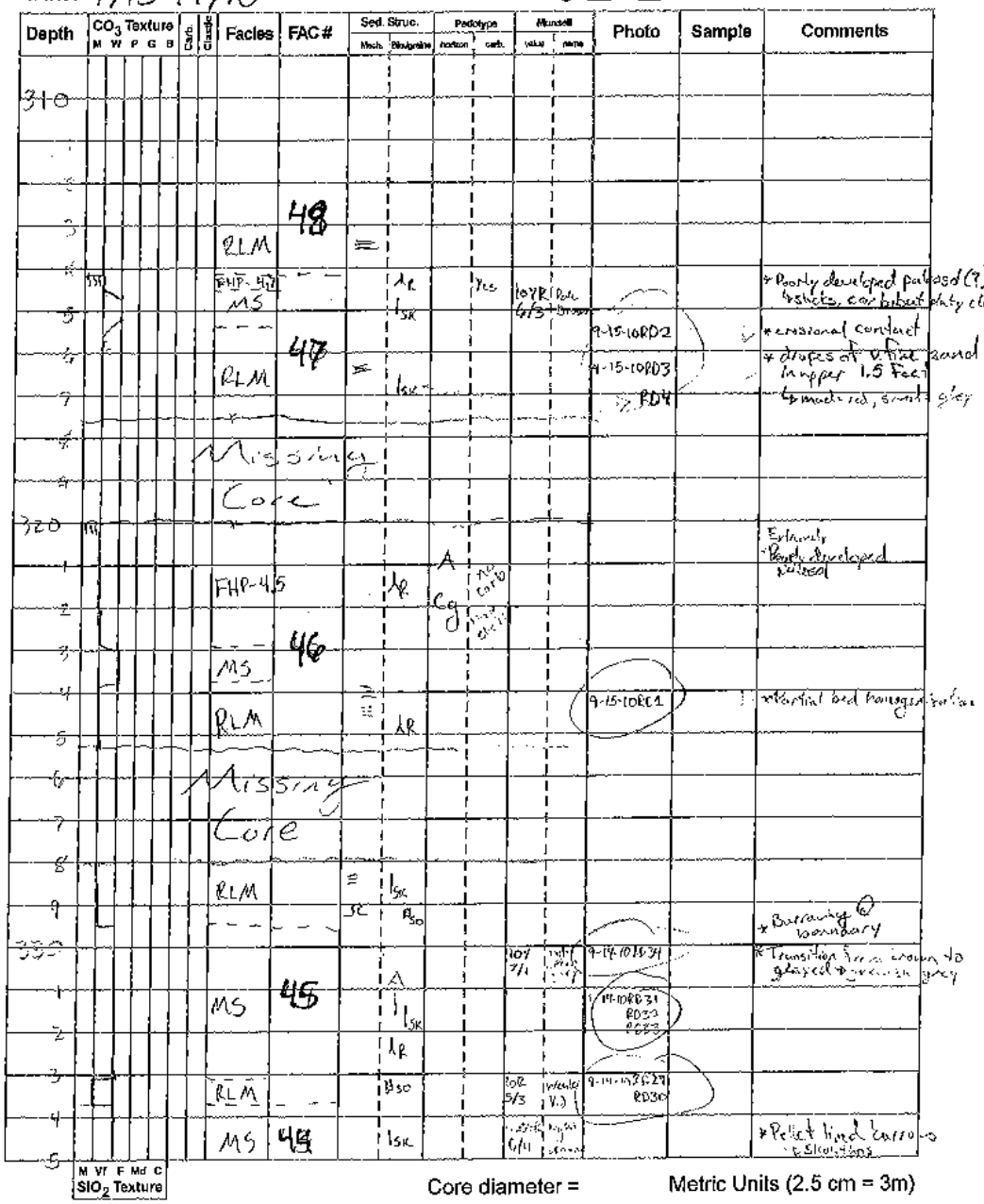

☆ Core photos = 9-16-10RD16 to RD27

FHP

Project/Location: FHF - TBEG well #12 **Logged By:** JSM + RD

Date: 9/14/16 **Page** 11 **of** 18

Depth	CO_3 Texture M W P G B	Carb.	Clastic	Facies	FAC #	Sed. Struc. Mech.	Sed. Struc. Bio/grains	Pedotype horizon	Pedotype carb.	Munsell value	Munsell name	Photo	Sample	Comments
289														Mudstone fully Undefined known from
290												9-14-16-JM-4		
291														
292														
293														
294														
295														
296														
297														
298										2.5Y 6/4				
299														
300														
301				MS						2.5Y 6/3				
302														
303				NOT RECOVERED										
304				RLM	55		H			10YR 5/3			X	
305				FMS								9-14-16-JM-3		
306								bw				in GHF 2.5 photo suite	X	
307					52			bk/c	C				X	
308				XBS						2.5Y 4/3		9-14-16-JM-2		
309				RLM XBS RLM	54 60									
310										2.5Y 5/4		9-14-16-JM-1		
311				MS	49									
312														
313				MS	48									

M W F Md C
SiO_2 Texture

Core diameter = 2.5" Metric Units (2.5 cm = 3m)

FHP

Project/Location: FH- well 22 | Logged By: JSM + RD | 12

Date: 9/14/10 | Page 12 of 18

Depth	CO3 Texture (M W P G B)	Carb.	Clastic	Facies	FAC #	Sed. Struc. (Mech.)	Sed. Struc. (Bio/grains)	Pedotype (horizon)	Pedotype (carb.)	Munsell (value)	Munsell (name)	Photo	Sample	Comments
263				MS RLM	60									
264														
265					14	Combine FAC's?								
266														
267				MS	58									unconsolidated sand
268				XSB			lith							
269					13									
270				FHP-7 RLM	58			A/C C		5YR 5/1	red gray	9/14/10-JSM-21/22; 9/14/10-JSM-20		[illegible] CAB [illegible] pedogenic [illegible] VEN/[illegible] slightly [illegible]
271				MS	57	Combine FAC's?								
272				XBS MS RLM								9/14/10 JSM 19		
273				XBS								9/14/10 JSM-16/17/18		
274				XBS RLM	58							9/14/10-JSM-13/14/15		
275				MS								9-14-10-JSM-11/12		Bedding every 2.5" in core
276														[illegible]
277				RLM	58					10YR 4/3		9-14-10-JSM-10		
278				FHP-6				BS Bg				9-14-10-JSM-9/10		
279				MS								9-14-10-JSM-7		
280				SPCa										submitted [illegible] very fine to fine [illegible]
281				SPCa	54									[illegible] fine sand [illegible] pebbles polymict [illegible]
282					58		UU					9-14-10-JSM-6		[illegible] include [illegible] granite [illegible]
283							UU							
284							VU							
285														
286														
287												9-14-10-JSM-5		surface [illegible] I think is pedotube [illegible] core [illegible]
288														

Margin notes: laminated (266–267); unlith (268); scabbled (277–279)

M VF F Md C SiO2 Texture

Core diameter = 2.5" Metric Units (2.5 cm = 3m)

FHP

Project/Location: FH-well 22   **Logged By:** JSM + RD   13

Date: 9/15/10   **Page** 13 **of** 18

Depth	CO_3 Texture (M W P G B)	Carb.	Clastic	Facies	FAC #	Sed. Struc. (Mech. / Bio/grains)	Pedotype (horizon / carb.)	Munsell (value / name)	Photo	Sample	Comments
237									[illegible]		[illegible] carbonized roots
238									9/15/10-[illegible] 24.1		no [illegible]; infrequent [illegible]
239					7Q			5YR 6/4			[illegible]
240											
241	Not Recovered										
242											
243											
244											
245				1C	69		[illegible]	[illegible]	(erosion surface?) deflation surface		rubbled – [illegible]
246				14.2				5YR 6/4	23, 22		This appears to be [illegible]
247				15	68		A, C		21		[illegible] occasional
248				14.1			A	2.5YR 5/6	20		3-5mm carbonate nodule [illegible]
249							B/C				Same as above except [illegible]
250				FS	67, 83		C		19		3mm pedolith fragment
251				FHP-14	66		Bw, C		18		
252				FHP-13	65	B/C		[illegible] 6/6			
253	[illegible] bottom of new run (taken every 10' - likely cored [illegible])										
254	[illegible] the bottom [illegible]										
255				FHP-12		[illegible]	Bk, B/C	5YR 3/4	9/15/10 [illegible]	X	[illegible]
256				FS, FHP-11	64		C, Bw	2.5YR 5/3	17, 16		[illegible] carbonized [illegible]
257				FS	63 ??		C		9/15/10 [illegible] 13		[illegible]
258				FHP-10			Bk	2.5YR 4/3	9-15-10-3[illegible]	3/6/-3/8 9/10 X	[illegible] carbonized root; [illegible]
259						[illegible]	Bk	2.5YR 5/4		X	[illegible]
260				FS	62		C				[illegible]
261				FHP-9	61		Bk, C, Bk	10R 4/3	FS	X	[illegible] 0.5cm [illegible]
262				FHP-8, FS	60		C		9/15/10-[illegible] 13	X	[illegible]

M VF F Md C — SiO_2 Texture

Core diameter = 2.5"   Metric Units (2.5 cm = 3m)

Project/Location: 9/15–9/16 | Logged By: JSM | 14

Date: FH - well 22 | Page 14 of 18

Depth	CO₃ Texture (M W P G B)	Carb.	Clastic	Facies	FAC#	Sed. Struc. Mech.	Sed. Struc. Bio/grains	Pedotype horizon	Pedotype carb.	Munsell value	Munsell name	Photo	Sample	Comments
211				RLM / FHP-20	80 / –89–					7.5YR 7/2	pink grey			
212					Bssg							15 – 20, 14	X	
213														Intraclasts: max = 12mm Avg: 2mm
214				IS	79	[illegible]				10YR 8/2	very pale brown	–17		
215				RLM		V						15		* Mudcracks @ boundary Ins
216				FHP-19	78			Bss				14, 13		
217								Bw				9/16/10 5m 6		
218								Bss				10/11/12	X	
219					77			ABss				5/9	X	
220				FHP-21/18	34			BA				7/8, 5		
221				FHP-17 (no hor)	76			Bw, Bk₁				9/16/10 Jm 1		
222				IS	36			Bk₂, C		7.5YR		4	[illegible]	[illegible]
223				FHP-16	75		[illegible]	A, Bk₁, Bk₂	[illegible]	5/2, 6/4		3, 2	X, X	[illegible]
224				IS / FHP-15				C, A						
225					74			Bg				9/15/10 5m 35		mottled 5GY 6/1 in matrix of 5YR 6/4
226				FHP-14.5	73			[illegible]		5/3		9/15/10 5m 34		? Entisol
227				14.45				A		5/6 6/4		9/15/10 5m 33		no carbonate nodules
228				IS				C						
229				IS 14.4	72			A		2.5YR 4/4		9/15/10 5m 32		[illegible]
230								C						[illegible]
231										7.5YR 6/4				[illegible]
232														
233				IS (?)								9/15/10 5m 30		[illegible]
234										7.5YR 7/1		9/15/10 5m 29		[illegible]
235				IS	71							9/15/10 5m 1		[illegible]
236				14.3	70							9/15/10 5m 25.1		

SiO₂ Texture (M VF F Md C)

Core diameter =

Metric Units (2.5 cm = 3m)

Project/Location: FHP | **Logged By:** RD + JM | 15

Date: 9/13-17/10 | **Page** 15 **of** 18

Depth	CO_3 Texture (M W P G B)	Carb.	Clastic	Facies	FAC #	Sed. Struc. (Mech. / Bio/grains)	Pedotype (horizon / carb.)	Munsell (value / name)	Photo	Sample	Comments
5											
6											
7											*Very fine to fine sand
8					82						*Clasts → 1-15mm
9				IS							
190											*Moderate clay content
1						Low weak bedding ~5-10mm thick					*Very sandy + low clay 9-28 inch
2											*Clay rich @ base → 9 inches
3											
4				Not Recovered							
5					82						
6				RLM					JM36		*A few white calcareous nodules present → ~10-15mm each
7								7.5YR 6/3 light brown	(drawing)		*Shift to fine sand matrix + lower clay content
8									JM35		
9				IS				5YR 6/4 light [illegible]			*Clasts: 2-15mm
200											Transition to v. fine sand matrix
201				IC	81			5YR 5/4 Red brown			↑ *Clasts: 2-35mm
202									JM33		*Matrix is Mud in the IC ↳ Diamict
203				RLM					JM32	boundary	
204				FHP-21			Bk		[illegible] -21	⊗	
205									26	X	
206							Bkm		24, 27		
207										X	
208							Bk		25	X	
209					80				JM34 → Nodules		
210							Bc		23, 22		
211				RLM			C				

M VF F Md C — SiO_2 Texture

Core diameter =

Metric Units (2.5 cm = 3m)

Project/Location: FHP　　　　Logged By: RD + JM　　16

Date: 9/13-17/10　　　　Page 16 of 18

Depth	CO_3 Texture (M W P G B)	Carb.	Clastic	Facies	FAC #	Sed. Struc. Mech.	Sed. Struc. Bio/grains	Pedotype horizon	Pedotype carb.	Munsell value	Munsell name	Photo	Sample	Comments
						(-)	λR							*Entisol - weakly developed
165				FHP-23										
166				IS						7.5YR 7/3	pink			↑ → Angular to subang
167				IC										*Clasts from 2-18 mm
168					83									*Matrix is fine-very fine sand
169				RLM						5YR 5/3	Red brown			
170				223	85									
171				222	84									
172				FHP-22										
173				FHP-221										
174					83									
175														*Deep vertical crack filled with mud → produced from overlying Entisol
176														
177				FHP-22										
178														
179														
180														*Some white carb nodules are present
181					82									
182												JM38 → X-beds in IS		
183				IS								9-16-10 JM37		
184												(core from 197-191 ft)		
185														

SiO_2 Texture (M Vf F Md C)

Core diameter =　　　　Metric Units (2.5 cm = 3m)

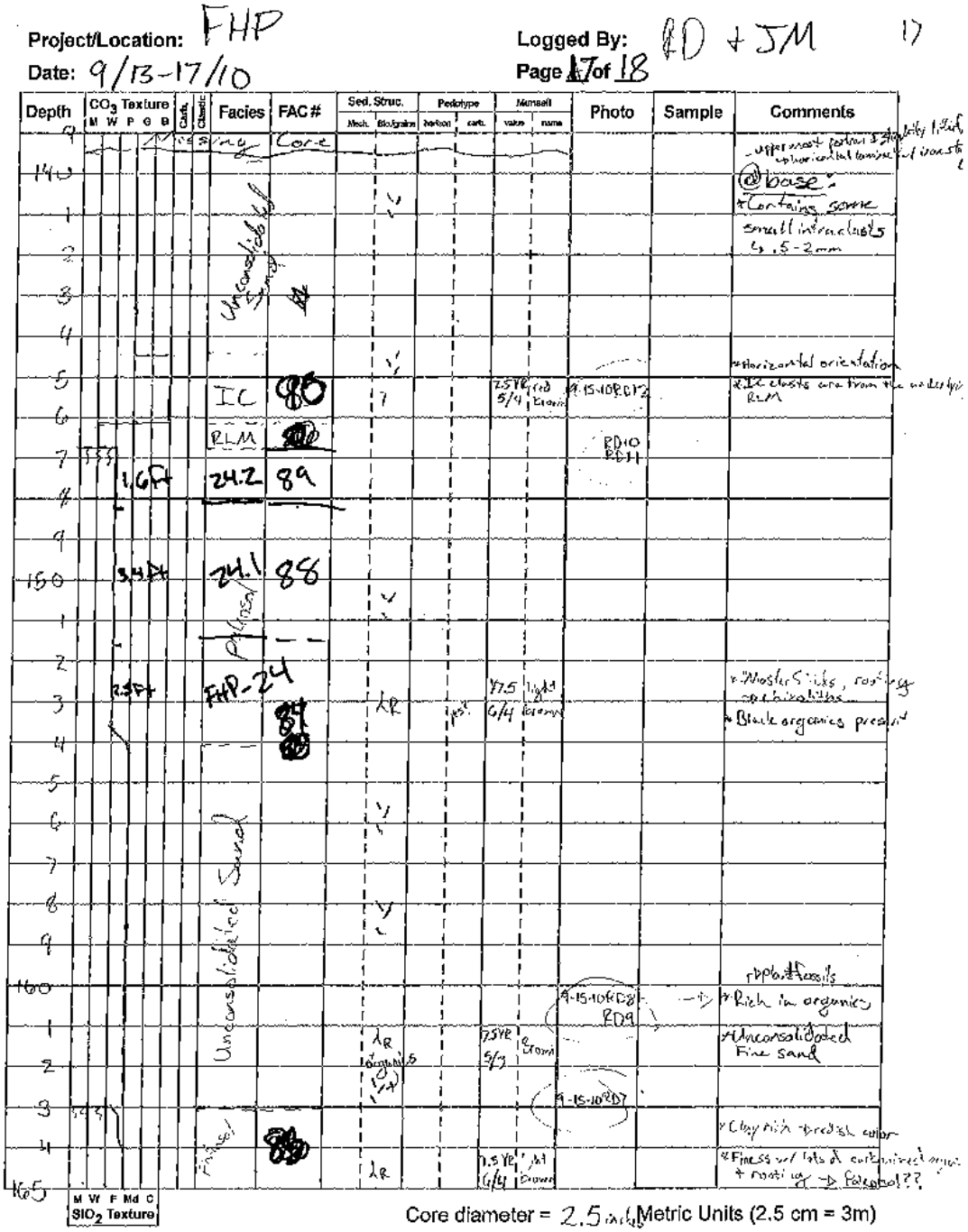
Project/Location: FHP
Logged By: RD + JM
Date: 9/13-17/10
Page 17 of 18
Depth
CO3 Texture M W P G B
Facies
FAC#
Sed. Struc. Mech. Bio/grains
Pedotype horizon carb.
Munsell value name
Photo
Sample
Comments
Core
Unconsolidated Sand
IC
RLM
24.2
24.1
FHP-24
Unconsolidated Sand
Paleosol
M W F Md C
SiO2 Texture
Core diameter = 2.5 inch
Metric Units (2.5 cm = 3m)

Project/Location: FHP

Logged By: RD + JM

Date: 9/17/11

Page 18 of 18

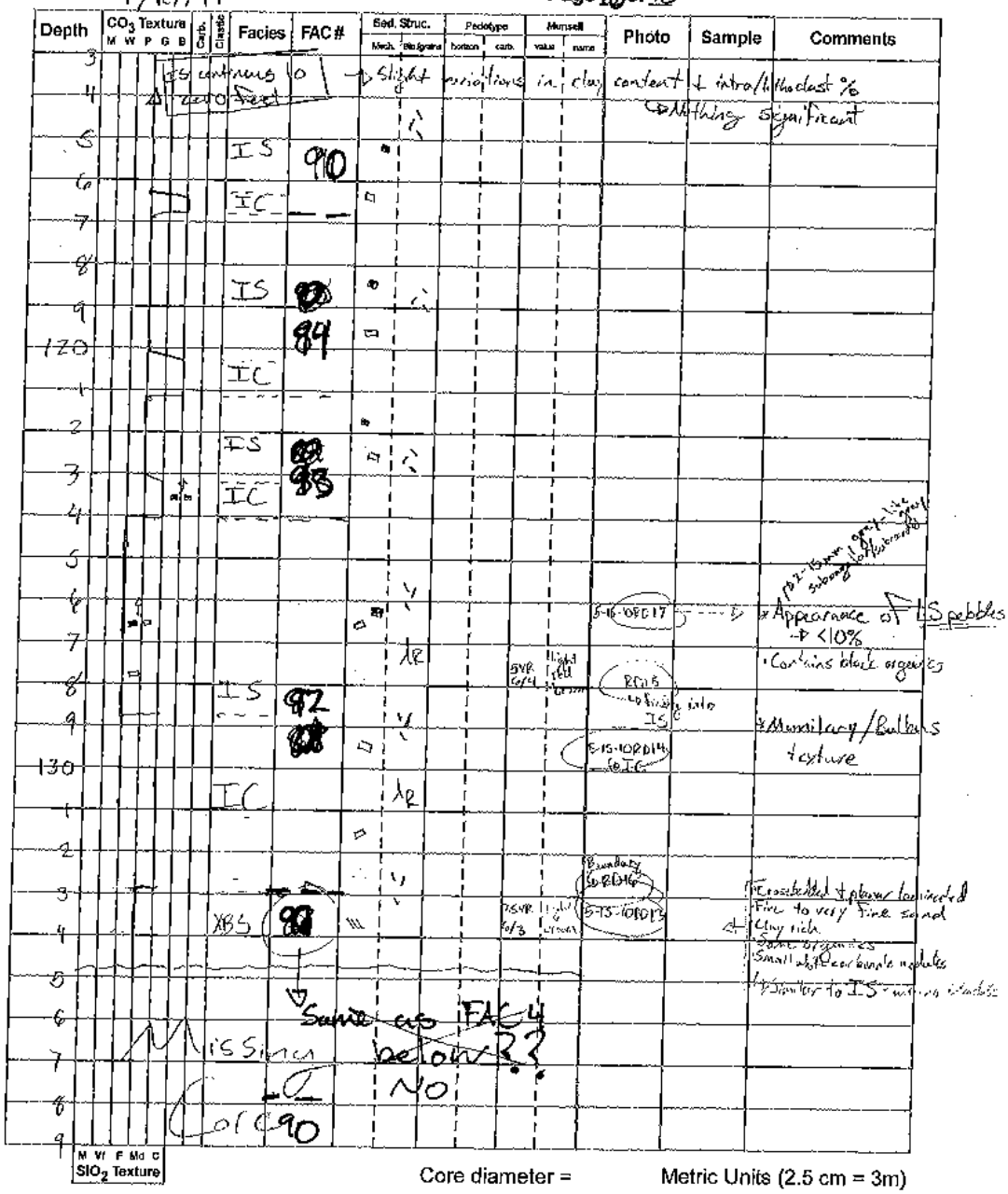

REFERENCES

Adams, J.M., 1997, Global land environments since the last interglacial. Oak Ridge National Laboratory, TN, USA. http://www.esd.ornl.gov/ern/qen/nerc.html.

Albritton, C. C. Jr. and Smith, J. F., 1965, Geology of the Sierra Blanca area, Hudspeth County, Texas: Geological Survey Prof Paper 479, p. 131.

An, Z., Wang, S., Wu, X., Chen, M., Sun, D., Liu, X., Wang, F., Li, L., Sun, Y., Zhou, W., Zhou, J., Liu, X., Lu, H., Zhang, Y., Dong, G., Qiang, X., 1999, Eolian evidence from the Chinese Loess Plateau: the onset of the Late Cenozoic Great Glaciation in the Northern Hemisphere and Qing-hai-Xizang Plateau uplift forcing: Sci. China, Series D, v. 42, n. 3, p. 258-271.

Arens, N. C., Jahren, A. H., and Amundson, R., 2000, Can C_3 plants faithfully record the isotopic composition of atmospheric carbon dioxide?: Paleobiology, v. 26, p. 137-164.

Atchley, S.C., Nordt, L.C., and Dworkin, S.I., 2004, Eustatic control on alluvial sequence stratigraphy: A possible example from the Cretaceous-Tertiary transition of the Tornillo basin, Big Bend National Park, West Texas, U.S.A.: Journal of Sedimentary Research, v. 74, p. 391-404.

Atchley, S.C., Nordt, L.C., Dworkin, S.I., Cleveland, D.M., Mintz, J.S., and Harlow, R.H., in review, Alluvial stacking pattern analysis and sequence stratigraphy: concepts and case studies: Special Publication, Society for Sedimentary Geology (SEPM).

Blakey, R. C. and Gubitosa, R., 1984, Sandstone body geometry and architecture of the Triassic Chinle Formation , Colorado Plateau: Sedimentary Geology, v. 38, p. 51-86.

Breeker, D. O., Sharp, Z. D., and McFadden, L. D., 2009, Seasonal bias in the formation and stable isotopic composition of pedogenic carbonate in modern soils from central New Mexico, USA: Geological Society of America Bulletin, v. 121, p. 630-640.

Bridge, J.S., 1984, Large-scale facies sequences in alluvial overbank environments: Journal of Sedimentary Petrology, v. 54, p. 583-588.

Burns, B. A., Heller, P. L., Marzo, M., and Paola, C., 1997, Fluvial response in a sequence stratigraphic framework: Example from Montserat fan-delta, Spain: Journal of Sedimentary Research, v. 67, p. 310-320.

Cerling, T. E., 1999, Palaeorecords of C_4 plants and ecosystems: *In* Sage, R. F., Monson, R. K. eds. C_4 plant biology, San Diego, CA, Academic Press, p. 445-469.

Cerling, T. E., and Harris, J. M., 1999, Carbon isotope fractionation between diet and bioapatite in ungulate mammals and implications for ecological and paleoecological studies: Oecologia, v. 120, p. 247-363.

Cerling, T. E., Harris, J. M., and MacFadden, B. J., 1998, Carbon isotopes, diet of North American equids,a nd the evolution of North American C_4 grasslands, *in* Griffiths, H., ed. Stable isotopes: Oxford, BIOS Scientific, p. 363-379.

Cerling, T. E., Harris, J. M., MacFadden, B. J., Leakey, M. G., Quade, J., Eisenmann, V., and Ehleringer, J. R., 1997, Global vegetation change through the Miocene/Pliocene boundary: v. 389, p. 153-158.

Cleveland, D. M., Atchley, S. C., and Nordt, L. C., 2007, Continental sequence stratigraphy of the Upper Triassic (Norian-Rhaetian) Chinle strata, northern New Mexico, U.S.A.: allocyclic and autocyclic origin of paleosol-bearing alluvial successions: Journal of Sedimentary Research, v. 77, p. 909-924.

Collins, E.W., and Raney, J.A., 1991, Neotectonic history and geometric segmentation of the Campo Grande fault: A major structure bounding the Hueco basin, trans-Peco Texas: Geology, v. 19, p. 493-496.

Collins, E.W., and Raney, J.A., 1994, Impact of late Cenozoic extension on Laramide overthrust belt and Diablo Platform margins, northwestern Trans-Pecos Texas: New Mexico Bureau of Mines and Mineral Resources Bulletin, v. 11, p. 71-81.

Dworkin, S. I., Nordt, L. C., and Atchley, S. C., 2005, Determining terrestrial paleotemperatures using the oxygen isotope composition of pedogenic carbonates: Earth and Planetary Science Letters, v. 237, p. 56-68.

Drummond, C. N., and Wilkinson, B. H., 1993, On the use of cycle thickness diagrams as records of long-term sea level change during accumulation of carbonate sequences: Journal of Geology, v. 101, p. 687-702.

Edwards, E.J, and Smith, S.A., 2010, Phylogenic analysis reveal the shady history of C_4 grasses: PNAS, v. 106, n. 6, p. 2532-2537

Ehleringer, J. R., Cerling, T. E., and Heliker, B. R., 1997, C_4 photosynthesis, atmospheric CO_2, and climate: Oecologia, v. 112, p. 285-299.

Ehleringer, J. R., Sage, R. F., Flanagan, L. B., and Pearcy, R. W., 1991, Climate change and the evolution of C_4 photosynthesis: TREE, v. 6, p. 95-99.

Ekart, D.D., Cerling, T.E., Montañez, I.P., and Tabor, N.J., 1999, A 400 million year carbon isotope record of pedogenic carbonate: Implications for paleoatmospheric carbon dioxide: American Journal of Science, v. 299, p. 805–827, doi: 10.2475/ajs.299.10.805.

Langford, R. P., 1993, Landscape evolution of Eagle Flat and Red Light basins, Chihuahuan Desert, South-Central Trans-Pecos Texas: The University of Texas at Austin, Bureau of Economic Geology, contract report, prepared for Texas Low-Level Radioactive Waste Disposal Authority under interagency Contract IAC (92-93)-0910, p. 23.

Flower, B. P., and Kennett, J.P., 1995, Middle Miocene deepwater paleoceanography in the southwest Pacific: Relations with East Antarctic Ice Sheet development: Paleoceanography, v. 10(6), p. 1095-1112.

Fox, D. L., and Koch, P.L., 2003, Tertiary histpry of C_4 biomass in the Great Plains, USA: Geology, v. 31, p. 809-812.

Goldhammer, R. K., Dunn, P. A. and Hardie, L. A., 1987, High frequency glacio-eustatic sealevel oscillations with Milankovitch characteristics recorded in middle Triassic platform carbonates in northern Italy: American Journal of Science, v. 287, p. 853-892.

Goldhammer, R. K., Dunn, P. A., and Hardie, L. A., 1990, Depositional cycles, composite sea level changes, cycle stacking patterns, and the hierarchy of stratigraphic forcing, examples from platform carbonates of the Alpine Triassic: Geological Society of America, Bulletin, v. 102, p. 535-562.

Goldhammer, R. K., and Elmore, R. D., 1989, Paleosools capping regressive carbonate cycles in Pennsylvanian Black Prince Limestone, Arizona: Journal of Sedimentary Petrology, v. 54, p. 1124-1137.

Gustavson, T. C., 1991, arid basin depositional systems and paleosols: Fort Hancock and Camp Rice Formations (Pliocene-Pleistocene), Hueco Bolsom, west Texas and adjacent Mexico: Texas Bureau of Economic Geology, Report of Investigation 198, p. 49.

Hatch, J. R., Jacobsen, S. R., Witzke, B. J., Rissatti, J. B., Anders, D. E., Watney, W. L., Newell, K. D., and Vuletich, A. K., 1987, Possible Late Ordovician organic carbon isotope excursion: evidence from Ordovician oil and hydrocarbon source rocks, mid-continent and east-central United States: American Association of Petroleum Geologists Bulletin, v. 71, p. 1342-1354.

Henry, C. D., and Price, J. G., 1985, Summary of the tectonic development of Trans-Pecos Texas: The University of Texas Austin, Bureau of Economic Geology Miscellaneous Map No. 36, p. 7.

Hönisch, B., Hemming, N.G., Archer, D., Siddall, M., and McManus, J.F., 2009, Atmospheric carbon dioxide concentration across the mid-Pleistocene transition: Science, v. 324, p. 1551-1554.

Kerans, C. and Fitchen, W. M., 1995, Sequence hierarchy and facies architecture of a carbonate-ramp system: San Andres Formation of Algerita Escarpment and western Guadalupe Mountains, West Texas and New Mexico: The University of Austin, Bureau of Economic Geology Geological Circular 95-2, 30 p.

Kraus, M. J., and Middleton, L. T., 1987, Contrasting architecture of two alluvial suites in different structural settings, in Ethridge, F. G., Flores, R. M., and Harvey, M. D., eds, Fluvial Sedimentology SEPM special publication 39, p. 253-262.

Kraus, M. J., 1999, Paleosols in clastic sedimentary rocks: their geological applications: Earth-Science Review, v. 47, p. 41-70.

Kraus, M. J., 2002, Basin-scale changes in floodplain paleosols: implications for interpreting alluvial architecture: Journal of Sedimentary Research, v. 72, p. 500-509.

Kraus, M. J., and Aslan, A., 1999, Paleosol sequences in floodplain environments: a hierarchical approach, *in* Thiry, M. ed., Paleoweathering, Paleosurfaces and Related Continental Deposits: International Association Sedimentological, Special Publication 27, p. 303-321.

Kottlowski, F. E., 1953, Tertiary-Quaternary sediments of the Rio Grande Valley in southern New Mexico: New Mexico Geoligical Society Guidebook of southwestern New Mexico, p. 144-148.

Langford, R.P., Jackson, M.L.W., Whitelaw, M.J., 1999, The Miocene to Pleistocene filling of a mature extensional basin in Trans-Pecos Texas: geomorphic and hydrologic controls on deposition: Sedimentary Geology, v. 128, p. 131-153.

Lehrmann, D. J., and Goldhammer, R. K., 1999, Secular variation in parasequence and facies stacking patterns of platform carbonates: a guide to application of stacking pattern analysis in strata of diverse ages and settings, *in* Harris, P. M., Saller, A. H., and Simmo, J. A., eds., Advances in Carbonate Sequence Stratigraphy: Applications to Reservoirs, Outcrops, and Models: SEPM, Special Publication 63, p. 187-225.

MacGinitie, H.D., 1962, The Kilgore flora; a Late Miocene flora from northern Nebraska: Univ. Calif. Publ. Geol. Sci, v. 35, p. 67–158.

Mack, G. H., and Seager, W. R., 1990, Tectonic controls on facies distribution of the Camp Rice and Palomas Formations (Pliocene-Pleistocene) in the southern Rio Grande rift: Geological Society of America Bulletin, v. 102, p. 45-53.

Miall, A. D., ed, 1978, Fluival Sedimentology, Canadian Society of Petroleum Geologists, Memoir 5 Calgary, 859.

Miller, K. G., Fairbanks, R. G., and Mountain, G. S., 1987, Tertiary oxygen isotope synthesis, sea level history, and continental margin erosion: Paleoceanography, v. 2, p. 1-19.

Miller, K. G., Wright, J. D., Fairbanks, R. G., 1991, Unlocking the Ice House: Oligocene-Miocene oxygen isotopes, eustasy, and margin erosion: Journal of Geophys..Res., v. 96, p. 6829-6848.

Mintz, J.S., 2011, Rise of the Givetian (385 Ma) forests, northern Appalachian Basin, Catskill State Park, New York, USA: Unpub. Ph.D. dissertation, Baylor University, Waco, TX, 143 p.

Mintz, J.S., Driese, S.G., Breeker, D.O., Ludvigson, G.A., 2011, Influence of changing hydrology on pedogenic calcite precipitation in vertisols, Dance Bayou, Brazoria County, Texas, U.S.A.: implications for estimating paleoatmospheric pCO_2: Journal of Sedimentary Research, v. 81, n. 6, p. 394-400.

Mintz, J.S., Harlow, R.H., Driese, S.G., Atchley, S.C., and Wright, T.C., in revision, Tectonic controls on terrestrial and marine sedimentation in Middle Devonian strata in the Appalachian basin, New York: to be submitted to Journal of Sedimentary Research.

Morgan, P., Seager, W. R., and Golombk, M. P., 1986, Cenozoic thermal, mechanical, and tectonic evolution of the RioGrande rift: Journal of Geophysical Research, v. 91, p. 6263-6276.

Muehlbereger, W.R., 1980, Texas Lineament revisited: *in* Dickerson, P.W., and Hoffer, J.M. eds., Trans-Pecos region, southwestern New Mexico and West Texas: New Mexico Geologic Society, 31st Annual Field Conference Guidebook, p. 113-121.

Pagani, M., Freeman, K. H., and Arthur, M. A., 1999, Late Miocene atmospheric CO_2 and the expansion of C_4 grasses: Science, v. 285, p. 876-879.

Pagani, M. Lui, Z., LaRiviere, J., and Ravelo, A. C., 2010, High Earth-system climate sensitivity determined from Pliocene carbon dioxide concentrations: Nature, v. 3 p. 27-30.

Prochnow, S. J., Nordt, L. C., Atchley, S. C., and Hudec, M. R., 2006, Multi-proxy paleosol evidence for middle and late Triassic climate trends in eastern Utah: Palaeogeography, Paleoclimatology, Paleoecology, v. 232, p. 53-72.

Price, J. G., and Henry, C. D., 1984, Stress orientations of volcanism in Trans-Pecos Texas: timing and transition from Laramide compression to Basin and Range extension: Geology, v. 12, p. 238-241.

Price, J. G., and Henry, C. D., 1985, Summary of Tertiary stress orientations and tectonic history of Trans-Pecos Texas, *in* Dickerson, P.W., and Muehlberger, W.R ., eds., Structure and tectonics of Trans-Pecos Texas: West Texas Geological Society, Publication 85-81, p. 149-151.

Romanek, C. S., Grossman, E. L., and Morse, J. W., 1992, Carbon isotopic fractionation in synthetic aragonite and calcite: Effects of temperature and precipitation rate: Geochemica et Cosmochimica Acta, v. 56, p. 419-430.

Retallack, G. J., 1988, Field recognition of paleosols: Geological Society of America Special Paper, v. 216, p. 1-20.

Retallack, G.J., 2001, Soils of the past, Second edition: Oxford, U.K., Blackwell Science, p. 404.

Ruddiman, W. F., 2010, A Paleoclimatic Enigma?, Science, v.328, p. 838-839.

Sadler, P. A., Osleger, D. A., and Montanez, I. P., 1993, On the labeling, length and objective basis of Fischer plots: Journal of Sedimentary Petrology, v. 63, p. 360-368.

Sanyal, P., Sarkar, A., Bhattacharya, S.K., Kumar, R., Ghosh, S.K., Agrawal, S., 2010, Intensification of monsoon, microclimate and asynchronous C_4 appearance: Isotopic evidence from Indian Siwalik sediments: Palaeogeography, Palaeoclimatology, Palaeoecology, v. 296, p. 165-173

Seager, W. R., Shafiquallah, M., Hawley, J. W., and Marvin, R. F., 1984, New K-Ar dates from basalts and the evolution of the southern Rio Grande: Geological Society of American Bulletin, v. 95, p. 87-99.

Ségalen, L., Renard, M., Lee-Thorp, J.A., Emmanuel, L., Le Callonnec, L., de Rafélis, M., Senut, B., Pickford, M., Melice, J., 2006, Neogene climate change and emergence of C4 grasses in the Namib, southwestern Africa, as reflected in ratite 13C and 18O: Earth and Planetary Science Latters, v. 244, p. 725-734.

Soil Survey Staff, 2010, Keys to Soil Taxonomy, 11th ed. Soil Management Support Services Technical Monograph 19: Blacksburg, Virginia, Virginia Polytechnic Institute and State University.

Smith, G.A., 1994, Climatic influences on continental deposition during late-stage filling of an extensional basin, southeastern Arizona: Geologic Society of American Bulletin, v. 106, p. 1212-1228.

Stevens, J.B., and Stevens M.S., 1985, Basin and range deformation and depositional timing, Tans-Pecos Texas, *in* Dickerson, P.W., and Muehlberger, W.R ., eds., Structure and tectonics of Trans-Pecos Texas: West Texas Geological Society, Publication 85-81, p. 157-163.

Stuart, C. J., and Willingham, D. L., 1984, Late Tertiary and Quaternary fluvial deposits in the Mesilla and Hueco bolsons, El Paso area, Texas: Sedimentary Geology, v. 38, p. 1-20.

Strain, W. S., 1966, Blancan Mammalian Fauna and Pleistocene Formations, Hudspeth County, Texas. Texas Memorial Museum, Bulletin 10, p. 55.

Tidwell, W. D., and Nambudiri, E. M. V., 1989, Tomlinsonia thomassonii, gen et sp. nov., a permineralized grass from the Upper Miocene Ricardo Formation, California: Palaeobot. Palynol, v. 60, p. 165–177.

Tripati, A. K., Roberts, C. D., and Eagle, R. A., 2009, Coupling of CO_2 and Ice Sheet Stability Over Major Climate Transitions of the Last 20 Million Years: Science, v. 326, p. 1394-1397.

Tripati, A. K., Roberts, C.D., Eagle, R. A., and Li, G., 2011, A 20 million year record of planktic foraminiferal B/Ca ratios: Systematics and uncertainties in pCO_2 reconstructions: Geochimica at Cosmochimica Acta, v. 75, p. 2582-2610.

Tipple, B. J. and Pagani, M., 2007, The early origins of terrestrial C_4 photosynthesis: Annual Review Earth Planetary Science, v. 35, p. 435-461.

Wright, J. D., Miller, K. G., Fairbanks, R. G., 1992, Early and middle Miocene stable isotopes: implications for deepwater circulation nd climate: Paleoceanography, v. 7, p. 357-389.

Zachos, J., Pagani, M., Sloan, L., Thomas, E., and Billups, K., 2001, Trends, Rhythms, and Aberrations in Global Climate 65 Ma to Present: Science, v. 292, p. 686-693